UNIVERSITÀ DEL PIEMONTE ORIENTALE
SCUOLA DI MEDICINA

Università degli Studi del Piemonte Orientale “Amedeo Avogadro”

Department of Health Sciences

PhD. Program in Food Health and Longevity

XXXVI Cycle

Biomaterials for bone regeneration possessing novel antibacterial and anti-inflammatory properties: Comprehensive biological evaluations.

Candidate: Reddy Ajay Kumar

Supervisor: Prof. Lia Rimondini

Tutor: Prof. Andrea Cochis

Co-Tutor: Prof. Diego Cotella

Table of contents

I. Aim of Thesis
II. Introduction
1. Bone Fracture
1.1 Bone Fracture Epidemiology
1.2 Bone Surgery and Treatments
1.3 Bone Grafts
1.4 References
III. Inflammation
2. Inflammation/Oxidative Stress
2.1 Oxidative Stress
2.2 Oxidative Stress After Implantation of Implants
2.2.1 Pre – Oxidative Stress Before Implantation
2.2.2 Post – Oxidative Stress After Implantation
2.3 References
IV. Bacterial Infection
3. Infection
3.1 Orthopaedic Implant-Associated Infection (IAI)
3.2 Biofilm Infection Formation During Surgery
3.2.1 Biofilm Attachment
3.2.2 Biofilm Maturation
3.2.3 Dispersal Of Biofilm
3.3 References
V. Aim

Abstract

Introduction

4. Antimicrobial Peptides
4.1 Material and Methods
4.1.1 Peptoid Synthesis
4.1.2 Surface Pre-treatment
4.1.3 Surface Functionalization
4.1.4 Zeta Potential Measurements on a Solid Sample
4.1.5 Contact Angle Measurements
4.1.6 Zeta Potential Measurements on a Liquid Sample
4.1.7 Cytocompatibility Evaluation
4.1.8 Antibacterial Properties
4.1.9 Selectively Targeted Activity
4.1.10 Statistical Data Analysis
4.2 Results and Discussions
4.2.1 Zeta Potential Measurements
4.2.2 Contact Angle Measurement
4.2.3 Cytocompatibility Evaluation
4.2.4 Antibacterial Properties
4.2.5 Selectively Targeted Activity
4.3 Conclusion
4.4 References

VI Aim

introduction

5. Phage Therapy
5.1.1 Endolysins or Lysins
5.1.2 Endolysins mechanism
5.2 Materials and Methods
5.2.1 Bioinformatic Analysis and Construction of LysK and PlyV12
5.2.2 Preparation of Competent *E. coli*
5.2.3 Bacterial Transformation and Protein Expression
5.2.4 Western Blot Analysis
5.2.5 Bacteria Culture
5.2.6 Protein Production by Bioreactor
5.2.7 Protein Extraction and purification by washing Method
5.2.8 Protein Denaturing and Refolding with Amino Acids
5.2.9 Protein Dialysis
5.2.10 Endolysins
5.2.11 Antibacterial Activity
5.2.12 Cytocompatibility
5.2.13 Statistical Data Analysis
5.3 Results and Discussion
5.3.1 Analysis and Construction of LysK and PlyV12
5.3.2 Bacterial Transformation and Protein Expression
5.3.3 Protein Production by Bioreactor
5.3.4 Protein Denaturing and Refolding with Amino Acids
5.3.5 Protein Extraction and Purification
5.3.6 Antibacterial Activity
5.3.7 Cytocompatibility
5.3.8 Conclusion
5.4 References
VII. Aim
Abstract
Introduction
6. Materials and Methods
6.1 Biological Characterization
6.1.1 Cytocompatibility Evaluation
6.1.2 Reactive Oxygen and Nitrogen Species
6.1.3 Osteogenesis
6.1.4 Antibacterial Activity
6.1.5 hMSCs-Bacteria Culture
6.1.6 Statistical Data Analysis
6.2 Results and Discussion
6.2.1 Cytocompatibility and ROS/RNS Scavenge Ability
6.2.2 Antibacterial Activity
6.2.3 Osteogenesis
6.2.4 hMSCs-Bacteria Culture
6.3 Conclusions
6.4 References

VIII. Aim

Abstract

Introduction

7. MBGs Powders Preparation for In Vitro Assays
7.1 MBGs Powders Preparation for In Vitro Assays
7.1.1 2D Cytocompatibility
7.1.2 3D cytocompatibility
7.1.3 MBGs Extracts Angiogenic Potential Assay
7.1.4 MBGs pellets preparation for In Vitro Assay
7.1.5 Statistical Data Analysis
7.2 Results and Discussion
7.2.1 MBGs Powders Cytocompatibility Assay: 2D
7.2.2 MBGs Powders Cytocompatibility Assay: 3D
7.2.3 MBGs Extracts Angiogenic Potential Assay
7.2.4 MBGs Pellets Cytocompatibility Assay
7.3 Conclusion
7.4 References

IX. Aim

8. Materials and Methods
8.1 Cytocompatibility Evaluation
8.1.1 Pre-inflammatory Model in Polystyrene
8.1.2 Pro-Inflammation Model in Polystyrene
8.1.3 Antioxidant Properties Evaluation
8.1.4 Statistical Data Analysis
8.2 Results and Discussion
8.2.1 Cytocompatibility Evaluation
8.2.2 Pre-inflammatory Model
8.2.3 Pro-inflammation Model
8.2.4 Antioxidant Properties Evaluation
8.3 Conclusion
8.4 References
9. Acknowledgement
10. Declaration of using software technologies in the writing process
11. Acronyms

Chapter I

Aim of Thesis

Bone fractures are a frequent type of injury caused by trauma globally, and their management typically results in a considerable economic burden on society, especially in individuals with osteoporosis and related fragile fractures. Fractures in human bones or tissues are frequently observed and typically occur because of sports injuries, falls, and vehicular accidents. Healthcare professionals worldwide encounter these situations daily. Improving quality of life increases the risk of lifestyle-related physical illnesses. Nevertheless, surgery may not always be required because the human body can naturally heal and regenerate up to a certain point. For example, small bone injuries can be treated without surgery, but spinal cord and cartilage damage may require transplantation or regenerative surgery for full recovery. The innate healing capacity of the body decreases with different factors, such as ageing, a decrease in progenitor cells, restricted tissue repair abilities, and inflammation resulting from damaged tissue.

Implants are commonly utilized in medical procedures such as microvascular surgery, orthopaedic surgery, and general surgery. These materials are designed to engage with biological systems, support the restoration or substitution of damaged tissues, and provide structural reinforcement. Orthopaedic surgeries often require the use of devices, such as implants, for procedures involving fracture fixation, osteoarthritis, spinal deformities, and hip and knee replacements, and the increase in the elderly population has led to an increase in the number of implant surgeries. Every year, millions of people receive bone implants for various traumatic conditions, such as open or closed fracture fixation, total hip and knee replacements, scoliosis, maxillofacial fixation, and other traumatic conditions. Implant failure is likely to occur after insertion into the host due to infection and severe inflammation, for instance, when a bone implant is placed, it disrupts the surrounding tissue, leading to a local inflammatory response. Fibroblasts, resident cells in connective tissue, become activated in response to the tissue injury caused by implant placement. The activation of fibroblasts is triggered by various signalling molecules released during the inflammatory process. The specific mechanisms by which fibroblasts contribute to bone inflammation may vary depending on the underlying cause of inflammation. So, the inflammation triggered by fibroblast activation plays a central role in implant failure. Thus, the host immune system may not be able to fight these infections. After implant placement, bacteria can quickly attach to the implant surface using different methods to adhere to natural and synthetic surfaces, increasing their chances of survival. Fixing open fractures carries a higher risk of microbial infection than fixing closed fractures, with rates varying between 8% and 13.6%. Most literature studies show that staphylococci are responsible for most biofilm formation on orthopaedic implants, accounting for about 80%, with *S. aureus* and *S. epidermidis* being the most common bacteria in bone infections. Biofilm formation allows bacteria to colonize the surface of an implant, making it easier for them to resist antibiotics and the human immune system, as well as enhancing their ability to adhere to surfaces. Bacteria can also cause peri-implant infections

and other complications. This leads to tissue necrosis around the implant, eventually resulting in cell and tissue damage.

Consequently, bone loss occurs, resulting in the loosening of the implant without infection. However, systemic drug administration is not a very effective method of targeted delivery and can lead to toxicity owing to the poor vascularity of the skeletal system. According to most studies, to effectively combat bacteria, antibiotics are directly used at the implant surgical site at higher concentrations, especially to prevent postsurgical infection. For example, during surgical closure, antibiotics in powder form, such as vancomycin, are directly sprinkled on the incision to significantly reduce the risk of surgical site infection (SSI) during the tibia plateau, spinal deformity, and fracture fixation procedures. The common organism in surgical site infection and bone implant infection is *S. aureus* and first-line treatment for these infections includes first-generation cephalosporins such as cefazolin for methicillin-susceptible strains and vancomycin for methicillin-resistant strains. Most studies have demonstrated that traditional antibiotics are ineffective against 5-10% of bacterial biofilms. Researchers are currently exploring new approaches to combat implant infections and biofilm formation. An antibacterial coating should be used on the implant to fight bacterial infections and enhance the results for patients with infected surgical implants. Several methods have been designed, including altering the implant surface, selecting appropriate implant materials, and applying natural or synthetic molecules (such as Peptides, Peptoids, and endolysins) to coat the implant. The orthopaedic field is rapidly evolving to keep up with the growing need for medical implants to treat injuries and trauma. Advancements have been propelled by the creation of novel materials and the incorporation of three-dimensional manufacturing methods, allowing for the creation of intricate geometric implants.

Peri-implantitis occurs in the hard and soft tissues surrounding dental implants, similar to periodontitis around natural teeth. It typically results in adverse biological effects, such as bleeding on probing, suppuration, and progressive bone loss beyond physiological remodelling, which eventually leads to complications and leading to implant removal. Recent studies have shown that pre-implantitis is a major concern for 28-56% of patients and is a leading cause of implant loss. Peri-implantitis is a disease associated with the biofilm around dental implants. It affects the tissues surrounding dental implants, causing inflammation in the peri-implant mucosa and a gradual reduction of supporting bone. The pathogenesis and clinical symptoms of peri-implantitis are similar to those of periodontitis, and its management is also based on periodontal therapy. Most patients with periodontitis respond well to treatment and have stable periodontal tissue in the long term. Similarly, throughout peri-implantitis treatment, the progression of bone resorption may be arrested, and the clinical condition may stabilize. However, clinical conditions such as bone resorption, suppuration, and bleeding progress rapidly in some cases. Most in vivo studies demonstrate that peri-implantitis progresses faster than periodontitis in animal models. Several studies have reported the predominance of common microbiota in these two diseases, and it is widely accepted that the implant surface

harbor's bacteria, forming a biofilm on the outer surface of the implant. Some studies have shown a higher presence of *Aggregatibacter actinomycetemcomitans* and *Prevotella intermedia* around infected implants, whereas other studies have documented that *Porphyromonas gingivalis* and *Fusobacterium nucleatum* are abundant in peri-implantitis sites. Additionally, dental implant surfaces are favourable to oral biofilm growth, similar to natural teeth. However, uncontrolled biofilm formation can lead to inflammation of surrounding tissues, and the outcome is implant failure. Although unconventional approaches have been reported to remove plaque from infected implants, none of these methods can fully and permanently solve the problem of bacterial invasion. Fortunately, the ongoing development of antibacterial implant materials is a promising solution to this situation.

My PhD project mainly concentrates on bone implants that have multifunctional properties aiming to improve tissue integration while decreasing bacterial infections. During the project, I focused on the most relevant biomaterial formulations used for bone repair, such as Bioglass and titanium implants and their combinations **(Kaou et al. 2023) (Stich et al. 2021)**. Focusing on antimicrobial peptoids, phage-derived endolysins, and natural extracts such as polyphenols and metal ions like Tellurium and cerium.

Firstly, we mainly focus on antimicrobial strategies to address the threat of bacterial infections, especially in the field of orthopaedics, due to the crucial issue of antibiotic resistance. To combat this, we are introducing synthetic Peptoids, specifically GN2-Npm9, known for their strong anti-bacterial effect.

In detail, Chapter V mainly focuses on the antibacterial properties: here we studied the synthesized Peptoid (GN2-Npm_9) that was used to functionalize a nanometric chemically treated (CT) titanium surface. Our objective was to bring out this Titanium coated with GN2-Npm_9 as an antibacterial, without compromising the cytocompatibility. The titanium samples were developed by the Politecnico di Torino and the GN2-Npm_9 Peptoids were synthesized at Roskilde University, Denmark. Here I was able to demonstrate strong antibacterial activity towards *S. epidermidis* in a co-culture system and at the same time cytocompatibility for the human bone marrow-derived stem cells (hMSCs). This chapter has been published as a 'research article' in Heliyon (https://doi.org/10.1016/j.heliyon.2024.e24246).

I have been exploring recombinant proteins derived from bacteriophages, specifically endolysins, as part of the same strategy. Endolysins are known for their ability to rapidly kill both Gram-positive and Gram-negative bacteria. This approach presents a new potential therapy that could overcome the limitations of traditional antibiotics. It could also address planktonic and biofilm forms of bacterial infections commonly associated with orthopaedic implants. By combining these two approaches, we developed a comprehensive strategy to fight bacterial infections. This involves modifying surfaces to prevent initial colonization and using recombinant proteins to directly target bacterial pathogens. Further research in this area has the potential to

improve our ability to combat bacterial infections in implants and could significantly improve orthopaedic implant treatments while reducing the occurrence of implant-related infections. Moreover, in **Chapter VI,** I tried to produce a recombinant protein that is derived from Bacteriophages during their lytic cycle, to target bacterial infection. Firstly, I assessed the effectiveness of specific endolysins, including LysK and Ply V12, in combating bacterial infections, and secondly, I evaluated the synergistic effects of these endolysins when used together. Finally, the antibacterial properties of the endolysins against both planktonic and biofilm forms of *S. aureus* and *S. epidermidis*, which are commonly associated with orthopaedic-related infections, were evaluated.

The transition from **Chapter VI** to **Chapter VII** underscores the importance of addressing both antibacterial and antioxidant properties in biomedical research, particularly in the context of implant materials. Inflammation plays a significant role in bone health, in particular, excessive production of inflammation reduces osteoblast activity, thus resulting in changes in bone architecture and bone loss. By addressing both antibacterial and anti-inflammatory aspects, we focused on metal ions that have multifunctional properties to develop comprehensive solutions for combating infections and inflammation. Ultimately improving patient outcomes and reducing the incidence of implant-related complications.

In **Chapter VII** explores the feasibility of creating novel bioactive glasses with a silica base containing a minimal level of tellurium dioxide. Our objective was to bring out these glasses with both antibacterial and antioxidant capabilities without compromising their cytocompatibility. The samples were developed by the Politecnico di Torino, and I was able to demonstrate the strong antibacterial and antioxidant effects of tellurium-doped glasses in comparison with non-treated glass as a control, showing that tellurium is a promising element to enhance the biological response of biomaterials. This chapter has been published as a 'research article' in Materials Science and Engineering: C (https://doi.org/10.1016/j.msec.2021.111957).

Furthermore, moving forward to **Chapter VIII** signifies a more in-depth exploration of bone tissue regeneration, which requires a complex approach considering not only antibacterial and anti-inflammatory properties, but also prioritizes the important role of blood supply; for example, vascularization is required for bone generation due to its capability of delivering some important components such as oxygen, nutrients and other signalling molecules. To achieve this aim, we focused on the unique properties of cerium in combination with natural polyphenols to improve bone regeneration.

In this chapter, to evaluate endothelial migration in conditions similar to *in vivo,* we prepared a 3D model of hMSCs spheroids as an *in vitro* model mimicking the "physiological" and "pathological" characterizations of bone. Then, this property of the glasses doped with cerium and polyphenol, which were referred to here as

Ce-MBGs and Ce-MBGs-Poly, respectively, was assessed. This research may offer valuable information on the potential use of Ce-MBGs-Poly as a therapy for bone regeneration. The biomaterials used in this chapter were kindly provided by the University of Modena and Reggio Emilia. This chapter has been published as a 'research article' in Biomaterials and Biosystems. (https://doi.org/10.1016/j.bbiosy.2024.100095).

Finally, in Chapter IX, we mainly focus on evaluating the anti-inflammatory properties of green chemistry components, specifically polyphenols, and their potential application in mitigating inflammation during and after surgery. In this work, the pro- and anti-inflammatory characterizations of treated titanium disks functionalized with green tea polyphenols were evaluated. The Politecnico di Torino produced and provided all the samples. This chapter has been published as a 'research article' in the MDPI Nanomaterials journal (https://doi.org/10.3390/nano13030479).

References

Gamna, Francesca, Seiji Yamaguchi, Andrea Cochis, Sara Ferraris, Ajay Kumar, Lia Rimondini, and Silvia Spriano. 2023. “Conferring Antioxidant Activity to an Antibacterial and Bioactive Titanium Surface through the Grafting of a Natural Extract.” Nanomaterials 13 (3): 479–79. https://doi.org/10.3390/nano13030479.

Gamna, Francesca, Andrea Cochis, Biljana Mojsoska, Ajay Kumar, Lia Rimondini, and Silvia Spriano. 2024. “Nano-Topography and Functionalization with the Synthetic Peptoid GN2-Npm9 as a Strategy for Antibacterial and Biocompatible Titanium Implants.” Heliyon 10 (2): e24246–46. https://doi.org/10.1016/j.heliyon.2024.e24246.

Kaou, Maroua H, Mónika Furkó, Katalin Balázsi, and Csaba Balázsi. 2023. “Advanced Bioactive Glasses: The Newest Achievements and Breakthroughs in the Area.” Nanomaterials 13 (16): 2287–87. https://doi.org/10.3390/nano13162287.

Miola, Marta, Jonathan Massera, Andrea Cochis, Ajay Kumar, Lia Rimondini, and Enrica Vernè. 2021. “Tellurium: A New Active Element for Innovative Multifunctional Bioactive Glasses.” Materials Science and Engineering: C 123 (April): 111957. https://doi.org/10.1016/j.msec.2021.111957.

Stich, Theresia, Francisca Alagboso, Tomáš Křenek, Tomáš Kovářík, Volker Alt, and Denitsa Docheva. 2021. “Implant-Bone-Interface: Reviewing the Impact of Titanium Surface Modifications on Osteogenic Processes in Vitro and in Vivo.” Bioengineering & Translational Medicine 7 (1). https://doi.org/10.1002/btm2.10239.

Lee, Chun-Teh, Yen-Wen Huang, Liang Zhu, and Robin Weltman. 2017. “Prevalences of Peri-Implantitis and Peri-Implant Mucositis: Systematic Review and Meta-Analysis.” Journal of Dentistry 62 (July): 1–12. https://doi.org/10.1016/j.jdent.2017.04.011.

Rakic, Mia, Pablo Galindo-Moreno, Alberto Monje, Sandro Radovanovic, Hom-Lay Wang, David Cochran, Anton Sculean, and Luigi Canullo. 2017. “How Frequent Does Peri-Implantitis Occur? A Systematic Review and Meta-Analysis.” Clinical Oral Investigations 22 (4): 1805–16. https://doi.org/10.1007/s00784-017-2276-y.

Ksenia Menshikh, Ajay Kumar Reddy, Andrea Cochis, Francesca Fraulini, Alfonso Zambon, Gigliola Lusvardi, and Lia Rimondini. 2024. “Bifunctional Mesoporous Glasses for Bone Tissue Engineering: Biological Effects of Doping with Cerium and Polyphenols in 2D and 3D in Vitro Models.” Biomaterials and Biosystems, May, 100095–95. https://doi.org/10.1016/j.bbiosy.2024.100095.

Chapter II

General Introduction of Bone Epidemiology

1. Bone Fracture Epidemiology

Fractures can occur in individuals of any age. Various factors, such as bone quality and trauma, can lead to a variety of bone fractures in different types and locations. Understanding the frequency of fractures in a particular demographic is crucial for effectively planning healthcare and preventive strategies. These measures could involve overall community planning, such as traffic flow and housing conditions for older individuals, as well as targeted preventative actions for vulnerable populations. Taking preventive steps is crucial for the elderly, as they frequently experience fragile fractures from mechanical forces that would not typically bring about a fracture. The occurrence of fractures is on the upward thrust, especially among older individuals. Fragility fractures, as defined by the World Health Organization (WHO), are fractures because of non-worrying forces. It is crucial to tackle this problem when strategizing healthcare and preventative actions. According to the Lancet Health Longevity Record, statistics on the global, local, and international costs and years lived with disability (YLDs) due to fractures were calculated between 1990 and 2019. In 2019, a total of 178 million new fractures had been reported globally, showing a 33.4% upward push from 1990. Additionally, there were 455 million instances of acute or long-term signs and symptoms of a fracture in 2019, which is 70.1% since 1990, at the side of 25.8 million YLDs, a 65.3% growth considering 1990. The age-standardized costs of fractures in 2019 were 2296.2 incident cases per one hundred thousand population, which is a decrease of 9.6% since 1990. The universal cases/ one hundred thousand population have been 5614.3. There, was a decrease of 6.7% since 1990. The YLDs / one hundred thousand population became 319.0, which is a lower of 8.4% since 1990. Whereas decreased leg fractures involving the patella, tibia, fibula, or ankle were the maximum not unusual and burdensome fractures in 2019, with an age-standardized occurrence rate of 419.9 cases /one hundred thousand population and an age-standardized rate of YLDs of 190.4/one hundred thousand population. In 2019, age-precise rates of fracture occurrence have been highest in the oldest age organizations, with, as an example, 15,381.5 incident cases/per one hundred thousand population in those elderly 95 years and older **(Wu et al. 2021)**.

Osteoporosis is a developing condition that leads to lower bone density and strength, raising the risk of fractures. Osteoporosis has the potential to become a major public health concern worldwide, resulting in substantial financial burdens, especially for the elderly population living with the condition. Standards of living, disabilities, rising healthcare costs, and significant strain on individuals, families, and healthcare systems can all be experienced. Research has indicated that a hip fracture replacement procedure at any hospital costs $10,075. Additionally, on a global scale, the average total healthcare expenses and personal care costs for one hip fracture after 12 months amount to $43,669 **(Wu et al. 2021)**. The International

osteoporosis foundation (IOF) has appointed a scientific committee to develop EU 6 including Italy, Germany, Spain, France, Sweden, and the United Kingdom. The total number of fractures reported in European Union (EU) countries is projected to rise from 2.7 million in 2017 to 3.3 million in 2030, representing a 23% increase. Men have a 66% lower risk of rupture compared to women. Fractures of the hip, femur, distal forearm, or proximal humerus make up 19.6%, 15.5%, and 17.9% of all osteoporotic fractures, according to **(Moriarty et al. 2016).**

1.1. Bone Surgery and Treatments

Surgeons have various treatment options for managing complex clinical situations that can be challenging to treat, leading to medical and socioeconomic difficulties. Standard methods in clinical practice for promoting bone regeneration involve processes like distraction osteogenesis, bone transport, and utilizing bone-grafting methods such as autologous bone grafts, allografts, substitutes, or growth factors. The Masquelet technique serves as a different approach to restoring and reconstructing a long-bone defect. The process consists of two steps utilizing a "biological" membrane created by a cement spacer in the initial stage, serving as a 'chamber' for inserting a non-vascularized autograft in the subsequent stage. Moreover, non-invasive methods are biophysical stimulation methods such as low-intensity pulsed ultrasound (LIPUS) and pulsed electromagnetic fields (PEMF) are utilized to boost bone regeneration.

1.2. Bone Grafts

Bone grafting is a surgical procedure that is often performed to enhance bone regeneration using several orthopaedic and maxillofacial methods. The gold standard for bone grafting is autologous bone, which has all the properties required in a bone graft, such as osteoinduction, osteogenesis, and osteoconduction. Autologous bone can be harvested as a tricortical graft for structural assistance or as a vascularized bone graft for the healing of long bone defects or avascular necrosis. The anterior and posterior iliac crests of the pelvis are normally used from the donor sites for bone-graft harvesting. The intramedullary canal of long bones can also be used as an alternative harvesting site, providing a huge extent of autologous bone graft, thanks to the development of a new reaming system called the reamer-irrigator-aspirator (RIA). Autologous bone is histocompatible and non-immunogenic because it’s the patient's tissue, decreasing the feasibility of immunoreactions and transmission of infections. However, harvesting requires an additional surgical procedure, with severe complications and irritation for the patient, and has the additional risks of quantity regulations and tremendous costs.

Biomaterials can restore the physiological function of diseased tissues by both replacing and regenerating tissue, as illustrated in Figure 1.1. In the orthopaedics field, the need for implants and medical devices has grown fast over the past few years, attributable to trauma, bone cancer, osteoporotic illnesses, and joint and spinal illnesses **(Stevens. 2008)**. Biomaterials have performed a crucial function in various healthcare

problems and feature fostered considerable advancements in various biomedical fields, which include tissue engineering (TE), clinical implants, drug delivery, and immunotherapies. Bone TE can be effectively carried out by following the diamond concept, which outlines the fundamental characteristics required for successful bone healing with bone TE **(Montoya et al. 2021)**. A good mechanical environment is necessary to provide sufficient stability for healing while mimicking the mechanical properties of natural tissue. Growth factors are required to facilitate cellular events and promote bone healing. A healthy population of osteoprogenitor cells is necessary to enable new bone regrowth. Additionally, adequate vascularity helps improve bone healing. However, it is crucial to consider the patient's medical history, as it may include risk factors that increase the chances of fractures, bone defects, or nonunion fractures. As an example, age can have significant implications for the skeletal system, as ageing is associated with higher fracture rates and lower fracture healing, as well as with conditions such as osteoarthritis and osteoporosis. Another critical consideration is the natural bone healing process. **(Kim et al. 2020).**

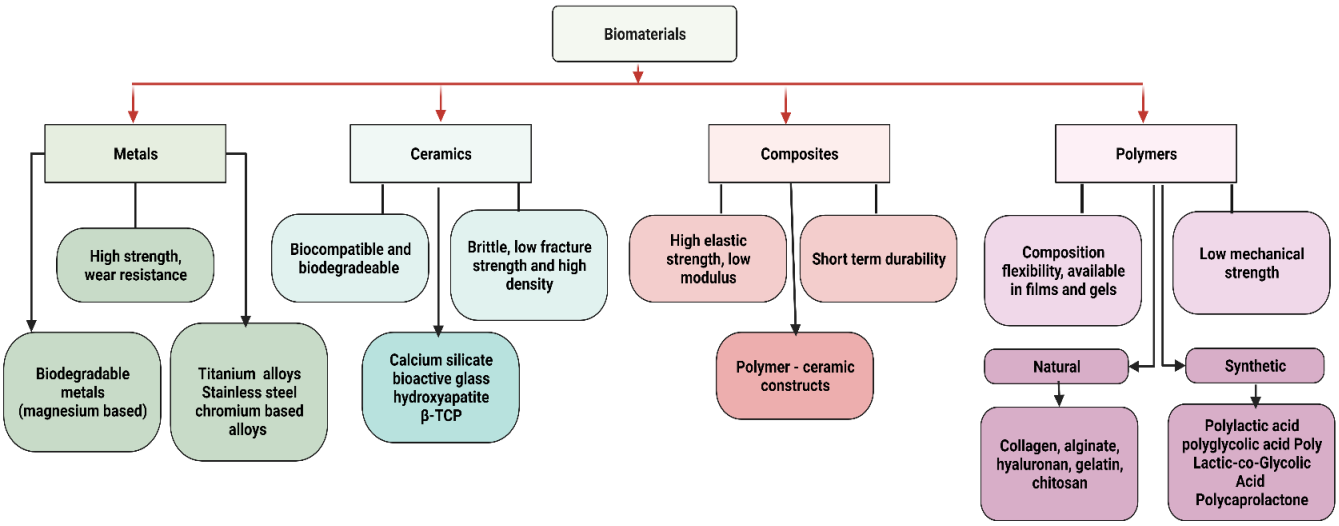

Figure 1.1: A schematic representation of biomaterials for tissue regeneration or replacement. Created with BioRender.com.

1.3 References

Kim, Tiffany, Carmine Wang See, Xiaochun Li, and Donghui Zhu. 2020a. “Orthopedic Implants and Devices for Bone Fractures and Defects: Past, Present and Perspective.” Engineered Regeneration 1: 6–18. https://doi.org/10.1016/j.engreg.2020.05.003. 2020b. “Orthopedic Implants and Devices for Bone Fractures and Defects: Past, Present and Perspective.” Engineered Regeneration 1: 6–18. https://doi.org/10.1016/j.engreg.2020.05.003.

Montoya, Carolina, Yu Du, Anthony L. Gianforcaro, Santiago Orrego, Maobin Yang, and Peter I. Lelkes. 2021a. “On the Road to Smart Biomaterials for Bone Research: Definitions, Concepts, Advances, and Outlook.” Bone Research 9 (1): 1–16. https://doi.org/10.1038/s41413-020-00131-z.

Moriarty, T. Fintan, Richard Kuehl, Tom Coenye, Willem-Jan Metsemakers, Mario Morgenstern, Edward M. Schwarz, Martijn Riool, et al. 2016. “Orthopaedic Device-Related Infection: Current and Future Interventions for Improved Prevention and Treatment.” EFORT Open Reviews 1 (4): 89–99. https://doi.org/10.1302/2058-5241.1.000037.

Stevens, Molly M. 2008. “Biomaterials for Bone Tissue Engineering.” Materials Today 11 (5): 18–25. https://doi.org/10.1016/s1369-7021(08)70086-5.

Wu, Ai-Min, Catherine Bisignano, Spencer L. James, Gdiom Gebreheat Abady, Aidin Abedi, Eman Abu-Gharbieh, Robert Kaba Alhassan, et al. 2021. “Global, Regional, and National Burden of Bone Fractures in 204 Countries and Territories, 1990–2019: A Systematic Analysis from the Global Burden of Disease Study 2019.” The Lancet Healthy Longevity 2 (9): e580–92. https://doi.org/10.1016/S2666-7568(21)00172-0.

Chapter III

General Introduction to Reactive Oxygen Species

2. Inflammation/Oxidative Stress

Inside a cell, reactive oxygen species (ROS) are generated utilizing different resources, which include enzymatic activation of cytochrome C, Nicotinamide adenine dinucleotide phosphate (NADPH) oxidases, xanthine oxidase, dysregulation of Nitric oxide Synthase (NOS), and release from the mitochondria. ROS are produced within a cell as detailed in Figure 2.1. Mitochondria are essential for cell metabolism, as they provide energy for cell functions through various redox reactions that help maintain cell balance. However, dysfunctional ROS metabolism, mainly within mitochondria, can cause severe outcomes for mitochondrial function and cellular integrity. This connection between mitochondrial dysfunction and ROS generation has been connected to numerous pathologies, including of neurodegeneration, endothelial dysfunction, cellular ageing, and cerebral ischemia-reperfusion damage. Mitochondrial ROS production can cause damage to mitochondrial proteins and mitochondrial DNA (Mt – DNA). It is currently increasingly recognized that two electrons or non–radical ROS such as hydrogen peroxide (H_2O_2) can play a crucial role in cell signalling when they exist at higher concentrations in cell injury. During normal metabolic reactions, the oxygen molecule is utilized to generate adenosine triphosphate (ATP) from adenosine diphosphate (ADP), a process called oxidative phosphorylation (OP), as well as results in the generation of superoxide radicals ($O_2-\bullet$). ROS such as $O_2-\bullet$ produces H_2O_2 and the hydroxyl radical (•OH), which have crucial roles in regulating everyday cell features at low concentrations. For example, they're worried about modulating reactions to noxious conditions, including hypoxia, and destroying cells inflamed with viruses. Reactive nitrogen species (RNS), along with nitric oxide (NO), are a result of NOS and affect vascular tone and inflammation.

Several studies have shown that ROS plays a crucial role in the autophagy process, which is an important pro-survival mechanism. During autophagy, cells selectively eliminate damaged mitochondria, misfolded proteins, toxic metabolites. ROS is responsible for activating the early feedback of the autophagic process by removing the potential source of pro-apoptotic stimulants **(Yun et al. 2020).** ROS can attack any cellular component, but they normally react with the first component they come across, mostly the lipids of cells or organelle membranes. Proteins and DNA are also susceptible to ROS attack, especially in mitochondria, where Mt-DNA is physically accessible to sites of ROS production. However, proteins, both structural and enzymatic, are exposed to free radical-mediated hydrolysis, which results in the loss of critical cellular functions such as cell growth, division, and repair processes **(Nissanka and Moraes, 2018).** ROS such as $O_2\bullet-$, •OH, and other oxygen-free radicals are known to cause DNA base hydroxylation and scission of DNA strands, leading to the disruption of cell integrity and lysis via activities such as apoptosis or necrosis. ROS are known to affect

apoptotic pathways; specifically, H_2O_2 is known to induce apoptosis via the activation of the mitogen-activated protein (MAP) kinase pathways and c-Jun N-terminal kinase (JNK).

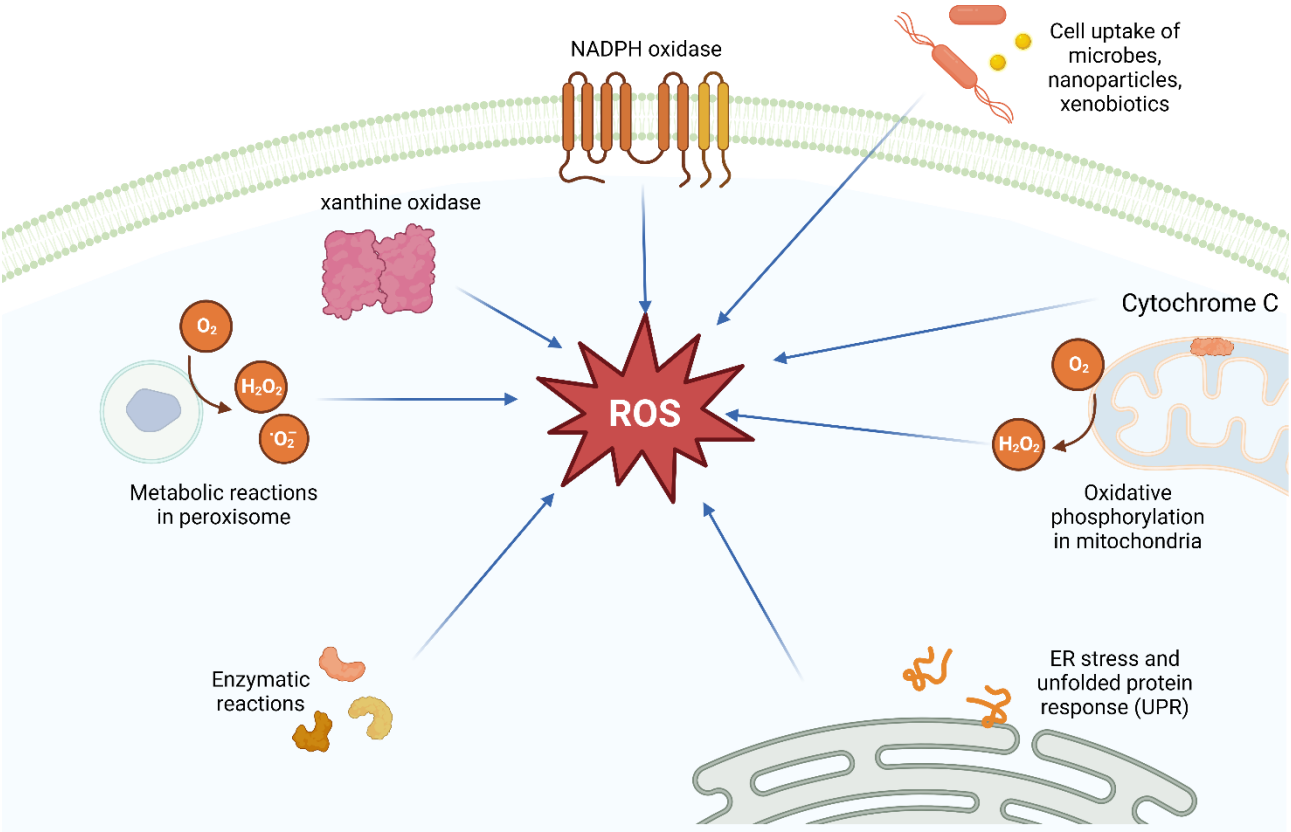

Figure 2.1: A schematic representation of Reactive oxygen species (ROS) produced inside a cell. Modified from (Jha et al. 2017) Created with BioRender.com

2.1 Oxidative Stress

Oxidative stress (OS) is a phenomenon caused by an imbalance between the production and accumulation of ROS in cells and tissues, and the capability of the biological system to purify these reactive products. ROS performs essential roles in cellular physiology, which includes cell signalling. Environmental stressors, such as UV radiation and ionising radiation, and environmental pollutants, (such as 1-nitropyrene (nitro-PAHs in diesel exhausts) and vanadium pentoxide (V_2O_5) **(Mudway, Kelly, and Holgate 2020),** Inorganic components (such as chloride, sulfates, nitrates, and ammonium) **(Kaloyianni et al. 2009)**, biological pollutants (such as bacteria, spores, and pollens), heavy metals (such as transition metals, such as iron (Fe), copper (CU), manganese (Mn), and zinc (Zn) **(Chen et al. 2018),** and xenobiotics, along with anti blastic drugs (such as doxorubicin, actinomycin D, Cisplatin) **(Deidda et al. 2016)** can seriously increase ROS production, directing to a substantial imbalance that causes cells and tissue damage. This phenomenon is a vital determinant of cell and tissue homeostasis and is implicated in the pathogenesis of various pathological conditions. ROS are particularly reactive molecules and are classified into 2 groups: 1. Non–radical and 2. Oxygen radicals are O2•−, •OH, NO• organic radicals (R•), peroxyl radicals (ROO•), thiyl peroxyl radicals (RSOO•) alkoxyl radicals

(RO•), thiyl radicals (RS•), sulfonyl radicals (ROS•), and disulfides (RSSR). Whereas the non – radical are H_2O_2, singlet oxygen ($^1O2$), trioxygen (O_3), nitronium (NO_2^+), dinitrogen dioxide (N_2O_2), organic hydroperoxides (ROOH), hypochlorite (HOCl), peroxynitrite (ONO−), nitroso peroxy carbonate anion ($O=NOOCO2^-$), and nitro carbonate anion ($O_2NOCO_2^-$), which are generated by using products of metabolic processes in biological structures. Most of them are reactive carbohydrates or lipid-derived carbonyl compounds. Some of them are H_2O_2, O2.-, and •OH which are well-studied ROS in cancer as well as normal disease conditions. ROS production plays a critical role in various cellular activities, consisting of protein phosphorylation, activation of transcriptional factors, apoptosis, immunity, and differentiation **(Sinenko et al. 2021).** However, it is important to maintain ROS levels within an optimum standard to inhibit harmful outcomes on cellular components, including proteins, lipids, and nucleic acids. When ROS production increases and reaches its minimum level (> 30 μM), it can cause oxidative stress, thereby promoting many diseases, such as cancer, diabetes (acute or chronic), metabolic diseases like obesity, insulin resistance, hyperglycemia, chronic inflammation, atherosclerosis, and heart disease. The most important source of ROS is the mitochondria, which produce O2•− during cellular respiration, in addition to lipoxygenase (LOX) and cyclooxygenase (COX) by metabolizing arachidonic acid (AA), endothelium, inflammatory cells such as macrophages, and neutrophils. Although mitochondria alone have intrinsic ROS scavenging activity, it is not sufficient to scavenge the high levels of ROS produced in the form of any physiological and pathological conditions, so cells protect themselves against ROS – induced cell damage by enzymatic adducts by superoxide dismutase (SOD), catalase (CAT), and glutathione peroxidase (GPx) **(Maria et al. 2022)**.

2.2 Oxidative Stress After Implantation of Implants

Most scientific studies have demonstrated that the presence of ROS in the microenvironment of bone tissue surrounding implant materials increases when a patient undergoes surgery for the implant. This is because the topography of the material surface plays a crucial role in determining how cells attach and ultimately influences the production of ROS in cells. The physicochemical properties and morphology of materials directly determine their wettability, which significantly affects the adsorption of various biomolecules and the attachment of cells. These characteristics are crucial in generating ROS, disrupting the natural balance between oxidation and anti-oxidation in the body, and leading to OS. This strain can increase the worsening of the implant by triggering inflammatory cells, resulting in a decrease in bone density near the implant. This reduction in bone density can significantly impact the implant's long-term strength and longevity. Before any biomaterial is implanted into the body, two crucial factors determine the reactivity or redox state of the implantation site. 1. The level of inflammation that already exists in the host tissue (pre–oxidative stress). 2. The immediate stress that is caused by the surgical wound (Post–oxidative stress). These two factors play a significant role in determining the success of the implantation procedure **(Mouthuy et al. 2016)**.

2.2.1 Pre – Oxidative Stress Before Implantation

Before biomaterial implantation, a particular level of inflammation may already exist because of tissue damage due to trauma or disease. Oxidative pressure is probably present throughout the healing process. The presence of H_2O_2 during recovery can stimulate the activity of NF-kB, which can generate the expression of inflammatory genes and NADPH oxidase (NOX) enzymes. Inflammatory cytokines, which include IL6, IL1b, and Interferon gamma (IFN-γ), can promote inflammatory gene expression and NOX enzymes, thus causing more ROS production. Pathological conditions related to oxidative stress can also show increased levels of oxidants, as seen in cardiovascular diseases characterized by infection and lipid oxidation **(Thomas and Puleo 2011)**. The oxidation of lipids in lipoproteins generates various oxidative stress markers that promote inflammation and oxidation. ROS levels are mostly elevated in nearly all types of cancer, inducing tumour initiation and progression with the aid of gene mutations. Tumours affect metabolic and signalling pathways such as nuclear issues, erythroid 2-related issues 2 (Nrf2) (anti-oxidative), and NF-kB (inflammation), causing an imbalance within the normal redox state. Pre-present oxidative stress can substantially affect the implanted biomaterials, especially degradable materials, which could degrade faster in environments with higher oxidant concentrations. These conditions can also affect the surrounding tissue for the surface chemistry, and the biological microenvironment, doubtlessly altering the overall performance of biomaterials. When deciding on a biomaterial, it is important to understand the quantity and nature of inflammation in the diseased or damaged site environment **(van der Vliet and Janssen-Heininger 2014)**.

2.2.2 Post – Oxidative Stress After Implantation

Implanting materials into the body during surgery causes tissue damage and the formation of wounds. This procedure results in the release of intracellular and extracellular components at the wound site, resulting in elevated oxidative stress levels. This occurs primarily due to the release of existing ROS from damaged cells. Additionally, the wound triggers an instantaneous Ca^{2+} flux, which activates the dual oxidase (DUOX) or lactoperoxidase system responsible for H_2O_2 production. H_2O_2 plays a crucial role in killing invading bacteria and recruiting phagocytic leukocytes from distant sites. Many other components are released from either dying cells or the breakdown of ECM components. These factors are known as damage-associated signals (DAMPs) or "alarmins," and other molecules include heat shock proteins, extracellular S-100 proteins, high mobility group box-1 (HMGB1), adenosine triphosphate (ATP), DNA, and proteins, among others. DAMPs in the innate immune system stimulate the defence mechanism and are recognized by sophisticated pattern recognition (PRR) systems, Tools-like receptors (TLRs) are the major PRRs responsible for inducing the NF-kB, p38, and JNK pathways. This leads to an increase in redox enzymes such as inducible isoform (iNOS) and inflammatory cytokines such as tumour necrosis factor-alpha (TNF-α), IL6, and the small inducible cytokine A2 (CCL2). Cells localized in the connective tissue surrounding the wound, such as mast cells, macrophages, and resident stromal cells, can respond to DAMPs early after tissue injury **(Goodman et al. 2019)**.

Mechanical stress during surgery can cause damage to the microvasculature and tissues, resulting in the breakdown of red blood cells. This can result in the release of pro-oxidant molecules like methemoglobin that can trigger the production of ROS, ultimately causing platelet and leukocyte activation, blood clot formation, and damage to cells at the wound site. Methaemoglobin can also combine with organic peroxides to create ferryl-haemoglobin and protein radicals, resulting in lipid peroxidation and protein damage from oxidation. Moreover, the breakdown of haemoglobin can also result in the generation of detrimental hydroxyl radicals via metal-catalyzed reactions. Temporary hypoxia can also happen during and after surgery because of a reduced blood supply to tissues, causing a rise in ROS production when blood flow returns. Hypoxia can also contribute to oxidative stress levels existing before surgery in case of a pre-existing disease. Additionally, hyperoxia can occur in normally less oxygenated tissues due to air exposure during surgery, creating gradients of oxygen that can contribute to oxidant production and tissue inflammation. Therefore, it is recommended to minimize air exposure during surgery to reduce the risk of OS **(Ikar et al. 2020)**.

Orthopaedic surgery is a common solution for patients who have severe bone damage and who are over 50 years old. However, this type of surgery is associated with higher mortality and morbidity rates when compared to normal fracture patients. Surgical operations such as spinal and arthroplasty surgery require open surgical procedures, which can lead to a higher level of soft tissue injuries **(Rosenfeldt et al. 2013)**. Furthermore, open surgical intervention is generally considered acceptable in providing therapeutic aid, most literature studies indicate that inflammation related to the procedure can contribute to post-operative problems and hinder recovery. This is particularly observed in elderly patients, where perioperative cardiovascular and pulmonary complications tend to be more common. To address these complications, the use of a tourniquet has been suggested to manage the inflammation that accompanies major limb surgery. Moreover, in knee replacement surgery, a leg tourniquet might be employed to establish a surgical area free of blood, enhancing the bond between bone and cement. On the other hand, releasing the tourniquet and allowing blood to flow back into the limb may cause ROS to be released into the bloodstream, thus resulting in OS. This could lead to various complications such as decreased blood flow to tissues post-surgery, higher chances of vascular and muscle damage, as well as delayed wound healing **(Rosenfeldt et al. 2014)**. Some reports suggest that the use of tourniquets in knee surgery can lead to these complications and create OS.

2.3 References

Chen, Pan, Julia Bornhorst, M. Diana Neely, and Daiana S. Avila. 2018. "Mechanisms and Disease Pathogenesis Underlying Metal-Induced Oxidative Stress." Oxidative Medicine and Cellular Longevity 2018 (September): 1–3. https://doi.org/10.1155/2018/7612172.

Deidda, Martino, Rosalinda Madonna, Ruggiero Mango, Pasquale Pagliaro, Pier P. Bassareo, Lucia Cugusi, Silvio Romano, Maria Penco, Francesco Romeo, and Giuseppe Mercuro. 2016. "Novel Insights in Pathophysiology of Antiblastic Drugs-Induced Cardiotoxicity and Cardioprotection." Journal of Cardiovascular Medicine 17 (May): e76–83. https://doi.org/10.2459/jcm.0000000000000373

Goodman, Stuart B., Jiri Gallo, Emmanuel Gibson, and Michiaki Takagi. 2019. "Diagnosis and Management of Implant Debris-Associated Inflammation." Expert Review of Medical Devices 17 (1): 41–56. https://doi.org/10.1080/17434440.2020.1702024.

Ikar, Marin, Tanja Grobecker-Karl, Matthias Karl, and Constanze Steiner. 2020. "Mechanical Stress during Implant Surgery and Its Effects on Marginal Bone: A Literature Review." Quintessence International (Berlin, Germany: 1985) 51 (2): 142–50. https://doi.org/10.3290/j.qi.a43664.

Kaloyianni, M., S. Dailianis, E. Chrisikopoulou, A. Zannou, S. Koutsogiannaki, D.H. Alamdari, G. Koliakos, and V.K. Dimitriadis. 2009. "Oxidative Effects of Inorganic and Organic Contaminants on Haemolymph of Mussels." Comparative Biochemistry and Physiology Part C: Toxicology & Pharmacology 149 (4): 631–39. https://doi.org/10.1016/j.cbpc.2009.01.006.

Maria, None Martins, Amanda Suellenn, Silva, Silva Primo, and Vanessa Brito. 2022. "Biological Indicators of Oxidative Stress [Malondialdehyde, Catalase, Glutathione Peroxidase, and Superoxide Dismutase] and Their Application in Nutrition." Biomarkers in Disease, January, 1–25. https://doi.org/10.1007/978-3-030-81304-8_49-1.

Mouthuy, Pierre-Alexis, Sarah J.B. Snelling, Stephanie G. Dakin, Lidija Milković, Ana Čipak Gašparović, Andrew J. Carr, and Neven Žarković. 2016. "Biocompatibility of Implantable Materials: An Oxidative Stress Viewpoint." Biomaterials 109 (December): 55–68. https://doi.org/10.1016/j.biomaterials.2016.09.010.

Mudway, I.S., F.J. Kelly, and S.T. Holgate. 2020. "Oxidative Stress in Air Pollution Research." Free Radical Biology and Medicine 151 (May): 2–6. https://doi.org/10.1016/j.freeradbiomed.2020.04.031.

Nissanka, Nadee, and Carlos T. Moraes. 2018. "Mitochondrial DNA Damage and Reactive Oxygen Species in Neurodegenerative Disease." FEBS Letters 592 (5): 728–42. https://doi.org/10.1002/1873-3468.12956.

Rosenfeldt, Franklin, Mark Wilson, Geraldine Lee, Christina Kure, Ruchong Ou, Lesley Braun, and Judy de Haan. 2013. "Oxidative Stress in Surgery in an Ageing Population: Pathophysiology and Therapy." Experimental Gerontology 48 (1): 45–54. https://doi.org/10.1016/j.exger.2012.03.010.

Rosenfeldt, Franklin, Mark Wilson, Geraldine Lee, Christina Kure, Ruchong Ou, Lesley Braun, and Judy. 2014. "Oxidative Stress in Surgery." Springer EBooks, January, 3929–46. https://doi.org/10.1007/978-3-642-30018-9_177.

Sinenko, Sergey A., Tatiana Yu. Starkova, Andrey A. Kuzmin, and Alexey N. Tomilin. 2021. "Physiological Signaling Functions of Reactive Oxygen Species in Stem Cells: From Flies to Man." Frontiers in Cell and Developmental Biology 9 (August): 714370. https://doi.org/10.3389/fcell.2021.714370.

Thomas, M.V., and D.A. Puleo. 2011. "Infection, Inflammation, and Bone Regeneration." Journal of Dental Research 90 (9): 1052–61. https://doi.org/10.1177/0022034510393967.

Vliet, Albert van der, and Yvonne M.W. Janssen-Heininger. 2014a. “Hydrogen Peroxide as a Damage Signal in Tissue Injury and Inflammation: Murderer, Mediator, or Messenger?” Journal of Cellular Biochemistry 115 (3): 427–35. https://doi.org/10.1002/jcb.24683.

Yun, Hyeong Rok, Yong Hwa Jo, Jieun Kim, Yoonhwa Shin, Sung Soo Kim, and Tae Gyu Choi. 2020. “Roles of Autophagy in Oxidative Stress.” International Journal of Molecular Sciences 21 (9): 3289. https://doi.org/10.3390/ijms21093289.

Chapter IV

General Introduction to Bacterial Infection

3. Infection

Implant infection poses a growing challenge in the field of orthopaedics. Despite progress in biomaterials, a considerable proportion of each type of implant is colonized by bacteria, potentially leading to implant-related infections. *Staphylococci* are the primary cause of these infections, accounting for approximately four out of five cases, especially two single *staphylococcal* species, respectively, *Staphylococcus aureus (S. aureus)* and *Staphylococcus epidermidis (S. epidermidis)* are the most common microorganisms that are involved. *S. aureus* is a widespread pathogen in wound infections **(Li et al. 2023)**. In contrast, *S. epidermidis* and coagulase-negative staphylococci are considered commensals of the human skin and mucous membranes. The pathophysiological mechanisms of both the *S. epidermidis* and *coagulase-negative staphylococci* (*CNS*) orthopaedic implant infection are the direct inoculation of skin colonizing at the time of surgery. Moreover, depending on the type of implant and location, distinct pathogens, together with, enterococci, streptococci, *Propionibacterium acnes*, and yeast, might also be the cause of biomaterial-related infection (BAI) **(Montanaro et al. 2011).**

3.1 Orthopaedic Implant-Associated Infection (IAI)

Even though the number of periprosthetic joint infections (PJI) is low, it dramatically increases the patient's health complications, such as septicaemia, and active cutaneous or deep tissue infections. It was very difficult to eliminate, resulting in a serious complication with a notable patient and economic burden. The present literature study suggests that the risk of secondary infection after PJI-induced re-evaluation surgery is 8% for hips as well as knees **(Borgström et al. 2020)**. Fracture-related infection (FRI) is caused by the severity of the trauma and is associated with damaged tissue. In open fractures, the incidence of FRI is up to 31% with consistent antibiotic treatment, but it can be reduced to 9% with secondary local antibiotics. Consequently, chronic orthopaedic implant-associated Infection (IAI) or bacterial biofilm-associated infection (BAI)-related bone infections have serious implications in current and future healthcare systems. The major pathogens sensible for IAI are shown in Table 3**.**1 Infections associated with orthopaedic implants can also be caused by different types of microorganisms, including aerobic Gram-negative bacteria such as *Escherichia coli* and *Pseudomonas aeruginosa*, and anaerobic bacteria like *Propionibacterium acnes*. The severity of the infection depends on the type and location of the implant, as well as the timing of the surgery.

Table 3.1 Major implant-infecting bacteria causing orthopaedic infections. Data from a European (EU) reference clinical setting, B- before the implant, A- After the implant. Modified from (Arciola, Campoccia, and Montanaro 2018).

Species	*Prevalence in medical device infection (%)*	*Prevalence in knee arthroplasty infection (%)*	*Prevalence in hip arthroplasty infection (%)*
Coagulase-negative staphylococci	*39.3%*	*37.0 %*	*40.7%*
Staphylococcus aureus	*B – 31.7%*	*21.1%*	*22.2%*
	A – 31.0%	*29.6%*	*32.6%*
Staphylococcus epidermidis	*39.5%*	*52.6%*	*48.1%*
Pseudomonas aeruginosa	*6.1%*	*10.5%*	*3.7%*
Escherichia coli	*2.4%*	*5.3%*	*0.0%*

Early infections can be caused by harmful microorganisms such as *S. aureus,* while delayed infections are often caused by less harmful microorganisms, such as CNS and *Propionibacterium acnes*. Late hematogenous infections can come from bacteria migrating from other infections inside the pores and skin, respiratory, dental, and urinary tracts. *Staphylococci* are the most common pathogens causing orthopaedic implant infections, and their occurrence varies amongst one-of-a-kind geographic areas. Biofilms are responsible for the persistence of implant infections due to their drug resistance (e.g., administration of antibiotics), thus requiring device surgical removal and leading to severe complications for patients. Moreover, antibiotic prophylaxis is a routine procedure in orthopaedic surgeries to reduce infection rates, but systemic or local administration of antibiotics may cause severe complications in other organs like the kidney and liver. More importantly, the rapid development and spread of antibiotic resistance in microbes as a result of the excessive use of antibiotics has become a major concern and has made it difficult to treat implant-associated infections. Additionally, excessive antibiotic use can lead to the speedy development and spread of antibiotic resistance in microbes, which has turned out to be a large concern in treating implant-related infections. Biofilms are groups of microorganisms that adhere to surfaces and are often associated with pathogens. Cell colonies consist of colonies or individual bacterial cells, surrounded by an ECM containing polymerases, extracellular DNA (eDNA), and proteins. Antimicrobial activity in biofilms is a particular challenge for researchers due to its association with biofilm formation. Various forms of antimicrobial resistance in biofilms are due to 1) slow penetration of antibiotics into the biofilm; 2) changes in the chemical environment of the biofilm, resulting in limited growth areas; 3) adaptive stress response; and 4) the presence of a small number of tolerant 'persistent' cells **(Martijn Riool and Sebastian 2022).**

Staphylococci are the most usual pathogens causing orthopaedic implant infections. Bacterial infections occur due to bacteria adhering to the implant surface, forming biofilm at the implantation site. These bacterial communities can cause chronic infections and are resistant to antibiotics, making them difficult to eliminate. In severe cases, the device may need to be surgically removed. While antibiotic prophylaxis is common in orthopaedic surgeries to reduce contamination, Systemic or nearby administration of antibiotics can cause excessive complications in different organs, like the kidney and liver. Additionally, excessive antibiotic use can lead to the speedy development and spread of antibiotic resistance in microbes, which has turned out to be a large concern in treating implant-related infections.

3.2 Biofilm Infections Formation During Surgery

Most of the researcher's studies in various bacteria species, such as *Pseudomonas aeruginosa, Pseudomonas fluorescens, Pseudomonas putida, Vibrio cholera, Yersinia pestis, Escherichia coli, Salmonella enterica, Burkholderia cenocepacia, Bacillus subtilis, and Clostridium difficile*, show that the level of intracellular second messenger c-di-GMP triggers the initiation of biofilm formation. Assessment methods primarily centred on genetic and microscopic techniques have established the foundation for today's models of bacterial biofilm development **(Sauer et al. 2022)**. This work has enabled researchers to define biofilm formation as a process that consists of specific stages as follows, as shown in Figure 3.1.

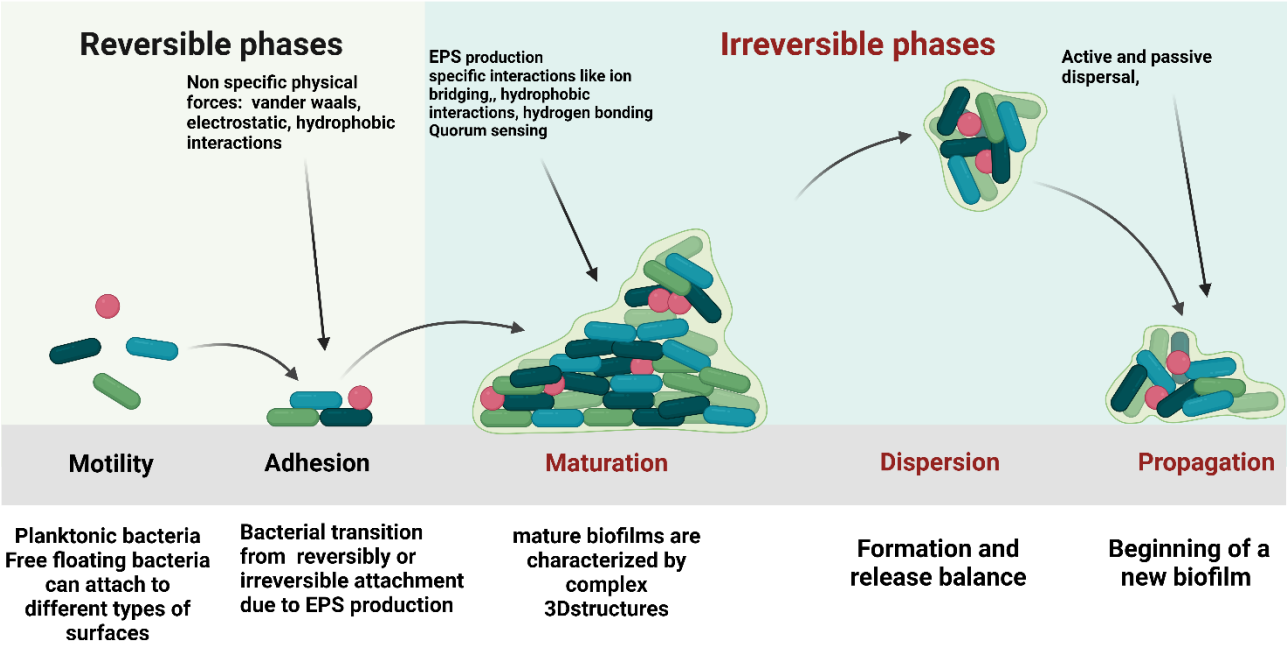

Figure 3.1: A schematic representation of bacterial biofilm formation on a surface. Modified from (Sauer et al. 2022) and created with BioRender.com.

3.2.1 Biofilm Attachment

Initial adhesion, also known as the reversible stage of biofilm formation, Biofilm formation starts when individual microorganisms in planktonic form adhere to surfaces. This step is essential for converting the floating microorganisms into an organized community (biofilm). The process of bacteria adhering to a surface is complicated and can be affected by different factors, including the duration of the bacterial exposure to the surface, the characteristics of the bacteria (including cell wall components, appendages, and motility), the availability of nutrients, and the concentration of bacteria. Bacteria promote adhesion by producing extracellular polysaccharides (EPS), metabolic activity, cell viability, charge, hydrophobicity, cell wall stiffness, and receptor-ligand binding mediated by adhesins, which are protein complexes that recognize and bind to the protein receptors on the host cell surface, and attachment with pili **(Limoli, Jones, and Wozniak 2015)**. Adhesion is the bond between cells, whereas cohesion is the attachment of cells to a substrate. The physical-chemical parameters of the substrate, which include surface charge, surface free energy, hydrophobicity, roughness, specific surface geometry (macro, micro, and nano), topography, and chemistry, also regulate the adhesion and initial formation of biofilm **(Donlan. 2002).** Irreversible attachment is where an increasing number of bacteria attach irreversibly and multiply, forming biofilms with complex structures and diverse bacterial species. Microcolonies, the biofilm precursor, is then formed and mature into matured microcolony biofilms. Encapsulated bacteria produce large amounts of EPS during the formation of microcolonies, which supports inner microbes and protects them from antibacterial molecules. EPS components differ between bacterial species or even strains of the same species, but they all contain polysaccharides, proteins, and eDNAs **(Mayton, Walker, and Berger 2021)**.

3.2.2 Biofilm Maturation

Complex Structure Development is a stage divided into maturation stages 1 and 2. The maturation stage (stage 1) of biofilm formation marks a significant phase in the growth of these intricate microbial colonies. This process is initiated by particular chemical signals within the EPS and micro-communities. In a biofilm, there are usually several different micro-communities present within bacterial colonies, which results in spatial variations in the number of nutrients available, the amount of oxygen present, and other elements. A structural framework that holds the biofilm together is provided by the ECM, which is made up of EPS. During stage 2 of biofilm maturation, quorum sensing, and microbial communication are both important. Microbial cells produce and detect signalling molecules as cell densities rise, which causes coordinated behaviour and changes in gene expression. The community of biofilms can react to environmental changes as a single unit thanks to this collective communication. The ECM and complex structure of the biofilm increase its resistance to immune responses and antimicrobial agents. The specialized roles of various microbial populations within the biofilm are the cause of this resistance. While some microorganisms may concentrate on nutrient uptake,

others may contribute to the breakdown of the matrix or the resilience of the biofilm **(Panlilio and Rice. 2021)**.

3.2.3 Dispersal of Biofilm

This is the last stage, which is characterized by the dispersal and colonization of newer sites by mature colonies and the propagation of disease: The dispersal stage of biofilm formation involves the detachment and release of cells from the established biofilm structure. During dispersal, cells within the biofilm initiate physiological changes that lead to reduced adhesion to the surface. They produce enzymes and molecules that weaken the extracellular matrix, facilitating detachment. Once detached, these cells are released into the surrounding environment. In this free-floating state, they can disperse and colonize new surfaces **(Kaplan. 2010)** forming new biofilm communities in different places. Therefore, microorganisms that form biofilms can explore and utilize new niches, enhancing their likelihood of surviving in evolving surroundings. The dispersal phase is crucial in the biofilm's lifecycle. By enabling microorganisms to spread and establish themselves elsewhere, it contributes to microbial diversity, adaptation, and the ongoing impact of biofilms in various environments.

3.3 References

Arciola, Carla Renata, Davide Campoccia, and Lucio Montanaro. 2018. “Implant Infections: Adhesion, Biofilm Formation and Immune Evasion.” Nature Reviews Microbiology 16 (7): 397–409. https://doi.org/10.1038/s41579-018-0019-y.

Borgström, Fredrik, Linda Karlsson, Gustav Ortsäter, Nicolas Norton, Philippe Halbout, Cyrus Cooper, Mattias Lorentzon, et al. 2020a. “Fragility Fractures in Europe: Burden, Management and Opportunities.” Archives of Osteoporosis 15 (1). https://doi.org/10.1007/s11657-020-0706-y.

Donlan, Rodney M. 2002. “Biofilms: Microbial Life on Surfaces.” Emerging Infectious Diseases 8 (9): 881–90. https://doi.org/10.3201/eid0809.020063.

Kaplan, J.B. 2010. “Biofilm Dispersal: Mechanisms, Clinical Implications, and Potential Therapeutic Uses.” Journal of Dental Research 89 (3): 205–18. https://doi.org/10.1177/0022034509359403.

Li, Panxin, Rui Yin, Jimin Cheng, and Jie Lin. 2023. “Bacterial Biofilm Formation on Biomaterials and Approaches to Its Treatment and Prevention.” International Journal of Molecular Sciences 24 (14): 11680–80. https://doi.org/10.3390/ijms241411680.

Limoli, Dominique H., Christopher J. Jones, and Daniel J. Wozniak. 2015. “Bacterial Extracellular Polysaccharides in Biofilm Formation and Function.” Microbiology Spectrum 3 (3). https://doi.org/10.1128/microbiolspec.mb-0011-2014.

Martijn Riool, and Sebastian. 2022. “Biomaterial-Associated Infection: Pathogenesis and Prevention.” Springer EBooks, January, 245–57. https://doi.org/10.1007/978-3-031-04484-7_20.

Mayton, Holly, Sharon L Walker, and Bryan W Berger. 2021. “Disrupting Irreversible Bacterial Adhesion and Biofilm Formation with an Engineered Enzyme.” Applied and Environmental Microbiology 87 (13). https://doi.org/10.1128/aem.00265-21.

Montanaro, Lucio, Pietro Speziale, Davide Campoccia, Stefano Ravaioli, Ilaria Cangini, Giampiero Pietrocola, Sandro Giannini, and Carla Renata Arciola. 2011. “Scenery of Staphylococcus Implant Infections in Orthopedics.” Future Microbiology 6 (11): 1329–49. https://doi.org/10.2217/fmb.11.117.

Panlilio, Hannah, and Charles V. Rice. 2021. “The Role of Extracellular DNA in the Formation, Architecture, Stability, and Treatment of Bacterial Biofilms.” Biotechnology and Bioengineering 118 (6): 2129–41. https://doi.org/10.1002/bit.27760.

Sauer, Karin, Paul Stoodley, Darla M. Goeres, Luanne Hall-Stoodley, Mette Burmølle, Philip S. Stewart, and Thomas Bjarnsholt. 2022. “The Biofilm Life Cycle: Expanding the Conceptual Model of Biofilm Formation.” Nature Reviews Microbiology 20 (10): 608–20. https://doi.org/10.1038/s41579-022-00767-0.

Chapter V

Surface Functionalization with the Synthetic Peptoid as a Strategy for Antibacterial and Biocompatible Titanium Implants

Aim

Peptoids have emerged as potent antimicrobial agents, demonstrating remarkable efficacy against a wide range of bacterial strains, including multi-drug resistant pathogens such as *S. aureus*. These synthetic compounds, designed to mimic the structure and function of antimicrobial peptides, exhibit high stability and selectivity, making them promising alternatives to traditional antibiotics. Peptoids have been shown to disrupt bacterial membranes, inhibit essential cellular processes, and effectively reduce bacterial growth without significant cytotoxic effects on mammalian cells. Their ability to target and kill bacteria through various mechanisms, such as membrane disruption and interference with intracellular processes, highlights their potential as strong antibacterial agents. Studies have emphasized the broad-spectrum activity of peptoids, their low hemolytic properties, and their capacity to inhibit biofilm formation, positioning them as valuable candidates for combating bacterial infections and addressing the challenges of antibiotic resistance.

Chapter V has been published as a 'research article' in Heliyon with several authors as a collaborator: Gamna, Francesca, Andrea Cochis, Biljana Mojsoska, Ajay Kumar, Lia Rimondini, and Silvia Spriano. 2024. "Nano-Topography and Functionalization with the Synthetic Peptoid GN2-Npm_9 as a Strategy for Antibacterial and Biocompatible Titanium Implants." (https://doi.org/10.1016/j.heliyon.2024.e24246). In this paper, the contribution of the author is as follows

Biljana Mojsoska: Synthesized the peptoid GN2-Npm_9 and verified the mass and purity.

Francesca Gamna and Silvia Spriano: Functionalized the GN2-Npm_9 peptoid onto the titanium surface, along with the physical and chemical characterization.

Ajay kumar: Performed the biological characterization of the samples in terms of cytocompatibility, antibacterial activity and co-culture studies.

Peptoid Synthesis and Surface Functionalization

GN2-Npm_9 was synthesized using solid-phase Fmoc chemistry with amidation at the carboxyl end (MHBA resin-loading capacity 0,65 mmol/g). Then the surface modifications with titanium alloy Ti6Al4V were chemically pre-treated (CT) and a solution of PBS containing 1 mg/mL GN2-Npm_9 was functionalized onto a titanium surface Samples were provided by the Politecnico di Torino in collaboration with Roskilde University, Denmark.

Abstract

In recent years, antimicrobial peptides (AMPs) have attracted great interest in scientific research, especially for biomedical applications such as drug delivery and orthopaedic applications. Since they are readily degradable in the physiological environment, scientific research has recently been trying to make AMPs more stable. Peptoids are synthetic N-substituted glycine oligomers that mimic the structure of peptides. They have a structure that does not allow proteolytic degradation, which makes them more stable while maintaining microbial activity. This structure also brings many advantages to the molecule, such as greater diversity and specificity, making it more suitable for biological applications. For the first time, a synthesized peptoids (GN2-Npm_9) was used to functionalize a nanometric chemically pre-treated (CT) titanium surface for bone-contact implant applications. A preliminary characterization of the functionalized surfaces was performed using contact angle measurements and zeta potential titration curves. These preliminary analyses confirmed the presence of the peptoid and its adsorption on CT. The functionalized surface had a hydrophilic behaviour (contact angle = 30°), but the hydrophobic tryptophan-like residues were also exposed. An electrostatic interaction between the lysine residue of GN2-Npm_9 and the surface allowed a chemisorption mechanism. The biological characterization of the CT_GN2-Nmp_9 surfaces demonstrated the ability to prevent surface colonization and biofilm formation by the pathogens *Escherichia coli* and *Staphylococcus epidermidis* thus showing a broad-range activity. Cytocompatibility was confirmed by human mesenchymal stem cells. Finally, a bacteria-cells co-culture model was applied to demonstrate the selective bioactivity of the CT_GN2-Nmp_9 surface that was able to preserve colonizing cells adhered to the device surface from bacterial infection.

Introduction

Antimicrobial peptides (AMPs) have become increasingly important in biomedical applications due to their different and multiple abilities. However, AMPs are not without limitations, particularly concerning their stability. One of the major limitations of peptides in biomedical applications is proteolytic degradation. peptides can be rapidly degraded by proteases in the body, which can result in a short half-life and reduced bioavailability **(Böttger, Hoffmann, and Knappe 2017).** Other limitations regard chemical reactions, such as oxidation, hydrolysis, and racemization which can affect the AMPs' stability and functionality **(Zapadka et al. 2017)**. Moreover, they often have greater problems of solubility in water or biological fluids, which can limit their bioavailability and efficacy **(Adessi and Soto 2002)**. Additionally, peptides can be sensitive to temperature changes, which can affect their stability and functionality **(Pucci, Bourgeas, and Rooman 2016)**. Another limitation of peptides in biomedical applications is their potential for immunogenicity. They can be recognized as foreign bodies by the immune system, leading to an immune response that can limit their effectiveness and cause adverse reactions **(Zapadka et al. 2017)**.

To overcome these limitations, efforts are being made to develop new strategies focused on the improvement of peptides stability. For these reasons, peptoids have been introduced as an alternative to peptides. Peptides and peptoids are two classes of molecules that are similar in structure but differ in several key features. Peptides are short chains of amino acids that are linked together by peptide bonds. Peptoids, on the other hand, are synthetic molecules that resemble peptides but have their side chains (R) attached to the nitrogen atoms instead of the alpha-carbon atoms. This difference in structure gives peptoids several advantages over peptides, including increased stability, diversity, and specificity. Peptoids are more stable than peptides because the side chains are not susceptible to cleavage by protease or acid hydrolysis, they are more bioavailable and have more stability to ionic strength and pH variations **(Saini and Verma 2017).** These properties make peptoids more suitable for use in biological applications that require long-term stability, such as drug development. Moreover, peptoids are highly flexible in composition and can be synthesized with a wide range of side chains. This diversity allows for the creation of large libraries of peptoids that can be screened for specific biological activities. Peptoids have a high degree of specificity due to their unique structure **(Sun and Zuckermann 2013) (T. Dohm, Kapoor, and E. Barron 2011)**. Currently, the synthesis of peptoids is complex and time-consuming but strategies for controlling the processes' efficiency and scale are proceeding quickly **(Abigail Mae Clapperton, Babi, and Tran 2022)**.

Among the various materials for implants, titanium and its alloys are frequently used, mostly in dental and orthopaedic implants, for their high osseointegration ability and biocompatibility. Because titanium is an example of bioinert material, scientific research has focused on topographic and surface modification as a means of making the implant bioactive, stimulating and accelerating the osseointegration process. The titanium alloys can become bioactive with proper chemical etchings and, in this way, the precipitation of the mineral component of the bone (hydroxyapatite) occurs on the surface from the physiological fluids **(Kim et al. 1996).** Physic-chemical properties of an implant surface such as topography, wettability, roughness, and surface potential regulate the protein adsorption and cell adhesion **(Hasan and Pandey 2020).** In particular, the topographical texture of implant surfaces has an important role in tissue response. Surface topography is fundamental for the adhesion and differentiation of osteoblasts in the initial stage of osseointegration. This is why micro, and nano-scale rough surfaces have greater surface area for tissue integration than smooth surfaces and increase the number and strength of focal adhesions (bone on-growth). Nanoscale roughness with size in the magnitude of protein and cell membrane receptors dimensions could also act in cell adhesion, proliferation, and spreading **(Vootla and Reddy 2017).**

AMPs are often conjugated with metal biomaterials, particularly titanium, to impart antibacterial properties to implant surfaces. Functionalization of AMPs on titanium surfaces can be achieved through various methods, such as covalent bonding **(Costa et al. 2015) (Holmberg et al. 2013)**, or physical adsorption **(Mehdi Kazemzadeh-Narbat et al. 2012) (Yoshinari et al. 2010).** Once the AMPs are functionalized on the titanium

surface, they can provide a potent antimicrobial barrier against bacterial infections. Despite the rich literature on AMPs functionalized on titanium, there are still no cases where peptoids are used for surface functionalization. The feasibility and advantages of the functionalization of titanium surfaces with peptoids are still to be proven.

In this chapter, a peptoid (GN2-Npm_9 – as shown in Figure 4.1), rich in lysine and tryptophan-like residues, was synthesized using a Solid Phase Synthesis protocol (SPS). Preliminary studies reported the ability of this peptoid to inhibit the growth of *E. coli,* by disrupting its membrane integrity **(Saporito et al. 2019) (Khara et al. 2020)**. So, here the peptoids antibacterial efficacy has been exploited to prevent the infection of implantable titanium as a potential alternative to common strategies. In addition, GN2-Npm_9 was carefully chosen as a good candidate for its low cytotoxicity. (IC50 104 µg/mL) compared with other synthesized peptoids **(Mojsoska, Zuckermann, and Jenssen 2015).** For these reasons, GN2-Npm_9 here it was used to functionalize a chemically pre-treated Ti6Al4V surface for permanent implant application.

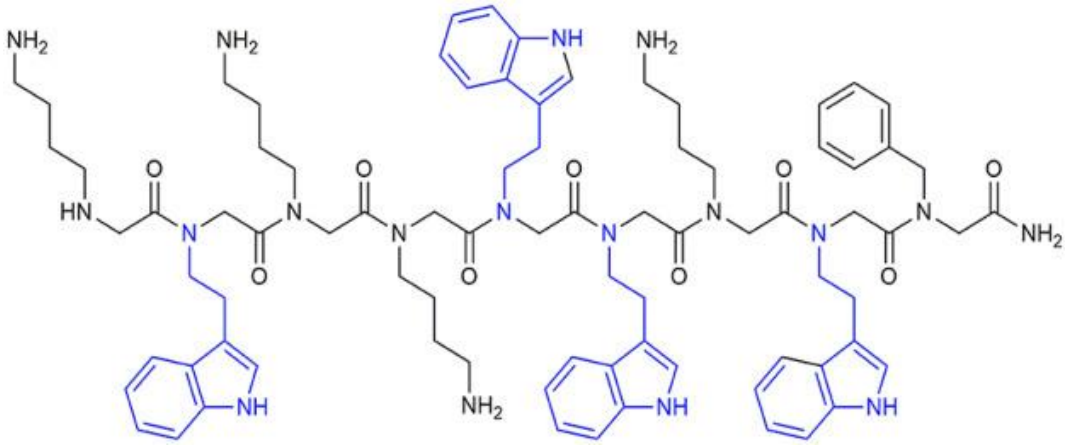

Figure 4.1: The chemical structure of GN2-Npm_9 peptoid. The figure is modified from (Lone et al. 2020). Re-acquired permission from Elsevier.

4.1 Materials and Methods

4.1.1 Peptoid Synthesis

GN2-Npm_9 was synthesized using solid-phase Fmoc chemistry with amidation at the carboxyl end (MHBA resin-loading capacity 0,65 mmol/g) and purified by reversed-phase HPLC using a C18 column (Higgins Analytical Inc. 10 µm 250 × 10 mm) and a water/acetonitrile gradient. The correct mass and purity >95 % were verified by Dionex Ultimate 3000 RP-UHPLC (C18 Kinetex 100 × 2.1 mm, 100 Å) electrospray ionization mass spectrometry (Finnigan LTQ).

4.1.2 Surface Pre-treatment

The substrate chosen for the surface modifications is titanium alloy Ti6Al4V (ASTM B348, Gr5, Titanium Consulting and Trading, 10 mm diameter discs). All discs were polished with SiC paper (up to 400 grit). To clean the surface, the samples were first immersed in acetone for 5 min and then twice for 10 min in high-purity Milli-Q (MQ, Millipore) water in an ultrasonic bath. The samples were subjected to a patented chemical treatment **(Yukari Iwaya et al. 2008)** involving initial acid etching in dilute hydrofluoric acid followed by controlled reoxidation with hydrogen peroxide. Before functionalization, the treated samples were irradiated with UV light for 1 h to reduce the water content and carbon impurity and to improve the reactivity of the hydroxyl groups. From now on, the samples treated as described above will be referred to as chemically pre-treated (CT), while the samples polished to a grain size of 4000, which served as a control, will be referred to as mirror polished (Ti64).

4.1.3 Surface Functionalization

A solution of PBS and 1 mg/mL GN2.Npm_9 was previously prepared by stirring the molecule in PBS for 5 min and then filtering through a 0.2 µm filter to leach out bacterial contamination. With the solution prepared, the CT samples were withdrawn from UV irradiation and placed on a Petri dish. A 100 µl drop of the solution was dropped onto the sample so that the entire surface of the sample was covered, taking care not to break the drop. The samples were left in an incubator at 37°C for 2 h. The samples were then rinsed in double distilled water to remove the non-adherent peptoids on the surface and dried under a hood. The functionalized samples were denoted as CT_GN2-Npm_9. Control samples (CT_PBS) were prepared with the same procedure, without adding the molecule (GN2-Npm_9) in PBS.

4.1.4 Zeta Potential Measurements on a Solid Sample

The zeta potential titration curves were measured by an electrokinetic analyzer (SurPASS, Anton Paar GmbH, Graz, Austria) for both functionalized and non-functionalized samples and control samples (CT_GN2-Npm_9, CT, and CT_PBS). The zeta potential was determined as a function of pH in an electrolyte solution of 0.001 M

KCl, and the pH value (which starts at approximately 5.5) was varied by adding 0.05 M HCl or 0.05 M NaOH using the automatic titration unit of the instrument. The isoelectric point (IEP) was established as the intercept of the titration curve with the x-axis (zeta potential = 0 mV). Two different sets of samples were used for each basic and acid curve. The expected IEP values of the monomers were calculated by using BACHEM software for peptide calculation (https://www.bachem.com/knowledge-center/peptide-calculator/2).

4.1.5 Contact Angle Measurements

Surface wettability was assessed by measuring the contact angle with the sessile drop method. After depositing a 10 µl drop of water on the treated side of the sample, the contact angle was measured through Image J software after acquiring images with a microscope (Kruss DSA 100). The contact angle was measured on CT, CT_GN2-Npm_9, and CT_PBS.

4.1.6 Zeta Potential Measurement on a Liquid Sample

The Zeta potential of an aqueous solution with the peptoids at a concentration of 1 mg/mL was measured with the Litesizer 500 particle analyzer (Anton Paar), using Smoluchowski as an approximation formula, and a debye factor of 1.5. Titration was done manually adjusting the pH with NaOH 0.005 M and HCl 0.005 M.

4.1.7 Cytocompatibility Evaluation

Samples were sterilized by UV-light exposure (30 minutes) before biological experiments. Sample names are shown in Table 4.1.

Table 4.1: Represent the samples' names and coatings.

No	Samples' names	Coating
1	**Ti64 (Mirror polished)**	**No coating (Control)**
2	**CT**	**Chemical treatment (CT)**
3	**CT_ GN2-Npm_9**	**GN2 _Npm_9 (peptoids)**

To test samples' cytocompatibility, human bone marrow-derived stem cells (hMSCs) were obtained from Merck (Promo Cell C-12974) and cultivated in low-glucose Dulbecco's modified Eagle Medium (DMEM, Merck) supplemented with 15% fetal bovine serum (FBS, Merck) and 1% antibiotics (penicillin/streptomycin, Merck) at 37°C, 5% CO_2 atmosphere. Cells were cultivated until 80-90% confluence, detached by a trypsin-EDTA solution (0.25% in PBS, from Merck), harvested, and used for the experiments.

Cells were directly dropwise seeded onto the samples' surface at a defined concentration (2.5 $x10^4$ cells/samples) and cultivated for 1 and 2 days; at each time-point, the viability of the cells has been deduced

in the function of their metabolic activity by the colourimetric assay Alamar blue (alamarBlue™, ready-to-use solution from Invitrogen™) following Manufacturer's instructions: accordingly, fluorescence signals were evaluated with a spectrophotometer (Spark®, Tecan Trading AG, CH) using excitation wavelength 570 nm, fluorescence emission reading 590 nm. Results are expressed in relative fluorescence units (RFU). Untreated mirror-polished Ti samples were considered as a positive control (100% viability).

To verify cells' spread and confluence onto samples' surface, on day 2 samples were washed with PBS, fixed with 4% paraformaldehyde (20 min, room temperature), permeabilized for 20 minutes with Triton (0.5% in PBS), and then stained with Texas Red™-X Phalloidin (Thermo Scientific; Invitrogen: T7471) and 4,6-diamidino-2-phenylindole (DAPI, Sigma, Aldrich) to visualize f-actins cytoskeleton filaments and nuclei, respectively. Images were collected by a confocal microscope (Leica SP8 confocal platform, Leica Microsystems, Germany). Finally, to better appreciate the adaptation of cells to the surfaces' morphology, scanning electron microscopy (SEM) was applied; accordingly, cells were fixed with 2.5% glutaraldehyde, dehydrated by the alcohol scale (50%, 70%, 90%, and 100%, 2 h each) and finally treated with hexamethyldisilazane (from Alfa Aesar, Waltham, MA, USA). Then, samples were mounted onto aluminum stubs, surface metalized by gold, and observed with an SEM-EDS JEOL JSM-IT 500.

4.1.8 Antibacterial Properties

Samples' ability to prevent surface bacterial infection was verified towards the Gram-positive *S. epidermidis* and the *Gram-negative E. coli* pathogens. Strains were obtained from the American Type Culture Collection (*S. epidermidis* ATCC 14990, *E. coli* ATCC 25922) and cultivated following the manufacturer's instructions. Fresh broth cultures were prepared before each experiment to test bacteria in their exponential growth phase; the final number of bacteria was adjusted to $1x10^5$ bacteria/mL by optical density (0.001 at 600 nm).

Samples' infection was performed according to the ISO 22196 standard; so, an aliquot of 100 µl of the above-mentioned bacterial suspensions was gently seeded onto the samples' surface, covered with a sterile polyethylene film, and placed in an incubator at 35°C for 24 h. Then, the cover film was gently removed, samples were washed 3 times with PBS to remove non-adherent bacteria, and Alamar blue was applied to determine bacterial viability in the function of the metabolic activity as previously detailed. Moreover, SEM imaging was applied to check the formation of biofilm-like 3D aggregates in the function of the surfaces' properties.

4.1.9 Selectively Targeted Activity

A cell-bacteria co-culture assay evaluated samples' ability to preserve cells from infection as previously reported by (**Cochis et al. 2020)**. Briefly, $2.5×10^4$ cells/sample of hBMSC were seeded onto the samples' surface and allowed to adhere and spread for 24 hours. The day after, samples were infected with 1 mL of antibiotics-free DMEM containing $1×10^3$ *S. epidermidis*. After 48 h of infection, samples were collected, and

surface-adhered cells and bacteria were detached by trypsin digestion; viable cells were counted by a Bürker chamber and trypan blue stain to determine the viable number, while bacteria were evaluated by the colonies forming unit (CFU) by seeding them into Luria Bertani semi-solid agar plates after serial dilutions. The final number of CFU was calculated according to **(Harrison et al. 2010)**. the following formula:

CFU = [(number of colonies × dilution factor) ^ (serial dilution)].

4.1.10 Statistical Data Analysis

Biological evaluations were performed using technical triplicates. Results were analyzed by using SPSS software (v25, IBM, New York City, NY, USA) and one-way ANOVA followed by Tukey's test as post hoc analysis. The significance level was set at $p < 0.05$.

4.2 Results and Discussions

The characterization of CT is already reported in previous works **(Ferraris et al. 2015) (Ferraris et al. 2011)**. The focus of this paper was on CT_GN2-Npm9, and data about CT as a control sample are here reported when needed.

4.2.1 Zeta Potential Measurements

Figure 4.2 displays the titration curves of the CT, CT_PBS, functionalized samples (CT, CT_GN2-Npm_9), and the solution of GN2-Npm_9. At a glance, the curve of CT_GN2-Npm_9 appears considerably different from that of control samples (CT and CT_PBS), confirming the effectiveness of the functionalization process. This is the first key information from this measurement.

CT and CT_PBS have the same titration curves, suggesting that the immersion of CT in PBS did not change its surface chemistry. The CT curve had an IEP at a very low pH (≈3), a low slope in the acid range of the titration with a change of the slope at pH 4, and a stable plateau (at around −45 mV) in the basic range, with an onset at pH 5.5. These features were due to the CT surface's chemistry **(Popat Mohite et al. 2023).** The CT sample, after undergoing the chemical pre-treatment, acquired a hydrophilic surface with a titanium oxide layer and a high density of OH groups. The hydroxyl groups were exposed and exhibited highly acidic behaviour, being deprotonated at pH as low as 3–5.5. An IEP at around 4 is expected for a surface without acidic/basic functional groups or a balance of them, while a shift towards lower values is expected in the presence of acidic functional groups. The prevalence of the negatively charged OH functional groups on the surface induced the low IEP of CT and a negative charge of the surface for all pH ranges, even at physiological pH. This feature makes CT a bioactive material. CT surface attracts Ca^{2+} ions from the physiological fluids and induces the *in vivo* precipitation of hydroxylapatite (bioactivity) **(Ferraris et al. 2015) (Ferraris et al. 2019).** Water

molecules adhered firmly to the hydrophilic CT surface and were not easily replaced by ions in the solution as the pH changed. This was the origin of the low slope of the curve in the acidic range of the titration. A plateau resulted from OH groups being completely deprotonated at pH values higher than 5.5.

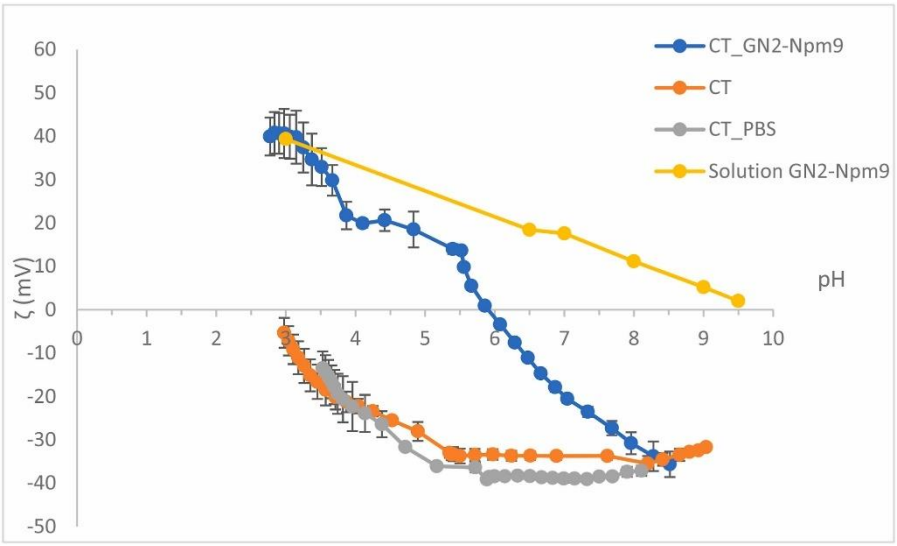

Figure 4.2: potential titration curve of CT, CT_PBS, CT_GN2Npm$_9$ and GN2-Npm$_9$ solution.

The zeta potential titration curve of a solution of the peptoids GN2-Npm$_9$ (Figure 4.2) shows an isoelectric point around 9.5 and a positive zeta potential in all the explored ranges of pH. This curve can be explained by considering its chemical structure. Lysine has an IEP of 9.7, the pKa of the alpha carboxylic group is 2.2, that of the ammonium group is 8.9, and that of the side chain is 10.5 **(Clemens Žváček et al. 2015)**. Tryptophan has an IEP of 5.9, the pKa of the alpha carboxylic group is 2.5, and that of the ammonium group is 9.4. It has a polar and hydrophobic side chain. The here used tryptophan-like residue is expected to be similar. The IEP of the dipeptide and polypeptides lysine-tryptophan was expected to be around pH 10 because carboxylic groups were engaged into the peptide bond, by adding more units, and were not available for deprotonation, while the number of the basic side chain of lysine were available for protonation. The titration curve was not expected to change by changing the sequence of the monomers inside the chain.

The IEP of the functionalized surface CT_ GN2-Npm$_9$ shifted towards more basic values vs CT, reaching a pH around 6, which confirmed the presence of the adsorbed peptoids on the CT substrate but without a complete coverage of the surface because the IEP of GN2-Npm$_9$ was not reached. The shape of the curve of CT_GN-Npm$_9$ can be explained as due both to the functionalities of CT and GN2-Npm$_9$. The positive zeta potential at pH 3–4 was likely due to the exposure of the positive surface charges (amine groups) of the peptoids. A plateau of the zeta potential was observed around pH 4–5.5 because of the deprotonation of the OH groups of CT not covered by the peptoids. Then, the high slope of the curve at pH 5.5–9 was due to the polar and hydrophobic side chain of the tryptophan-like residue. It could be assumed that the hydrophilic

residues of GN2-Npm_9 (lysine) were attracted by the substrate surface and were facing it, while the hydrophobic ones (tryptophan-like) were facing the solution.

At the pH value chosen for the functionalization process (pH = 7.4), the CT substrate had a negative surface charge with completely deprotonated –OH groups, whereas GN2-Npm_9 had an overall positive charge. Based on these conditions, an electrostatic attraction between the substrate and the peptoids, resulting in a chemisorption mechanism, could be predicted.

4.2.2 Contact Angle Measurement

Figure 4.3 illustrates the water contact angles measured on a surface-functionalized sample (CT_GN2-Npm_9), and two reference samples: CT and CT_PBS. A protocol analogous to CT_GN2-Npm_9 was used to prepare CT_PBS but without the addition of GN2-Npm_9 to the solution. The CT sample exhibited a contact angle of approximately 40°, as supported by the zeta potential curve and the expected high density of OH groups, making the surface more hydrophilic compared to the Ti64 samples' surface which exhibits a higher contact angle of approximately 65°. CT_PBS sample had a contact angle of approximately 5°. The exact origin of the high hydrophilicity of this control sample is not completely clear, but it lies outside the scope of this study. Comparing the CT_PBS and CT_GN2-Npm_9 samples, the presence of the adsorbed peptoids was confirmed by the different contact angles. Thus, it can be inferred that the CT_GN2-Npm_9 sample exhibited a hydrophilic behaviour but the exposure of GN2-Npm_9 (exposing hydrophobic moieties) significantly increased the contact angle vs CT_PBS, reaching values of approximately 25°, which was statistically different from both the controls ($p < 0.05$). Surface roughness can affect the wettability of a surface together with its chemistry. The measured roughness of CT (Ra = 0.25 µm) did not increase the real surface area **(Barberi et al. 2022)** and it is not expected to significantly affect wettability. Moreover, the zeta potential titration curve is not sensitive to roughness but shows an evident hydrophilic behaviour of CT. In conclusion, a major role of chemistry in the wettability of these samples' is expected. In the case of CT and GN2-Npm_9 From the perspective of an implant, surface wettability is important as it affects cell adhesion and well-being. It has been found that a surface suitable for cell adhesion is a hydrophilic surface with contact angles ranging from 30 °C to 65 °C and above 40 mN/m in terms of surface energy **(Wang et al. 2020) (Hollinger 2012).**

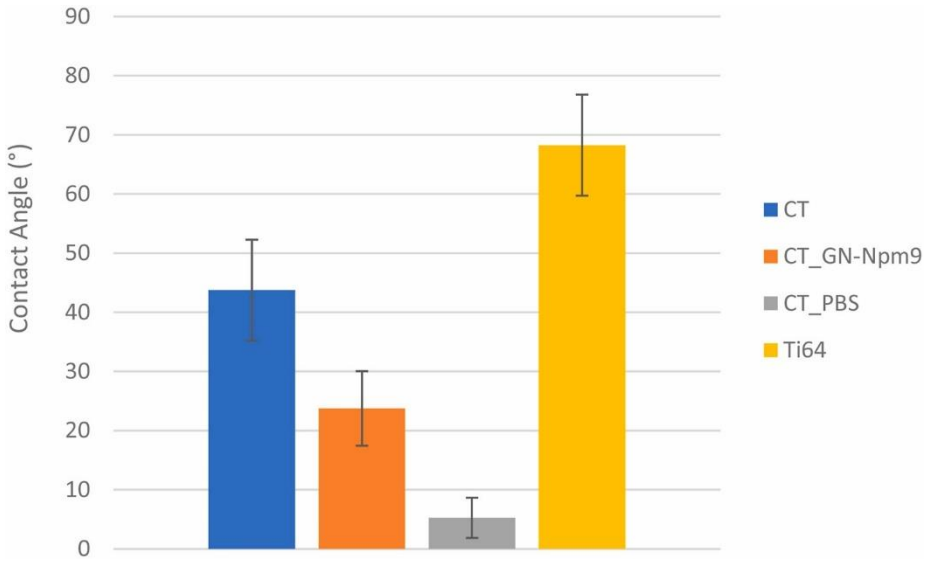

Figure 4.3: Contact angle of CT, CT_GN2-Npm$_9$, CT_PBS and Ti64.

4.2.3 Cytocompatibility Evaluation

Cytocompatibility evaluation was performed on mesenchymal stem cells as they represent a frequent and consolidated pattern to test in vitro the ability of an implantable device to support the recruitment and colonization from the progenitor cells migrating towards the injured site. The bulk titanium alloy (Ti64) has been considered a positive control due to the large literature, including clinical revisions, suggesting its biocompatibility and successful osteointegration after months upon implantation **(Popat Mohite et al. 2023) (Clemens Žváček et al. 2015)**. Accordingly, it has been considered as 100 % viability to rank the results coming from CT and CT_GN2-Npm$_9$ samples.

Results are reported in Figure 4.4. In general, the presence of the peptoid did not impair the ability of the hMSCs to colonize the samples' surface, thus being metabolically active at both 1 or 2 days after seeding as demonstrated by the Alamar blue assay (Figure 4.4a) where the reported RFU were not significantly reduced comparing CT and CT_GN2-Npm$_9$ with the Ti64 control ($p > 0.05$). So, the percentage of viable cells was always >90 % as reported in Figure 4.4b. As a confirmation of the presence of viable cells, SEM imaging (Figure 4.4c) showed that cells were able to adapt to the CT_GN2-Npm$_9$ surface similarly to the untreated Ti64 controls reporting a similar morphology despite the presence of the functionalized layer and the microtopography due to CT pre-treatment. Fluorescence staining of cells' cytoskeleton and nuclei (Figure 4.4d) provided further evidence of the cell-friendly behaviour of the test CT_GN2-Npm$_9$ surfaces. In particular, the density of the DAPI-stained nuclei demonstrated a comparable cellular confluence between the Ti64 control and CT_GN2-Npm$_9$ thus confirming the ability of the test samples to support the colonization of progenitor cells, albeit with all the limitations relating to an in vitro experiment.

In general, ranking our results in comparison to previous works is not easy due to the large variety of synthesized peptoids available in the current literature. However, some articles report on peptoids cytocompatibility and bioactivity toward mesenchymal stem cells. As an example (**Morton et al. 2023)** exploited unstructured, helical, and non-helical peptoids to tune the biomechanical properties of hydrogels to realize 3D cultures of stem cells that did not report any toxic effect after seeding and cultivating in direct contact **(Barberi et al. 2022)**. **(Statz et al. 2009)**. were able to correlate the length and the surface density of peptoids on titanium substrates with their antifouling activity towards fibroblasts. Results showed that cells' adhesion can be prevented by reducing pro-adhesion protein surface accumulation but toxic effects due to the peptoids coating were not reported **(Wang et al. 2020)**. Similarly, **(Zhao et al. 2022)** reported the use of peptoid-loaded microgels as a bioactive coating to prevent bacterial contamination of Ti substrates in a simulated surgery infection model reporting that such treatment was not toxic toward human progenitor fetal osteoblasts that were used as cells deputed to drive the implant colonization **(Hollinger 2011).** So, our results seem to be in line with previous literature suggesting the use of the GN2-Nmp_9 Peptoid as a cytocompatible tool to coat biomedical Ti substrates.

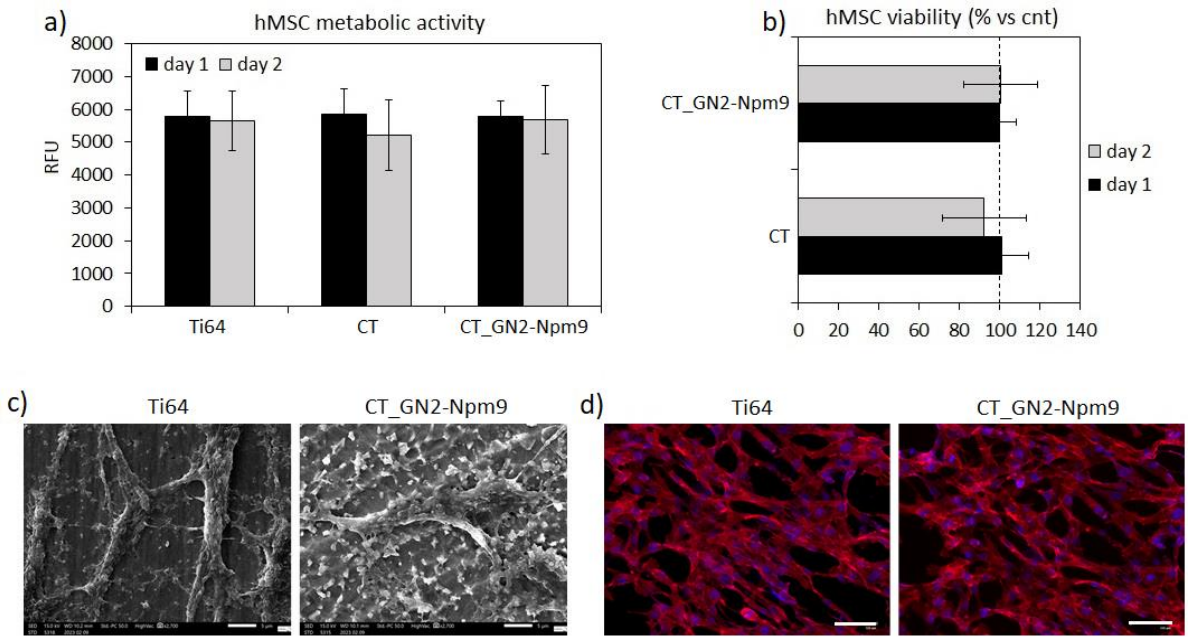

Figure 4.4: Cytocompatibility evaluation of CT, Ti64, and CT_GN2-Npm_9 (a) Cells seeded onto peptoid-doped surfaces (CT_GN2-Npm_9) reported a comparable metabolic activity in comparison to the Ti64 control and the CT ones ($p > 0.05$). (b) Accordingly, the viability ranged between 90 and 100 % in comparison with Ti64 controls. (c) SEM images confirmed the ability of cells to adapt onto the CT_GN2-Npm_9 surface as well as (d) fluorescent staining demonstrated a comparable cell density between test and control samples. Bars represent mean±sdev.st; replicates n = 3. SEM bar scale = 5 µm (2700x); fluorescence bar scale = 125 µm. Re-acquired permission from Elsevier.

4.2.4 Antibacterial Activity

Orthopaedic implant infection represents a huge clinical burden strongly reducing the patient's quality of life due to the frequent need to remove infected devices **(Cho et al. 2010)**. Therefore, there is an urgent need to develop new strategies conferring antibacterial properties to the materials aimed for implantation to prevent bacterial infections thus avoiding further surgeries.

In this direction, peptoids have been reported to represent an attractive tool as much proof about their antibacterial properties has been provided by the literature **(Froimson et al. 2007) (Morton et al. 2023)** So, here the GN2-Nmp_9 peptoid was exploited to coat the surface of the CT chemically pre-treated surfaces to combine the peptoids bioactivity and the nanostructured surface topography of the samples, considering that such peptoid was previously reported to efficiently determine *E. coli* death by membrane irreversible destruction (MIC = 16 μg/mL). **(Saporito et al. 2019a).**

Accordingly, samples were infected with *S. epidermidis* (Gram-negative) and *E. coli* (Gram-positive). These strains were selected because they are often involved in orthopaedic infections and to test the antibacterial efficacy of the peptoids against both the Gram species. The results are reported in Figure 4.5. In general, the CT nano-topography reduced the metabolic activity of both pathogens but only *E. coli* was significant in comparison with Ti64 controls (Figure 4.5a, c, $p < 0.05$ indicated by #). As previously shown by the authors, this effect is due to the needle-like nanostructures formed after the chemical pre-treatment that can directly cause bacteria death by irreversible membrane damage thus preventing proliferation or preventing their adhesion by reducing the anchorage sites in the early adhesion phase **(Ferraris et al. 2019).** So, this was a predictable difference as the Gram-positive strains are expected to be more sensitive to the surface morphology due to the membrane thickness and the relative difficulty of modifying the cytoskeleton based on topography. However, the presence of the peptoid significantly improved the ability of the CT samples to further reduce the colonization in comparison with the CT (Figure 4.5a, c indicated by the §). CT_GN2-Npm_9 resulted as significant towards both Ti64 control and CT for *S. epidermidis* and *E. coli* (Figure 4.5a–c), thus confirming their antibacterial and broad-range activity. As a consequence, bacterial viability was reduced by ~ 77 % for *S. epidermidis* (Figure 4.5b) and by ~ 89 % for *E. coli* (Figure 4.5d). Accordingly, it can be hypothesized that also those bacteria being able to adapt to the nano-topography of the CT samples were prevented from proliferation by the presence of the peptoid onto the surface that bonded to the bacteria membranes after surface colonization. Finally, SEM images (Figure 4.5e, representative of the *S. epidermidis* strain) validated the results obtained by the metabolic assay. While Ti64 reported a highly colonized surface with bacteria aggregated into dense and thick biofilm-like 3D structures, only a few colonies mostly arranged in small aggregates were observed on CT_GN2-Npm_9 samples.

So, our results confirmed the antibacterial activity provided by the peptoids that significantly improved the preventive antifouling and antiadhesive effect due to the CT nano-topography. Such a synergistic effect can be expected since the mechanism underlying the antibacterial effect of peptoids is different from the membrane rupture caused by the needle-like effect of the nano-topography. Amine residues with a positive electrostatic charge allow a strong bond between GN2-Nmp_9 and the bacterial membrane. Such interaction brings in the formation of irreversible pores in the membrane causing bacterial death due to the loss of the balanced homeostasis affected by the intra/extra-cellular trafficking of ions and nutrients **(Lee et al. 2018).** Accordingly, the authors hypothesize that the strong antibacterial effect observed on CT_GN2-Nmp_9 can be ascribed to the synergistic activity of the reduced bacterial adhesion due to the CT nano-topography combined with the disruptive effect of the peptoid towards the bacterial membrane.

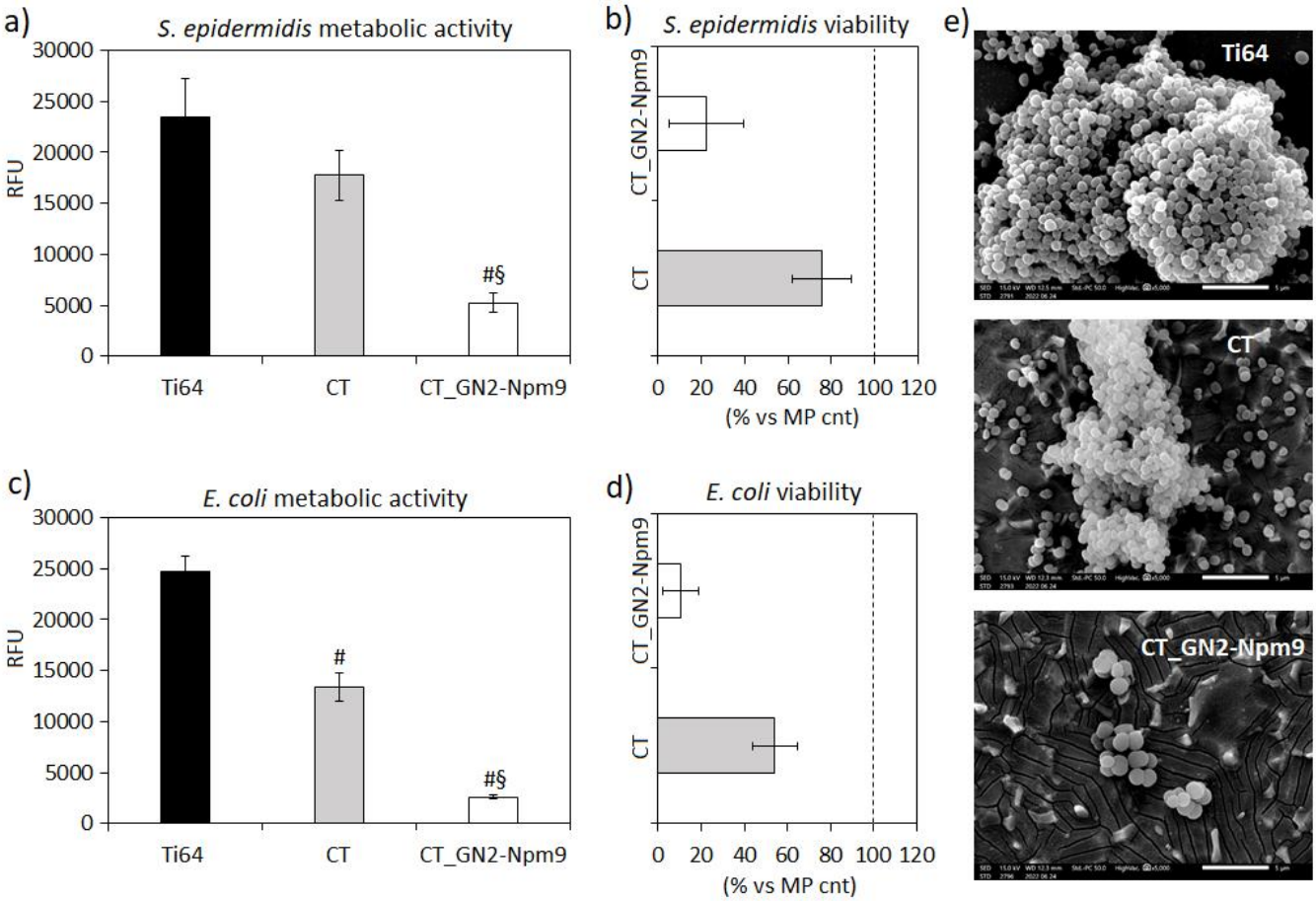

Figure 4.5: Antibacterial properties of CT, Ti64, and CT_GN2-Npm_9. The nano-topography of the CT samples determined a significant reduction of *E. coli* metabolic activity (c, $p < 0.05$ indicated by #) but only the introduction of peptoids significantly decreased bacterial metabolic activity in comparison to both Ti64 controls (a-c, $p < 0.05$ indicated by #) and CT (a-c, $p < 0.05$ indicated by §). This led to a reduction of bacterial viability ranging between 70 and 90 % in comparison with Ti64 controls (b–d). SEM images confirmed the strong reduction of colonies into the CT_GN2-Npm_9 surfaces as well as the prevention of dense 3D biofilm-like aggregates (e, representative for *S. epidermidis*). Bars represent mean±sdev.st; replicates n = 3. SEM bar scale = 5 µm (5000x). Re-acquired permission from Elsevier.

Lastly, as the authors already described in previous findings related to the antimicrobial peptide Nisin **(Lallukka et al. 2022) (Virginia Alessandra Gobbo et al. 2023)**, the functionalization through a chemisorption mechanism is advantageous both in comparison with physisorption, which is a weak and poorly controlled bond with the surface, and covalent grafting, that does not allow the release of the antibacterial agent (such as the Peptoid, in this case), resulting in a weak antibacterial effect.

4.2.5 Selectively Targeted Activity

After demonstrating CT_GN2-Npm_9 samples' cytocompatibility and antibacterial activity, bacteria-cells co-cultures were used to verify whether the antibacterial effect was targeted to preserving cells' viability in an environmental competition between hMSCs and *S. epidermidis* **(Cochis et al. 2020)**. It must be considered that cells and bacteria are not separate entities in the real clinical scenario, but, on the contrary, they compete to adhere and colonize the same surface (in this case the newly implanted biomedical device) putting in place a sort of "race for the surface" **(Gristina, Naylor, and Myrvik 1990).**

Results are reported in Figure 4.6. In general, such experiments confirmed previous findings related to antibacterial and cytocompatibility studies. In fact, in the absence of any antibacterial agent, bacteria adhered, proliferated and infected the Ti64 controls thus reducing the number of viable cells colonizing the surface. The number of viable cells decreased by ≈ 47 % (Figure 4.6a) in comparison to the seeded number, while, on the contrary, the number of bacteria increased by > 2 logs (Figure 4.6b) compared to the early stage of the infection. SEM images (Figure 4.6c) confirmed the presence of bacterial aggregates (indicated by the red circle) in proximity to apoptotic cells (indicated by the black arrows). According to the previous findings related to the antibacterial studies (Figure 4.5), the results obtained by the Ti64 samples were considered to rank the CT and CT_GN2-Npm_9 as it was demonstrated that untreated samples were not able to counteract bacterial infection. So, CT samples reported mostly a bacteriostatic effect since the number of viable bacteria increased only by < 1 log (Figure 4.6b) and the number of viable cells was increased compared to the Ti64 control (Figure 4.6a). SEM images reported the presence of cells with a proper morphology, but also the accumulation of biofilm aggregates overhanging cells' cytoskeleton (indicated by the red circles). Those results can be expected. As it was previously discussed, nano-topography is a physical hurdle for bacteria during the adhesion phase and a cause of membrane rupture in the proliferation stage. Finally, the presence of the peptoid chemisorbed on the CT surface was effective in reducing the number of viable bacteria of ≈1 log (Figure 4.6b) as well as the number of cells increased by ≈ 17 % compared to the seeded number. SEM images (Figure 4.6c) confirmed the presence of cells displaying regular morphology and only a few bacterial colonies mostly in a single conformation rather than in the biofilm-like 3D arrangement which appears not to interact with cells.

So, coming back to the basic hypothesis of the co-culture experiment, it can be speculated that the CT_GN2-Npm_9 surfaces are a very promising combination of nano-topography and adsorbed bioactive compound selectively preventing bacterial infection while preserving cells' ability to colonize the device. Further studies are still necessary to confirm samples' properties for tissue engineering applications in a more biologically rich in vivo environment where other factors such as blood protein surface accumulation can change the scenario. A more in-depth physical-chemical analysis is required to better understand the orientation of the adsorbed peptide on the surface and image its distribution on the surface, whether homogenous or not. The study of the release kinetics is also required to study how and whether the peptoid is released from the surface.

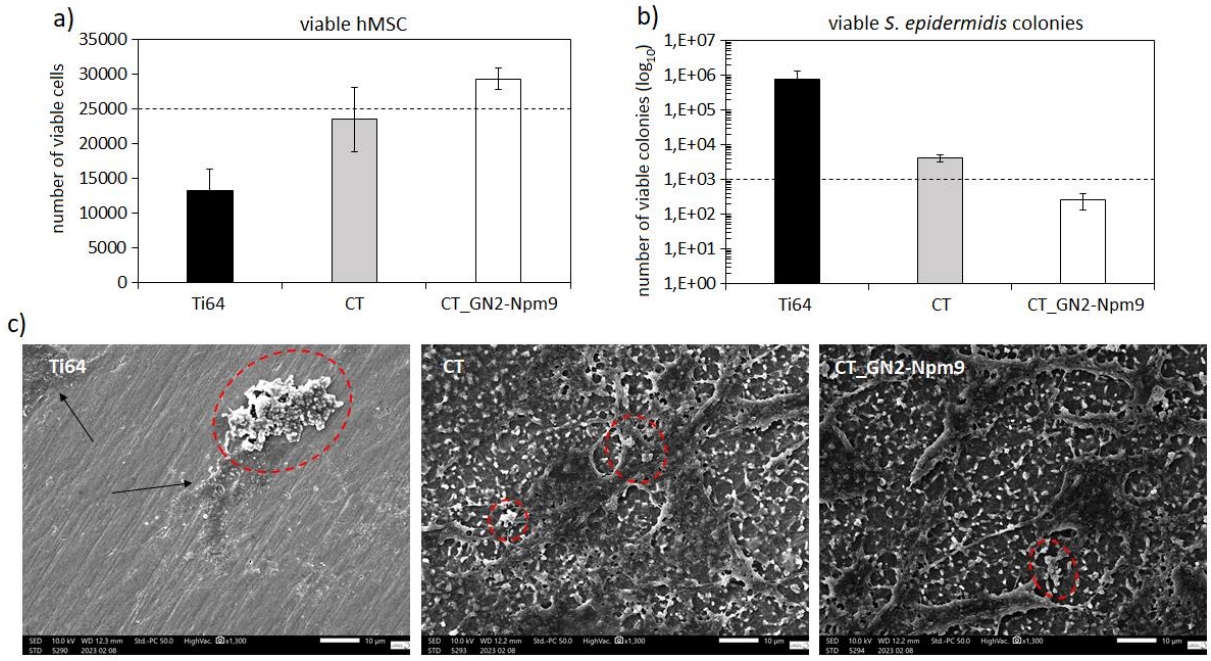

Figure 4.6: Peptoids selectively targeted activity. The peptoid doping allowed for a parallel increase of the cells seeded onto the surface (a, the dashed line indicates the starting number of cells) and a decrease of bacteria colonizing the surface (b, the dashed line indicates the starting number of bacteria) in this competition model. SEM images c) demonstrated that on Ti64 surfaces biofilm-like bacteria aggregates were visible (indicated by the red circles) and cells appeared as degraded (indicated by the arrows), while on CT_GN2-Npm_9 cells were intact and homogeneously distributed while only a few single bacteria were visible. Bars represent mean±sdev.st; replicates n = 3. SEM bar scale = 10 µm (1300x). Re-acquired permission from Elsevier.

4.3 Conclusion

In this work, the antimicrobial peptoid GN2-Npm_9 was used to functionalize a chemically pre-treated Ti6Al4V alloy (CT). A preliminary physical-chemical characterization (zeta potential titration and contact angle measurements) of CT_GN2-Npm_9 showed a hydrophilic surface, suitable for cell proliferation and adhesion, and an effective functionalization through a chemisorption mechanism. Biological tests showed a strong antibacterial activity without any cellular cytotoxicity even when cells and bacteria competed in a co-culture. The functionalized surface was a very promising combination of nano-topography and adsorbed peptoid selectively preventing bacterial infection while preserving cells' ability to colonize the device for permanent bone contact applications.

4.4 References

Abigail Mae Clapperton, Jon Babi, and Helen Tran. 2022. “A Field Guide to Optimizing Peptoid Synthesis” 2 (6): 417–29. https://doi.org/10.1021/acspolymersau.2c00036.

Adessi, Celine, and Claudio Soto. 2002. “Converting a Peptide into a Drug: Strategies to Improve Stability and Bioavailability.” Current Medicinal Chemistry 9 (9): 963–78. https://doi.org/10.2174/0929867024606731.

Barberi, J, L. Mandrile, L. Napione, A.M. Giovannozzi, A.M Rossi, A Vitale, S Yamaguchi, and S. Spriano. 2022. “Albumin and Fibronectin Adsorption on Treated Titanium Surfaces for Osseointegration: An Advanced Investigation.” Applied Surface Science (Print) 599 (October): 154023–23. https://doi.org/10.1016/j.apsusc.2022.154023.

Barberi, J, L. Mandrile, L. Napione, A.M. Giovannozzi, A.M Rossi, A Vitale, S Yamaguchi, and S. Spriano. 2022. “Albumin and Fibronectin Adsorption on Treated Titanium Surfaces for Osseointegration: An Advanced Investigation.” Applied Surface Science (Print) 599 (October): 154023–23. https://doi.org/10.1016/j.apsusc.2022.154023.

Böttger, Roland, Ralf Hoffmann, and Daniel Knappe. 2017. “Differential Stability of Therapeutic Peptides with Different Proteolytic Cleavage Sites in Blood, Plasma and Serum.” PLoS ONE 12 (6): e0178943. https://doi.org/10.1371/journal.pone.0178943.

Cho, Jin-Ho, Jonathan P Garino, Suk Jung Choo, Kye Young Han, Jung Hyun Kim, and Hyoung Keun Oh. 2010. “Seven-Year Results of a Tapered, Titanium, Hydroxyapatite-Coated Cementless Femoral Stem in Primary Total Hip Arthroplasty.” Clinics in Orthopedic Surgery 2 (4): 214–14. https://doi.org/10.4055/cios.2010.2.4.214.

Clemens Žváček, Gerald Friedrichs, Leonhard Heizinger, and Rainer Merkl. 2015. “An Assessment of Catalytic Residue 3D Ensembles for the Prediction of Enzyme Function.” BMC Bioinformatics 16 (1). https://doi.org/10.1186/s12859-015-0807-6.

Clemens Žváček, Gerald Friedrichs, Leonhard Heizinger, and Rainer Merkl. 2015. “An Assessment of Catalytic Residue 3D Ensembles for the Prediction of Enzyme Function.” BMC Bioinformatics 16 (1). https://doi.org/10.1186/s12859-015-0807-6.

Cochis, Andrea, Jacopo Barberi, Sara Ferraris, Marta Miola, Lia Rimondini, Enrica Vernè, Seiji Yamaguchi, and Silvia Spriano. 2020. “Competitive Surface Colonization of Antibacterial and Bioactive Materials Doped with Strontium And/or Silver Ions.” Nanomaterials 10 (1): 120. https://doi.org/10.3390/nano10010120.

Costa, Fabíola M.T.A., Sílvia R. Maia, Paula A.C. Gomes, and M. Cristina L. Martins. 2015. “Dhvar5 Antimicrobial Peptide (AMP) Chemoselective Covalent Immobilization Results on Higher Antiadherence Effect than Simple Physical Adsorption.” Biomaterials 52 (June): 531–38. https://doi.org/10.1016/j.biomaterials.2015.02.049.

Dohm, Michelle, Rinki Kapoor, and Annelise E. Barron. 2011. “Peptoids: Bio-Inspired Polymers as Potential Pharmaceuticals.” Current Pharmaceutical Design 17 (25): 2732–47. https://doi.org/10.2174/138161211797416066.

Ferraris, S., A. Bobbio, M. Miola, and S. Spriano. 2015. “Micro- and Nano-Textured, Hydrophilic and Bioactive Titanium Dental Implants.” Surface and Coatings Technology 276 (August): 374–83. https://doi.org/10.1016/j.surfcoat.2015.06.042.

Ferraris, Sara, Andrea Cochis, Martina Cazzola, Mauro Tortello, Alessandro Scalia, Silvia Spriano, and Lia Rimondini. 2019. “Cytocompatible and Anti-Bacterial Adhesion Nanotextured Titanium Oxide Layer on

Titanium Surfaces for Dental and Orthopedic Implants." Frontiers in Bioengineering and Biotechnology 7 (May). https://doi.org/10.3389/fbioe.2019.00103.

Ferraris, Sara, Andrea Cochis, Martina Cazzola, Mauro Tortello, Alessandro Scalia, Silvia Spriano, and Lia Rimondini. 2019. "Cytocompatible and Anti-Bacterial Adhesion Nanotextured Titanium Oxide Layer on Titanium Surfaces for Dental and Orthopedic Implants." Frontiers in Bioengineering and Biotechnology 7 (May). https://doi.org/10.3389/fbioe.2019.00103.

Ferraris, Sara, Silvia Maria Spriano, Guanjun Pan, Alberto Venturello, Claudia L Bianchi, Roberto Chiesa, Maria Giulia Faga, Giuseppe Maina, and Enrica Verne. 2011. "Surface Modification of Ti–6Al–4V Alloy for Biomineralization and Specific Biological Response: Part I, Inorganic Modification" 22 (3): 533–45. https://doi.org/10.1007/s10856-011-4246-2.

Froimson, Mark I, Jonathan P Garino, A. Machenaud, and Jean-Pierre Vidalain. 2007. "Minimum 10-Year Results of a Tapered, Titanium, Hydroxyapatite-Coated Hip Stem." Journal of Arthroplasty 22 (1): 1–7. https://doi.org/10.1016/j.arth.2006.03.003.

Godballe, Troels, Line L. Nilsson, Pernille D. Petersen, and Håvard Jenssen. 2011. "Antimicrobial β-Peptides and α-Peptoids." Chemical Biology & Drug Design 77 (2): 107–16. https://doi.org/10.1111/j.1747-0285.2010.01067.x.

Gristina, Anthony G, Paul T Naylor, and Quentin N Myrvik. 1990. "Biomaterial-Centered Infections: Microbial Adhesion versus Tissue Integration." Springer EBooks, January, 193–216. https://doi.org/10.1007/978-1-4471-3454-1_25.

Harrison, Joe J, Carol A Stremick, Raymond J Turner, Nick D Allan, Merle E Olson, and Howard Ceri. 2010. "Microtiter Susceptibility Testing of Microbes Growing on Peg Lids: A Miniaturized Biofilm Model for High-Throughput Screening." Nature Protocols 5 (7): 1236–54. https://doi.org/10.1038/nprot.2010.71.

Hasan, Abshar, and Lalit M Pandey. 2020. "Surface Modification of Ti6Al4V by Forming Hybrid Self-Assembled Monolayers and Its Effect on Collagen-I Adsorption, Osteoblast Adhesion and Integrin Expression." Applied Surface Science 505 (March): 144611. https://doi.org/10.1016/j.apsusc.2019.144611.

Hollinger, Jeffrey O. 2011. An Introduction to Biomaterials, Second Edition. Hoboken: CRC Press.Holmberg, Kyle V., Mahsa Abdolhosseini, Yuping Li, Xi Chen, Sven-Ulrik Gorr, and Conrado Aparicio. 2013. "Bio-Inspired Stable Antimicrobial Peptide Coatings for Dental Applications." Acta Biomaterialia 9 (9): 8224–31. https://doi.org/10.1016/j.actbio.2013.06.017.

Hollinger, Jeffrey O. 2012. An Introduction to Biomaterials. Boca Raton, Fl: Crc Press/Taylor & Francis.Popat Mohite, Sunny Shah, Sudarshan Singh, Tanavirsing Rajput, Shubham Munde, Nitin Ade, Bhupendra G Prajapati, Himanshu Paliwal, Dhaval D Mori, and Ashvin Dudhrejiya. 2023. "Chitosan and Chito-Oligosaccharide: A Versatile Biopolymer with Endless Grafting Possibilities for Multifarious Applications." Frontiers in Bioengineering and Biotechnology 11 (May). https://doi.org/10.3389/fbioe.2023.1190879.

Khara, Jasmeet Singh, Biljana Mojsoska, Devika Mukherjee, Paul R. Langford, Brian D. Robertson, Håvard Jenssen, Pui Lai Rachel Ee, and Sandra M. Newton. 2020. "Ultra-Short Antimicrobial Peptoids Show Propensity for Membrane Activity against Multi-Drug Resistant Mycobacterium Tuberculosis." Frontiers in Microbiology 11 (March). https://doi.org/10.3389/fmicb.2020.00417.

Kim, Hyunmin, Fumiaki Miyaji, Tadashi Kokubo, and Takashi Nakamura. 1996. "Preparation of Bioactive Ti and Its Alloys via Simple Chemical Surface Treatment" 32 (3): 409–17. https://doi.org/10.1002/(sici)1097-4636(199611)32:3%3C409::aid-jbm14%3E3.0.co;2-b.

Lallukka, Mari, Francesca Gamna, Virginia Alessandra Gobbo, Mirko Prato, Ziba Najmi, Andrea Cochis, Lia Rimondini, Sara Ferraris, and Silvia Spriano. 2022. “Surface Functionalization of Ti6Al4V-ELI Alloy with Antimicrobial Peptide Nisin.” Nanomaterials 12 (23): 4332. https://doi.org/10.3390/nano12234332.

Lee, Jiyoun, Dahyun Kang, Jieun Choi, Wei Huang, Mayken W Wadman, Annelise E Barron, and Jiwon Seo. 2018. “Effect of Side Chain Hydrophobicity and Cationic Charge on Antimicrobial Activity and Cytotoxicity of Helical Peptoids.” Bioorganic & Medicinal Chemistry Letters 28 (2): 170–73. https://doi.org/10.1016/j.bmcl.2017.11.034.

Lone, Abdullah, Anis Arnous, Paul Robert Hansen, Biljana Mojsoska, and Håvard Jenssen. 2020. “Synthesis of Peptoids Containing Multiple Nhtrp and Ntrp Residues: A Comparative Study of Resin, Cleavage Conditions and Submonomer Protection.” Frontiers in Chemistry 8 (April). https://doi.org/10.3389/fchem.2020.00370.

Masip, Isabel, Enrique Perez-Paya, and Angel Messeguer. 2005. “Peptoids as Source of Compounds Eliciting Antibacterial Activity.” Combinatorial Chemistry & High Throughput Screening 8 (3): 235–39. https://doi.org/10.2174/1386207053764567.

Mehdi Kazemzadeh-Narbat, Shahryar Noordin, Bassam A Masri, Donald S Garbuz, Clive P Duncan, Robert, and Rizhi Wang. 2012. “Drug Release and Bone Growth Studies of Antimicrobial Peptide-Loaded Calcium Phosphate Coating on Titanium” 100B (5): 1344–52. https://doi.org/10.1002/jbm.b.32701.

Mojsoska, Biljana, Ronald N. Zuckermann, and Håvard Jenssen. 2015. “Structure-Activity Relationship Study of Novel Peptoids That Mimic the Structure of Antimicrobial Peptides.” Antimicrobial Agents and Chemotherapy 59 (7): 4112–20. https://doi.org/10.1128/aac.00237-15.

Morton, Logan D., David A. Castilla-Casadiego, Ajay C. Palmer, and Adrianne M. Rosales. 2023. “Crosslinker Structure Modulates Bulk Mechanical Properties and Dictates HMSC Behavior on Hyaluronic Acid Hydrogels.” Acta Biomaterialia 155 (January): 258–70. https://doi.org/10.1016/j.actbio.2022.11.027.

Popat Mohite, Sunny Shah, Sudarshan Singh, Tanavirsing Rajput, Shubham Munde, Nitin Ade, Bhupendra G Prajapati, Himanshu Paliwal, Dhaval D Mori, and Ashvin Dudhrejiya. 2023. “Chitosan and Chito-Oligosaccharide: A Versatile Biopolymer with Endless Grafting Possibilities for Multifarious Applications.” Frontiers in Bioengineering and Biotechnology 11 (May). https://doi.org/10.3389/fbioe.2023.1190879.

Pucci, Fabrizio, Raphaël Bourgeas, and Marianne Rooman. 2016. “Predicting Protein Thermal Stability Changes upon Point Mutations Using Statistical Potentials: Introducing HoTMuSiC.” Scientific Reports 6 (1). https://doi.org/10.1038/srep23257.

Saini, Avneet, and Gaurav Verma. 2017. “Peptoids: Tomorrow’s Therapeutics.” Elsevier EBooks, January, 251–80. https://doi.org/10.1016/b978-0-323-46142-9.00010-4.

Saporito, Paola, Biljana Mojsoska, Anders Løbner Olesen, and Håvard Jenssen. 2019. “Antibacterial Mechanisms of GN-2 Derived Peptides and Peptoids againstEscherichia Coli.” Biopolymers 110 (6). https://doi.org/10.1002/bip.23275.

Statz, Andrea R, Jinghao Kuang, Cheng Ren, Annelise E Barron, Igal Szleifer, and Phillip B Messersmith. 2009. “Experimental and Theoretical Investigation of Chain Length and Surface Coverage on Fouling of Surface Grafted Polypeptoids.” Biointerphases 4 (2): FA22–32. https://doi.org/10.1116/1.3115103.

Sun, Jing, and Ronald N Zuckermann. 2013. “Peptoid Polymers: A Highly Designable Bioinspired Material.” ACS Nano 7 (6): 4715–32. https://doi.org/10.1021/nn4015714.T.

Virginia Alessandra Gobbo, Mari Lallukka, Francesca Gamna, Mirko Prato, Alessandra Vitale, Sara Ferraris, Ziba Najmi, et al. 2023. “Functionalization of a Chemically Treated Ti6Al4V-ELI Alloy with Nisin for Antibacterial Purposes.” Applied Surface Science 620 (May): 156820–20. https://doi.org/10.1016/j.apsusc.2023.156820.

Vootla, Dr. Naveen Reddy, and Dr. K. Varun Reddy. 2017. “Osseointegration- Key Factors Affecting Its Success-an Overview.” IOSR Journal of Dental and Medical Sciences 16 (04): 62–68. https://doi.org/10.9790/0853-1604056268.

Wang, Yifei, Yu Zhou, Kangmei Li, and Jun Hu. 2020. “Effects of Surface Properties of Titanium Alloys Modified by Grinding, Sandblasting and Acidizing and Nanosecond Laser on Cell Proliferation and Cytoskeleton.” Applied Surface Science 501 (January): 144279–79. https://doi.org/10.1016/j.apsusc.2019.144279.

Wang, Yifei, Yu Zhou, Kangmei Li, and Jun Hu. 2020. “Effects of Surface Properties of Titanium Alloys Modified by Grinding, Sandblasting and Acidizing and Nanosecond Laser on Cell Proliferation and Cytoskeleton.” Applied Surface Science 501 (January): 144279–79. https://doi.org/10.1016/j.apsusc.2019.144279.

Yoshinari, Masao, Tetsuo Kato, Kenichi Matsuzaka, Tohru Hayakawa, and Kiyotaka Shiba. 2010. “Prevention of Biofilm Formation on Titanium Surfaces Modified with Conjugated Molecules Comprised of Antimicrobial and Titanium-Binding Peptides.” Biofouling 26 (1): 103–10. https://doi.org/10.1080/08927010903216572.

Yukari Iwaya, Miho Machigashira, Kenji Kanbara, Motoharu Miyamoto, Kazuyuki Noguchi, Yuichi Izumi, and Seiji Ban. 2008. “Surface Properties and Biocompatibility of Acid-Etched Titanium.” Dental Materials Journal 27 (3): 415–21. https://doi.org/10.4012/dmj.27.415.

Zapadka, Karolina L., Frederik J. Becher, A. L. Gomes dos Santos, and Sophie E. Jackson. 2017. “Factors Affecting the Physical Stability (Aggregation) of Peptide Therapeutics.” Interface Focus 7 (6): 20170030. https://doi.org/10.1098/rsfs.2017.0030.

Zhao, Wenhan, Haoyu Wang, Xixi Xiao, Lauren De Stefano, Jordan Katz, Jennifer S Lin, Annelise E Barron, Thomas P Schaer, Hongjun Wang, and Matthew Libera. 2022. “Peptoid-Loaded Microgels Self-Defensively Inhibit Staphylococcal Colonization of Titanium in a Model of Operating-Room Contamination.” Advanced Materials Interfaces 9 (31). https://doi.org/10.1002/admi.202201662.

Chapter VI

Phage Derived Endolysins as a Recombinant Protein

Aim

Bacterial infections are common in developing countries, and their high occurrence has caused a rise in rates of both morbidity and mortality. Most studies have focused on determining the number of deaths attributed to antibiotic-resistant infections and sepsis, highlighting that infections remain a significant contributor to worldwide death rates. Moreover, the discovery of new antibiotics is a time-consuming and expensive procedure, requiring an average of 10 to 15 years for completion. In June 2019, the European Medicines Agency began supporting the creation of clinical trials for novel antibacterial agents to ensure they comply with different regulatory organizations. During my PhD programme, my main focus was finding innovative methods to prevent and control bacterial infection: Phage therapy is one of the suggestions that is well-liked in this aspect. Phages, which are viruses, require a bacterial host for survival as they are unable to reproduce on their own. Bacteriophages attach to particular receptor sites on the surface of bacterial cells, transfer their genetic material into the host cell, and proceed to either incorporate this material into the bacterial DNA and replicate vertically, or take control of the bacterial replication mechanism to generate new phage offspring, eventually resulting in cell lysis. I mainly focused on lysins as an alternative to antibiotics. While the pathway might not be the same, I still followed the existing guidelines for antibiotics according to the European Agency.

Recombinant Endolysins Preparation

Diego Cotella: The design of phage endolysins from staphylococcal bacteriophage K (LysK) and enterococcus phage ϕ1 (Ply V12) and the construction of plasmids were done. plasmid preparation and protein production were described in section 5.2.

Ajay Kumar: Here, I produced the recombinant protein by using the *E. coli* BL21 (DE3) strain. After protein production, I performed the antibacterial and cytocompatibility studies.

Introduction

5. Phage Therapy

Bacteriophages are defined as the most common reproducing biological system on the planet. These bacteriophages, which can infect and lyse bacteria, were discovered by Frederick William Twort and Félix d'Hérelle. Shortly after making this breakthrough, d'Hérelle identified the opportunity to make use of bacteriophages for the treatment of human and animal infections. **(Summers 2001).** In 1919, a mixture of phages was created to treat a child with dysentery, and after being tested on some healthy people to check its safety, it was given to the child. The boy was successfully treated with one phage dose, and three additional patients were treated the same way, all recovering shortly after receiving the treatment. Nevertheless, these findings were not made public. An increasing concern has been observed regarding the development of bacterial strains that are resistant to all categories of antibiotics commonly used in medical treatment. Despite the vast selection of antibiotics that are available. Resistance to bacteria has been acknowledged for all antimicrobial drugs created so far. Additionally, recent case studies and clinical trials indicate some promise in tackling these issues of drug resistance. Due to resistance to antibiotics, there's an urgent requirement for unconventional scientific therapies to address bacterial infections. Moreover, it is very crucial to expand an alternative to conventional antibiotics for treatment. A potential alternative to regular antibiotics is the use of lytic enzymes or endolysins produced by bacteriophages during lytic infection. In the process of lytic infection, bacteriophage enzymes degrade the peptidoglycan layer of the bacterial cell wall, leading to the lysis of the host cell **(Schmelcher et al. 2012).** Phage therapy is a unique method of treating bacterial infections by using bacteriophages, also known as phages, which are viruses that specifically attack and destroy bacteria, including antibiotic-resistant strains. Furthermore, bacteriophage-derived endolysins and other peptidoglycan hydrolases may serve as a potential substitute for conventional antibiotics by targeting specific bacteria such as *S. aureus*, *S. epidermidis*, and *E. coli*. Phage therapy has been retained in the past five years due to increased concerns about antibiotic resistance and the limited availability of new antibiotics, Research studies have found increasing evidence supporting how phage treatment is effective in treating severe bacterial infections. **(Dedrick et al. 2022)** recently performed phage therapy in 20 patients with resistant mycobacterial infections. Following the treatment, no negative impacts were observed in any patients, with most patients showing positive clinical and/or microbiological responses. In 11 patients, neutralizing antibodies were detected in the serum after receiving intravenous phage delivery. Out of the 11 patients who received only one phage administration, none exhibited phage resistance. **(Petrovic Fabijan et al. 2020)** have shown that phage therapy is safe for treating severe *S. aureus* infections. The primary focus was on safety and effectiveness, with no reported side effects. The findings indicate that phage treatment is safe for *s. aureus* infections, including cases of infective endocarditis and septic shock.

Few literature studies have a minor discrepancy regarding the use of phages as antibacterial agents in medicine. Hence, there are a variety of phages available for a specific bacterium, and the current approach involves utilizing phage cocktail mixes to identify various phages that attack the pathogens in different ways, thus managing the significant phage resistance shown by bacteria. Most phages are not harmful to human health. Nevertheless, phages are versatile genetic components that can engage with host bacteria and, in certain instances, facilitate the transfer of genes between bacteria via horizontal gene transfer. Therefore, viral particles that impact specific traits like virulence gene transfer can have a detrimental impact on human health by enhancing bacterial virulence and pathogenicity. Bacteriophages can move genes in two distinct ways. Generalized transduction: In this stage, fragments of degraded bacterial DNA are combined with newly created viral particles rather than viral genomes **(Biondo 2022)**. At the same time, Specialized transduction is limited to phages that can form aggregates and undergo lysogeny by integrating their genome into the bacterial chromosome. During the lytic cycle, the prophage is removed without specificity, resulting in the inclusion of surrounding bacterial genes in newly formed viral particles that are transferred to other bacteria. Nevertheless, therapeutic phages need to be free of harmful genes, and virulent yet unable to undergo lysogeny to minimize transduction risks. The primary obstacle hindering the advancement of phage therapies is the lack of globally acknowledged human clinical trials. Therefore, the majority of countries do not authorize phage therapies for human clinical trials. Most researchers have created an antibacterial product using bacteriolytic proteins encoded by phages to combat phage therapies. Studies show that the key proteins are phage-encoded peptidoglycan hydrolases, also known as lysins or endolysins. These endolysins cause the breakdown of the bacteria's peptidoglycan layer in the later stage of lytic phage replication, leading to the bursting of bacterial cells and the release of newly produced viral particles, as depicted in Figure 5.1.

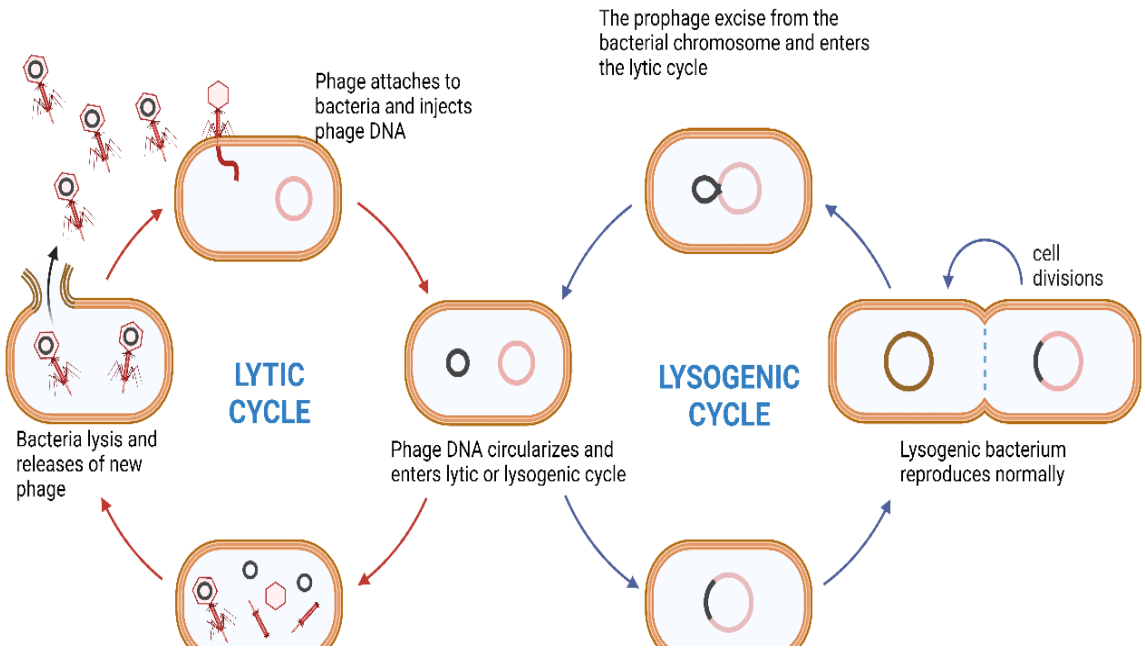

Figure 5.1: Figure: A schematic representation of phages lytic and lysogenic cycle of a bacteriophage. Modified from (Tu et al. 2023). Created with BioRender.com.

5.1 Endolysins or Lysins

With antibiotic-resistant strains on the rise, phage endolysins are being considered as potential alternative antimicrobials for treating bacterial infections. These enzymes derived from phages are effective in different animal models of bacterial infection as well as in removing bacteria from mucosal surfaces. While some endolysins have widespread lytic activity, many phage endolysins exhibit specificity towards particular species, which is considered advantageous in the face of increasing antibiotic resistance to avoid impacting beneficial bacteria **(Schmelcher et al. 2012)**. Additionally, it is improbable for resistance to develop against endolysins due to various other factors. Hence, the phages and host bacteria are co-evolving. Endolysins have adapted to target and break down well-preserved cell wall structures that are harmful to the host. These endolysins utilized in treatments are effective against various resistance mechanisms, unlike traditional antibiotics. It is believed that multiple endolysins have two catalytic domains that can break down various bonds in the peptidoglycan, potentially decreasing the likelihood of resistance emergence. Based on literature research, these lysins offer various benefits compared to antibiotics including their ability to quickly eliminate bacteria as soon as they come into contact. They may target certain pathogens, especially Gram-positive bacteria, thus preserving the normal microbiota, 3. Additionally, the unlikelihood of resistance development may be attributed to the enzymes targeting a crucial and widely preserved structural component like peptidoglycan, which cannot be easily altered without consequences. The team won the championship after a series of impressive victories. They have efficacy against multidrug-resistant bacteria. They can act synergistically with other lysins or antibiotics and thus theoretically reduce the development of resistance while increasing therapeutic efficiency, 6. Endolysins are very effective in killing colonizing pathogens growing on mucosal surfaces and also on biofilms **(Nelson et al. 2012)**.

5.1.1 Endolysins Mechanism

Endolysins work by breaking the bacterial peptidoglycan layer. The peptidoglycan layer of Gram-positive bacteria is 20 to 80 nm in thickness, which is thicker compared to the 10 nm thickness in Gram-negative bacteria. Along with alternating N-acetylglucosamine (N-Glc) residues and N-acetylmuramic acid (N-Mur). The amide bonds connecting the linear strands to the stem peptide are aimed through the covalent bonds among the N-Mur residues and the conserved stem peptide L-alanine. The oligopeptides consist primarily of L and D amino acids, which are connected either directly to the opposite stem peptide or adjacent to the interpeptide bridge. The majority of endolysins are recognized for their catalytic function within peptidoglycan structures, such as glycosidase, that breaks down glycan residues, as illustrated in Figure 5.2. Amidase splits the amide bond between N-Mur and the stem L-alanine residue, while endopeptidases split peptide bonds between 2 amino acid residues. Additionally, glycosidases are categorized into muramidase and glucosaminidases. Muramidase cleaves the bond between N-Mur and N-Glc as lysozymes do. Glucosaminidases are enzymes that can break the bond between N – Glc and N – Mur, and they are frequently

found in autolysins. The source of endolysin activity comes from phages that target gram-positive hosts and typically feature a typical domain structure with an N-terminal enzymatically active domain (NAD) connected to a C-terminal Cell wall binding domain (CBD) by a short linker region. This domain arrangement is common among endolysins from gram-positive phages and differs in endolysins from Gram-negative phages. Typically, they have a rounded shape and lack CBDs. For instance, staphylococcal phage – K endolysins (Lys K) have a very efficient histidine or cysteine-dependent peptidase (CHAP). These enzymes eliminate the bacteria by using a specific hydrolysis method. Glycosidic links between the N - Mur and N - Glc monomers hold peptidoglycan polymers together. Once the endolysins are externally introduced, they begin to break down these 2 bonds, causing the bacterial peptidoglycan cell wall to rupture due to compromised structural integrity. As a result, there is an alteration in osmotic pressure which leads to the bursting of the bacterial cell and the release of cellular substances **(Broendum et al. 2018)**.

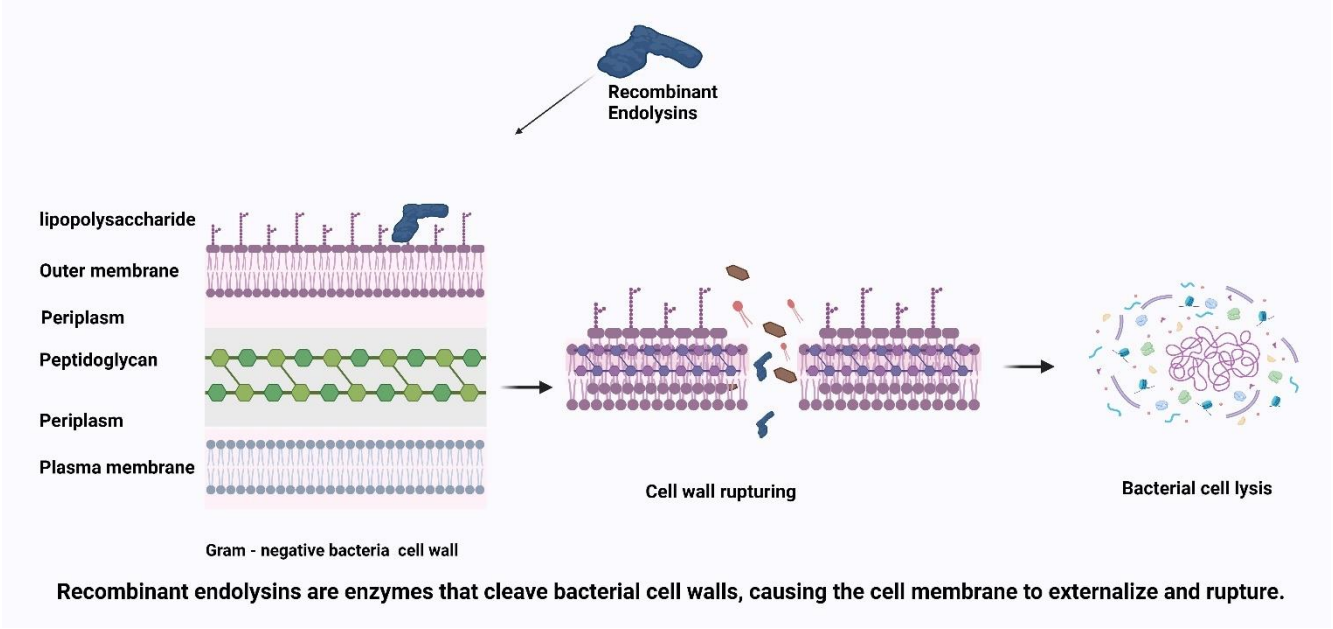

Figure 5.2: A schematic representation of endolysin antibacterial mechanism. Modified from (Camacho-González et al. 2022). Created with BioRender.com

Aim of the study

Both LysK and PlyV12 recombinant proteins were first tested with antibacterial activity to verify whether the recombinant production was successfully produced or not. To test this, I performed an antibacterial activity towards the Gram-positive *S. aureus* and *S. epidermidis* as well as the Gram-negative *E. coli* and *Aggregatibacter actinomycetemcomitans* pathogens. Furthermore, I also tested the cytocompatibility with the human mesenchymal stem cells to determine safe concentrations for the cells.

5.2 Materials and Methods

5.2.1 Bioinformatic Analysis and Construction of LysK and PlyV12

The basic local alignment search tool, BLASTp (https://blast.ncbi.nlm.nih.gov/Blast.cgi, accessed 1 June 2021) was used to identify sequences of Protein Data Bank (PDB). These sequences were then used in a Multiple-sequence alignment by Florence Corpet. (http://multalin.toulouse.inra.fr/multalin/ accessed 1 June 2021) LysK from Staphylococcus phage K (it is annotated as ORF30/ORF32 [Staphylococcus virus K] GenBank: AAO47477.2 and then we repeat the Multiple sequence alignments, the protein is identical to most LysK. Reverse-translate the protein sequence, by using a sequence manipulation web tool (http://www.bioinformatics.org/sms2/). Consider the *E. coli* as a host. LysK DNA was ordered from thermo scientific from gene Art with pet100/D-TOPO vector (https://www.thermofisher.com/it/en/home/life-science/cloning/gene-synthesis.html).

PlyV12, the basic local alignment search tool, BLASTp (https://blast.ncbi.nlm.nih.gov/Blast.cgi accessed 1 June 2021) was used to identify sequences of Protein Data Bank (PDB). PlyV12 AND Enterococcus faecalis Gene Bank: AAT01859.1. Reverse-translate the protein sequence, by using the Sequence Manipulation Suite (SMS) web tool (http://www.bioinformatics.org/sms2/). Consider the codon usage of E. coli as a host. Both the DNA was ordered from thermo scientific from gene Art with pet100/D-TOPO vector (https://www.thermofisher.com/it/en/home/life-science/cloning/gene-synthesis.html).

5.2.2 Preparation of Competent *E. coli*

E. coli cells are grown on the early log phase (OD600 = 0.3 - 0.5) in 2xTY broth (Thermo Fisher, USA). Briefly, cells were centrifuged at 25000 rpm for 15 min at 10°C using a swing-bucket rotor. The cells are then resuspended in 8 mL (1/12 culture volume) of CCMB80 buffer (10% glycerol, 10 mM K-Acetate, 80 mM Calcium chloride dihydrate ($CaCl_2$), 20mM Manganese chloride tetrahydrate ($MnCl_2$), Magnesium chloride hexahydrate ($MgCl_2$)) and incubated on ice for 20 min and recentrifuged the cells ab above mentioned. Gently re-suspended each pellet in 2 mL (1/12 culture volume in CCMB80 buffer and cells were aliquot 80 µl each in cold (pre-chilled on ice) 1.5 mL centrifuge tubes and stored at -80°C.

5.2.3 Bacterial Transformation and Protein Expression

The *E. coli* strain BL21 (DE3) was grown at 37°C in 2xTY (Thermo Fisher, USA) medium. The 2xTY medium was then supplemented with Ampicillin 1X for plasmid selection. The artificial gene LysK and plyV12 were subcloned using synthetic oligonucleotides and inserted into pET100/D-TOPO. The plasmids were then transformed into *E. Coli* BL21(DE3) for protein expression at 100 ng/mL, as targeted in the preceding phase. To produce the recombinant proteins, the *E. Coli* BL21(DE3) was grown at 37°C and the optical density was measured hourly till reaching the mid-log segment (OD600 = 0.5 to 0.8 for LysK and 0.4 to z0.6 for Plyv12), then the cells had been frozen with 10% glycerol and saved at -80°C. Briefly, the BL21 (DE3) strain was induced

with the use of 1 mM Isopropyl β-D-1-thiogalactopyranoside (IPTG) and then kept at 37°C for 4 hours for expression inside the logarithmic phage, attaining an OD 600 of 2.0 (LysK) and 1.8 (PlyV12). Bacteria were collected every hour for 3 h and stored at -20°C and protein expression was analyzed using 12.5% SDS-PAGE stained with Coomassie blue.

5.2.4 Western Blot Analysis

In brief, the lysate containing the protein expressed utilizing LysK and PlyV12 turned into analyzed on a 12.5% SDS-PAGE gel (biorad) after which transferred to a nitrocellulose membrane with a semi-dry transfer system. The membrane was blocked with 4% milk serum for 1 h at room temperature, followed by incubation with primary antibody 1:10000 (anti-His tag monoclonal antibody (mAb) (Abcam Inc., MA, USA) for two hours with shaking at room temperature. Then samples were washed with 05% Tween 20). Followed by alkaline phosphate (colourimetric assay) with nitro blue tetrazolium chloride (NBT) and 5-Bromo- 4-chloro-3-indolyl phosphate (BCIP) (NBT/BCIP, Sigma).

5.2.5 Bacteria Culture

The Production of the LysK and PlyV12 recombinant lysins is detailed in Figure 5.3. Bacteria were freshly streaked on 2xTY Agar (Thermo scientific, USA. Agar Germany) in the presence of Ampicillin 1X and incubated at 37°C overnight until round single colonies were formed, then 1 colony were collected and spotted into 50 mL of 2xTY each. Broth cultures were incubated overnight at 37°C under agitation at 200 rpm in an orbital shaker after overnight each culture was transferred separately into bioreactors for protein production.

5.2.6 Protein Production by Bioreactor

The Production of the LysK and PlyV12 recombinant lysins, the transformed E. coli BL21 (DE3) strain was cultivated in 2 litres of 2× YT broth (Thermo Scientific, USA) in the presence of Ampicillin 1X at 37°C. Briefly, both the culture's OD was observed each hour until the mid-log phase (OD600 = 0.5 for LysK) and 0.7 for Plyv12). Then both BL21 (DE3) strain was induced with 0.5 mM Isopropyl β-D-1-thiogalactopyranoside (IPTG) and incubated at 37°C and cultured was continued for 4h to allow expression at logarithmic phase (OD 600 = 1.0 (LysK) and 2.0 (PlyV12) and both the cultures were stopped after 4h and both the cultures were collected into 500 mL for ultra-centrifuge bottles (Avanti J – 26 XP, Beckman Centrifuge, USA.) JA-10 Router and the cultures were centrifuged at 10000 RPM for 10 min at 10°C. Both the Cell pellets were frozen at −20°C until use.

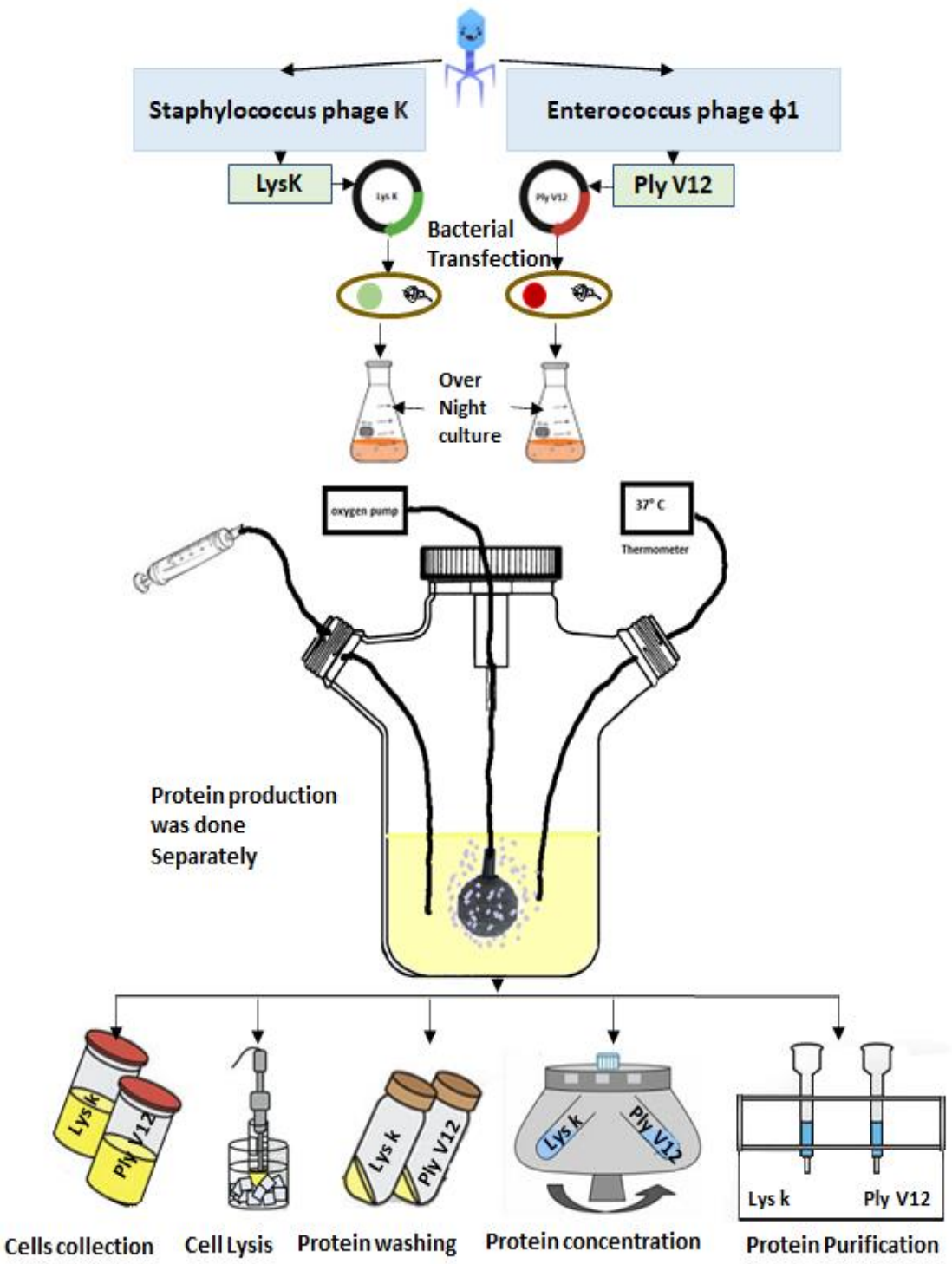

Figure 5.3: A schematic representation of endolysin protein production.

5.2.7 Protein Extraction and Purification by Washing Method

Both the pellets were resuspended in Lysis Solution with 200 µg/mL Lysozyme from chicken egg white (Sigma-Aldrich) and 1% Triton (Sigma Life Science) in 50 mL of 1X PBS, and vortex for 1 minute each. In short, the pellet was sonicated four times at 70% pulse on ice for 1 minute each with a 20 to 40 seconds rest period between pulses. After that, it was centrifuged for 10 minutes at 12000 rpm at 10°C and each supernatant was stored at 4°C. The pellet was subsequently resuspended in 1X triton in 50 mL 1X PBS, sonicated again,

centrifuged, and the supernatant stored at 4°C. Moreover, both pellets were rinsed with 50 mL of sterile Distilled H_2O containing 0.01 % Triton and the step was repeated with 0.01 % Triton and the resulting supernatant was stored at 4°C. Finally, the supernatant was stored at -20°C then the purity of each protein was evaluated using SDS-PAGE gel electrophoresis and the gel was stained with Coomassie blue.

5.2.8 Protein Denaturing and Refolding with Amino Acids

After the evaluation of the purity of the protein. Both the LysK and PlyV12 supernatant were centrifuged at 12000 rpm at 10°C and both the pellets were resuspended in 5 mL each 8M Urea pH= 8.0 (denaturing buffer) and incubated on a share for room temperature. Briefly, 1 mL of each protein was diluted to 1:10 with a refolding Buffer (500 mM L-Arginine, 5 mM L-Cystine HCL and 0.5mM L-cysteine in 1X PBS) incubated for 30 mins on ice and transferred to 10 mL solution to a protein concentration tubes (pierce™ Protein Concentrator PES 10K MWCO, 5-20 mL, Thermo Scientific, Lot # WK338227. The UK) by following the manufacturing instructions, tubes were centrifuged at 5000 RPM for 1h and finally, 1 mL of concentrated protein was collected from the tube The purity of LysK and PlyV12 was >90% as according to the manufacture and both the proteins were verified SDS-PAGE gel electrophoresis and the gel was stained with Coomassie blue.

5.2.9 Protein Dialysis

Finally, the collected proteins were subjected to buffer exchange by dialysis using 1X PBS by a mini dialysis tool (Slide-A-Lyzer® MINI Dialysis Device, 10K MWCO, 2 mL, Thermo Scientific, Lot # P00090804, USA) following the manufacturer instructions. Briefly, LysK and Ply V12 protein samples were placed in a dialysis chamber with 2 mL and incubated for 2 h on a shaking at 200 rpm at 20°C, after 2 h 1x PBS was replaced and incubated overnight at 200 rpm at 20°C. The purity of the protein was evaluated using SDS-PAGE gel electrophoresis and the gel was stained with Coomassie blue. Furthermore, both the recombinant proteins were verified by western blot analysis using an anti-His monoclonal antibody as described in the section.

5.2.10 Endolysins

Both the LysK and Ply V12 Protein concentrations were determined by Bradford assay (Bio-Rad Quick Start™ Bradford 1x Dye Reagent #5000205) following the manufacturer's instructions and the proteins were stored at -20°C, respectively solutions were thawed before each experiment by diluting the proteins in the proper cell or bacteria culture medium. Proteins were tested at the concentrations that are described in detail in Table 5.1.

Table 5.1. Proteins tested concentrations (in the appropriate Bacteria and Cells medium).

Proteins	Concentrations (µg/µl)	Concentrations (µg/mL)
	Bacteria	**Cells**
LysK	**25, 50 & 100 µg/µl**	**100, 150 & 200 µg/mL**
Ply V12		

5.2.11 Antibacterial Activity

Gram – positive strains *Staphylococcus aureus* (*S. aureus* (ATCC 43300)) and *Staphylococcus epidermidis.* (*S. epidermidis* (ATCC14990)) Gram – Negative strains *Escherichia coli* (*E. coli* (ATCC 25922)) and *Aggregatibacter actinomycetemcomitans* (*Aggregatibacter* (ATCC 33384)) strains were purchased from the American Type Culture Collection (ATCC). Bacteria were cultivated onto Trypticase Soy Agar (TSA, Sigma-Aldrich) and incubated at 37°C until single colonies were formed; then, 3 – 5 colonies were collected and cultured into 20 mL of Luria Bertani broth (LB, Sigma-Aldrich) for *S. aureus*, *S. epidermidis* and *E. coli.* In contrast, *Aggregatibacter* were cultured in Brain Heart Infusion Broth (BHI) all the Broth cultures were incubated overnight at 37°C in agitation at 120 rpm in an orbital shaker. Always a fresh culture was prepared during each experiment.

In brief, each well-contained 100µl of the $1x10^5$ cells/mL (0.001 O.D.) and biofilm formation was explained previously. supernatants containing planktonic cells were removed and replaced with 200µl of fresh media along with LysK and Ply V12 concentrations as shown in Table 5.1 and biofilm was grown at 37°C. Bacterial viability was determined by Alamar blue colourimetric assay as described in int section 4.1.7.

5.2.12 Cytocompatibility

To assess the cytocompatibility of samples, hMSCs cells were seeded onto the multiwell at a specific concentration of 1 $x10^4$ cells and cultured for 1 and 2 days. The viability of the cells was determined at each time point based on their metabolic activity using the Alamar blue colourimetric assay as described in the 4.1.7 section. The outcomes are reported in relative fluorescence units (RFU). cells without any treatment were used as a positive control. After each time point, cell viability was evaluated by the fluorescent live/dead assay (LIVE/DEAD, from Invitrogen, L3224, Thermo Fisher, USA) following the manufacturer's instructions. Briefly, cells were washed with PBS for 1 time 2 µM calcein and 4 µM EthD-1 were dissolved in fresh medium and 150 µL of live /dead were added to each sample and then incubated for 45 min after incubation samples were washed 1 time with PBS and Images were collected by a confocal microscope (Leica SP8 confocal platform, Leica Microsystems, Germany).

5.2.13 Statistical Data Analysis

Triplicates were utilized for conducting biological evaluations. Firstly, the normal distribution of data and homogeneity of variance were checked with the use of Shapiro-Wilk's and Levene's checks, after confirming that the records met the assumptions. The results were assessed using SPSS software (v25, IBM, New York City, NY, USA) through one-way ANOVA followed by Tukey's test for post hoc analysis. The level of significance was established as $p < 0.01$.

5.3 Results and Discussion

5.3.1 Analysis and Construction of LysK and PlyV12

Both the synthetic genes LysK and Ply V12 were assembled from synthetic oligonucleotides and/or PCR products. The fragment was inserted into pET100/D-TOPO and genes were codon-optimized. The plasmid DNA was purified from transformed bacteria and the final construct was verified by sequencing. The sequence identity within the insertion sites was 100% verified by Thermo Scientific. The LysK protein is encoded by the ORFO42 open reading frame of the Staphylococcal Phage and consists of 495 Amino acids (AAs, 54.75kDa) The protein search results showed that the N-acetyl-muramoyl-L-alanine-amidase. Whereas the Ply V12 protein is encoded by the open reading frame Enterococcus sp. phage 1 and consists of 314 Amino acids (AAs, 34.13kDa). The protein search results showed that the N-acetylmuramoyl-L-alanine amidase, where both endolysins have the same function that hydrolase the cell wall of bacteria.

5.3.2 Bacterial Transformation and Protein Expression

To analyze Lys K and Ply V12 protein expression, a classical induction setup was performed based on comparing both protein profiles of cell lysates obtained from Induced (No Induction) and Induced (induction). So, the results confirmed that the IPTG can induce the specific protein expression of LysK (54.75 kDa) and Ply V12 (34.13 kDa) and the expressed recombinant protein was verified in the lysate by western blot analysis using an anti-His monoclonal antibody as shown in Figure 5.4. Thus, suggesting that the protein was the His-tagged recombinant protein. However, both the proteins did not show any high similarity results with the reported proteins in the database, thus confirming the expression of the protein is in line with the previously published authors. In the present work, both the lysins were successfully expressed and the expression of both LysK and Ply V12 protein bands corresponded to the exact molecular weight represented in the protein database. LysK=54.75 kDa Ply V12= 34.13 kDa.

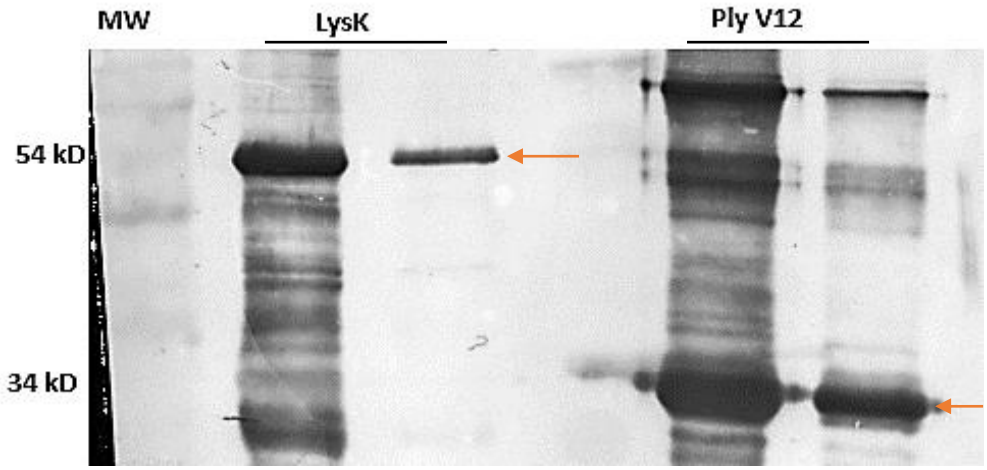

Figure 5.4: western blot analysis using an anti-His monoclonal antibody. Both the protein expressions were indicated by an orange arrow, LysK=54.75 kDa Ply V12= 34.13 kDa.

5.3.3 Protein Production by Bioreactor

We introduced a new molecular approach to achieving high-level protein production by using a customized bioreactor as shown in Figure 5.3 to produce a low-cost recombinant protein production process by closely monitoring controlled environments. For LysK and Ply V12 recombinant protein production, the cultivation of the *E. coli* BL21 (DE3) strain was performed under the same conditions as previously described, but with an additional supply of complex nutrients, 1% Glucose and 0.5mM IPTG under aerobic conditions and culture was stopped after 4h and there is a high-level expression of inclusion bodies that are normally formed in the cytoplasm. To overcome these Inclusion bodies in the final protein both the cell lysates were centrifuged at low speed to purify the protein followed by washing both the pellets with 2 times PBS 1X and 2 times sterile ddH_2O. By using appropriate centrifugation and washing steps, more than 50% of inclusion bodies were removed by the process when compared to the bacterial transformation protein expression and the results are shown in Figure 5.4.

5.3.4 Protein Denaturing and Refolding with Amino Acids

High-level expression of recombinant proteins in *E. coli* often leads to the formation of insoluble protein aggregate, it is an important step that the recombinant protein requires refolding into its active structure to function. To achieve a biologically active recombinant protein from the aggregates, a refolding step is required, most commonly refolding is performed after solubilization in denaturing solution (8 M urea) followed by concentration and dialysis. In the present work, protein refolding is done by amino acids (L-Arginine, L-Cystine HCL and L-cysteine in PBS).

5.3.5 Protein Extraction and Purification

The concentration of LysK and Ply V12 protein was purified from a culture as shown in Figure 5.5. Furthermore, when analyzing the protein content from the bioreactor the result is similar to the first experiment that was obtained. The protein expressions are shown in Figure 5.4.

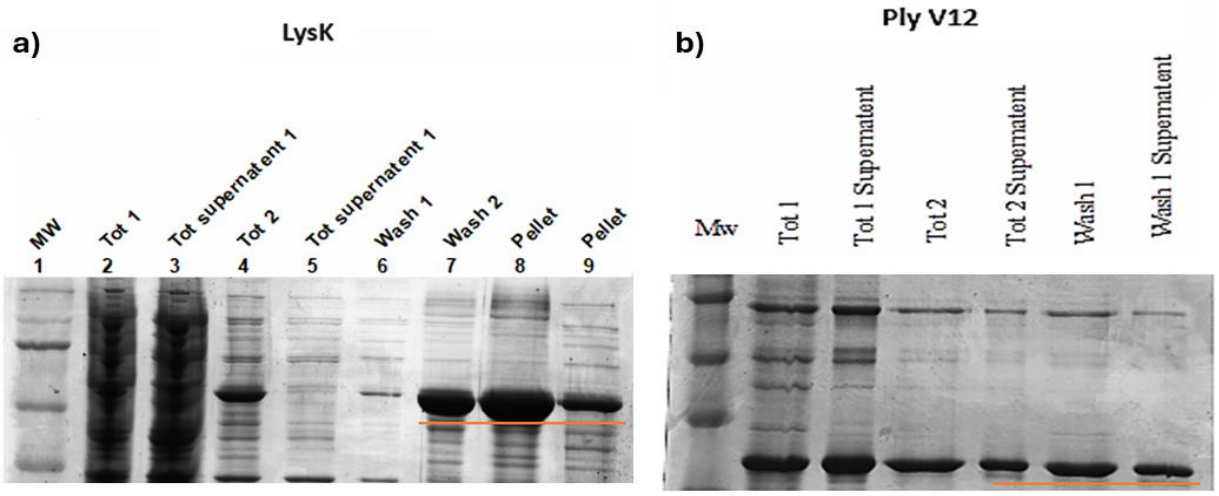

Figure 5.5: Represents the LysK (a) and Ply V12 (b) protein expression derived from cultures are indicated by the orange line, and results are shown by SDS-PAGE (12.5%).

5.3.6 Antibacterial Activity

Firstly, both the recombinant protein's antibacterial activity was performed with low concentrations (shown in Table 5.1). Both the proteins were applied to two Gram-positive strains, *S. aureus* and *S. epidermidis*, as well as to two Gram-negative bacteria that is *E. coli* and *A. actinomycetemcomitans*. Although *S. aureus* and *S. epidermidis* have been primarily linked to bone infections, in this study, I also included two Gram-negative strains. This was because most of the literature suggests that endolysins are only effective against the species (or subspecies) of bacteria from which they were produced. For instance, enzymes produced by streptococcal phage are effective against specific streptococci, and enzymes produced by pneumococcal phage are effective against pneumococci. Therefore, my hypothesis is to test the purified recombinant proteins against both Gram-positive and Gram-negative bacteria. To evaluate any difference in efficacy of the selected recombinant proteins. **(Fischetti 2005)**, when the protein was applied to bacteria it rapidly hydrolyzes the peptidoglycan layer, thus resulting in cell lysis and bacterial death. Both Lys K and Ply V12 results are represented in relative fluorescence units (RFU).

Results are reported in Figure 5.6 a-b; Lys K has shown a strong metabolic reduction towards Both Gram-positive strain *S. aureus* (Figure 5.6a) and Gram-negative strain *E. coli* (Figure 5.6b) when compared to the Untreated controls. All concentrations resulted in significantly reduced bacteria metabolism when compared to the controls at all time points. Moreover, at concentrations of 50µg/µl and 100µg/µl more significant reduction in bacteria metabolism is observed. These results are in line with the previous literature studies,

suggesting that Lys K is an active protein in lysis Gram-positive bacteria through hydrolases that can cleave the bonds in peptidoglycan chains of the Bacteria cell wall. Lys K also showed a metabolic reduction toward Gram-negative bacteria *E. coli*. Furthermore, we couldn't perform the antibacterial activity towards *A. actinomycetemcomitans* and *S. epidermidis* due to protein aggregation.

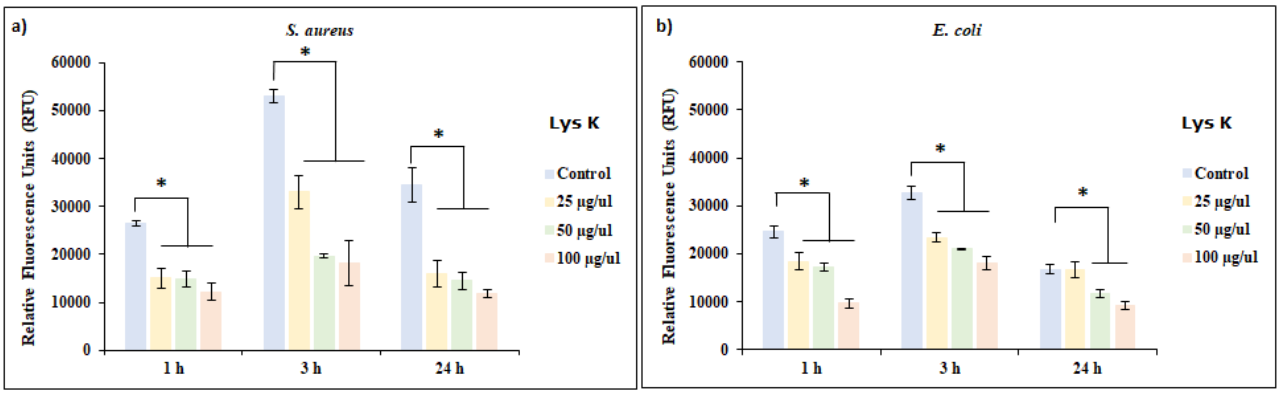

Figure 5.6: Lys K antibacterial activity towards *Staphylococcus aureus* (a) and *Escherichia coli* (b). Lys K was shown as very effective toward the Gram-positive strains *S. aureus* and Gram-negative *E. coli*, especially at 100µg/µl Lys K showed an antibacterial activity when compared to control. Bars represent means and standard deviations. All the tested concentrations were significant towards the control (Indicated by * p<0.01)

Coming to ply V12 Results are reported in Figure 5.7 a – d; Ply V12 is more effective towards Gram-positive strains *S. aureus* and *S. epidermidis* when compared to controls. All the concentrations resulted in a significant reduction of the bacteria metabolism in comparison to controls. Moreover, when increasing protein concentration to 100 µg/µl a more evident metabolic reduction was seen when compared to the controls. Results are in line with the Lys K. Differently, Ply V12 did not show any metabolic activity reduction towards *E. coli* as shown in Figure 5.7d; in fact, there is no difference between the controls and the concentrations. While on the other hand, Ply V12 showed a strong metabolic activity reduction towards *A. actinomycetemcomitans*, especially during at 3 h time points. After 24 h the metabolic activity reduction is seen only in 100 µg/ mL concentration. *A. actinomycetemcomitans* Ply V12 protein lysed the bacteria rapidly at all time points. Thus, confirming the recombinant protein of phages has a strong antibacterial activity towards Gram-positive and Gram-negative bacteria.

These phage-derived peptidoglycan hydrolases are recombinant proteins that cleave the bonds of peptidoglycan chains found in bacterial cell walls and when these proteins are added to bacteria externally as recombinant proteins, it rapidly ruptures the peptidoglycan layer, causing cell rupture and leading to death **(Oliveira, São-José, and Azeredo 2018).** The findings show that the two proteins were effective against Gram-positive and Gram-negative bacteria because they are eliminated rapidly in 1 to 3 h. According to the obtained results from the Alamar blue assay, these recombinant proteins can be a promising tool for development as

next-generation antibiotics to prevent infection in the orthopaedic field **(Chen et al. 2023) (Łusiak-Szelachowska, Weber-Dąbrowska, and Górski 2020).**

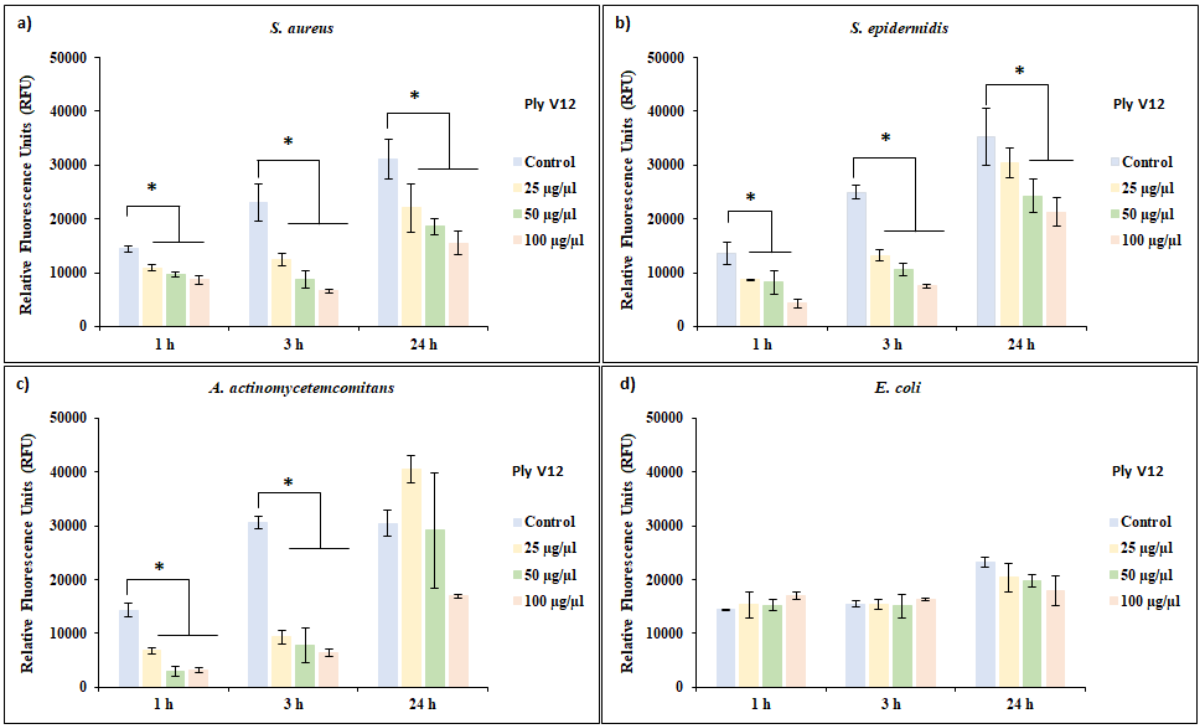

Figure 5.7: Ply V12 antibacterial activity against *S. aureus* (a), *S. epidermidis* (b), *A. actinomycetemcomitans* (c) and *E. coli* (d). Ply V12 was very effective towards all the bacteria, except *E. coli*. All the tested concentrations were significant towards the control (Indicated by * p<0.01).

5.3.7 Cytocompatibility

After the antibacterial activity we, furthermore, tested the Lys K and Ply V12 recombinant proteins to be cytocompatible. According to the literature, these endolysins have emerged as a promising tool for development as the next generation of antibiotics. hMSCs have been selected as emblematic cells due to their pivotal role in bone healing and regeneration. To do this, hMSCs were incubated with the high concentrations shown in Table 5.1.

Figure 5.8 a-b shows the results of hMSCs viability in contact with Lys k and ply V12 protein at both experimental time points (24 and 72 h). No difference in viability was observed between the treated cells and the control after 24 h. In contrast, after 72 h, significant differences were noted between the concentrations and control. However, by comparing the results in function of days, on day 3 both in Lys k and Ply V12 the number of cells was significantly higher when compared to day 1. The metabolic activity for Lys K and Ply V12 proteins was not toxic for the hMSCs after 24 and 72 h. Furthermore, to confirm the cell viability of hMSCs, we performed a live and dead assay at each time point. As shown in Figure 5.8c, the fluorescent live and dead staining confirmed that most of the cells, even in the presence of the high concentrations, the

cells were found to be alive (stained in green). So, our results are in line with the Alamar blue where both the proteins favour the metabolic activity of hMSCs at all time points.

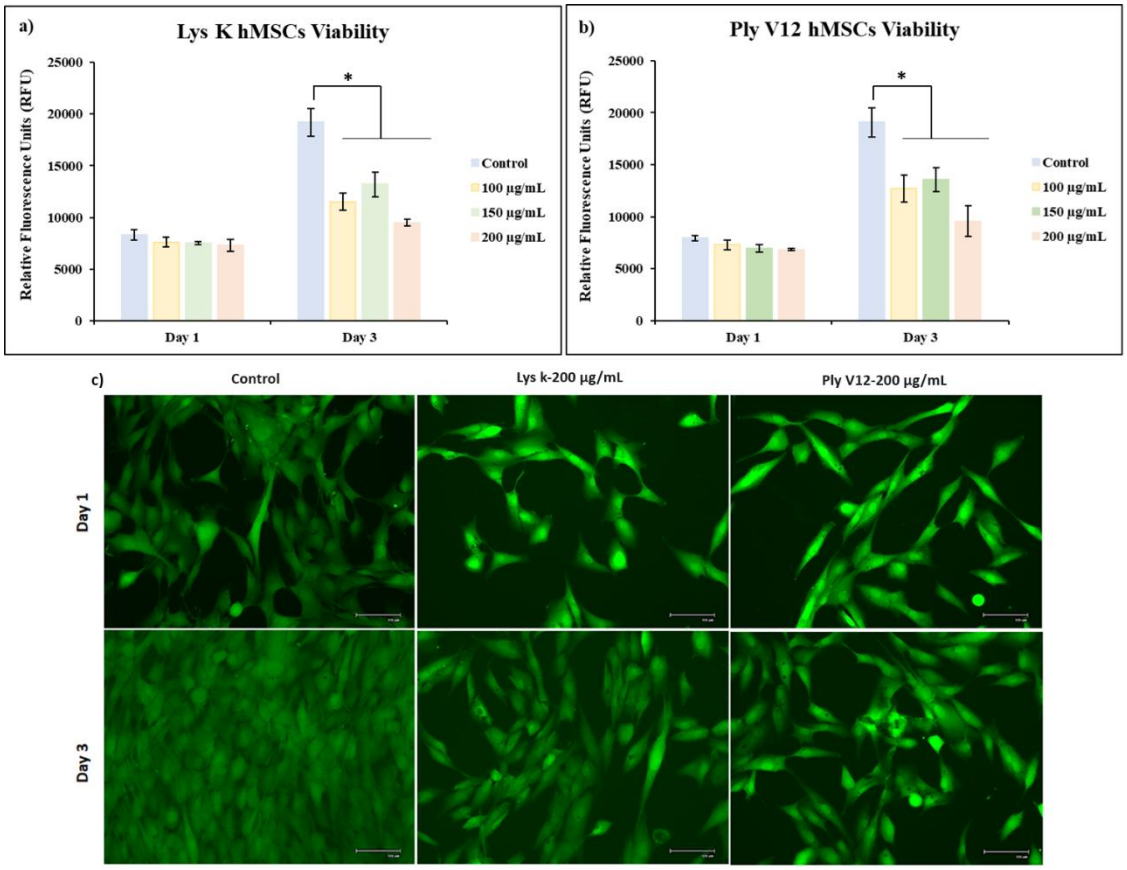

Figure 5.8: Lys K and Ply V12 cytocompatibility. LysK (a) & Ply V12 (b) were shown to be *in vitro* cytocompatible at all tested concentrations in both time points. (c) live and dead staining demonstrated a comparable cell density between test concentrations. Bars represent means and standard deviations. All the tested concentrations were significant towards the control (Indicated by * p<0.01).

5.4 conclusion

By concluding the obtained results, these recombinant proteins can somehow act on Gram-positive and Gram-negative bacteria. It can be a useful antibacterial agent in an era of increasing antibiotic resistance. Further analysis should be addressed to verify the minimum inhibitory concentrations (MICs), biofilm thickness and cell differentiation studies. Endolysins are antibacterial agents with a distinctive way of working, making them very efficient at killing bacteria. Their rapid killing and unlikely resistance development make them an attractive option over traditional antibiotics. These characteristics make them a hopeful option for creating new medications to fight against bacteria that are resistant to multiple drugs, particularly in cases of infections caused by Gram-positive and Gram-negative bacteria. Furthermore, more in vitro validation is required to confirm the hypothesis.

5.5 References

Biondo, Carmelo. 2022. "New Insights into Bacterial Pathogenesis." Pathogens 12 (1): 38. https://doi.org/10.3390/pathogens12010038.

Broendum, Sebastian S., Ashley M. Buckle, and Sheena McGowan. 2018. "Catalytic Diversity and Cell Wall Binding Repeats in the Phage-Encoded Endolysins." Molecular Microbiology 110 (6): 879–96. https://doi.org/10.1111/mmi.14134.

Chen, Xionggang, Jianhong Zhou, Yu Qian, and LingZhou Zhao. 2023. "Antibacterial Coatings on Orthopedic Implants." Materials Today Bio 19 (April): 100586. https://doi.org/10.1016/j.mtbio.2023.100586.

Dedrick, Rebekah M., Bailey E. Smith, Madison Cristinziano, Krista G. Freeman, Deborah Jacobs-Sera, Yvonne Belessis, A. Whitney Brown, et al. 2022. "Phage Therapy of Mycobacterium Infections: Compassionate-Use of Phages in Twenty Patients with Drug-Resistant Mycobacterial Disease." Clinical Infectious Diseases, June. https://doi.org/10.1093/cid/ciac453.

Fischetti, Vincent A. 2005. "Bacteriophage Lytic Enzymes: Novel Anti-Infectives." Trends in Microbiology 13 (10): 491–96. https://doi.org/10.1016/j.tim.2005.08.007.

Łusiak-Szelachowska, Marzanna, Beata Weber-Dąbrowska, and Andrzej Górski. 2020. "Bacteriophages and Lysins in Biofilm Control." Virologica Sinica 35 (2): 125–33. https://doi.org/10.1007/s12250-019-00192-3.

Nelson, Daniel C., Mathias Schmelcher, Lorena Rodriguez-Rubio, Jochen Klumpp, David G. Pritchard, Shengli Dong, and David M. Donovan. 2012. "Endolysins as Antimicrobials." Advances in Virus Research, 299–365. https://doi.org/10.1016/b978-0-12-394438-2.00007-4.

Oliveira, Hugo, Carlos São-José, and Joana Azeredo. 2018. "Phage-Derived Peptidoglycan Degrading Enzymes: Challenges and Future Prospects for in Vivo Therapy." Viruses 10 (6): 292. https://doi.org/10.3390/v10060292.

Petrovic Fabijan, Aleksandra, Ruby C. Y. Lin, Josephine Ho, Susan Maddocks, Nouri L. Ben Zakour, and Jonathan R. Iredell. 2020. "Safety of Bacteriophage Therapy in Severe Staphylococcus Aureus Infection." Nature Microbiology 5 (3): 465–72. https://doi.org/10.1038/s41564-019-0634-z.

Schmelcher, Mathias, David M Donovan, and Martin J Loessner. 2012. "Bacteriophage Endolysins as Novel Antimicrobials." Future Microbiology 7 (10): 1147–71. https://doi.org/10.2217/fmb.12.97.

Summers, William C. 2001. "Bacteriophage Therapy." Annual Review of Microbiology 55 (1): 437–51. https://doi.org/10.1146/annurev.micro.55.1.437.

Chapter VII

Tellurium: An active Element with Multifunctional Properties

Aim

As alternatives to antibiotics, there is now considerable academic research on the use of metal ions to combat pathogenic bacteria and inflammation, as a possible alternative to antibiotics. Metal ions have been increasingly recognized for their potential in reducing bacterial infections and controlling excessive inflammatory responses at the site of injury. Copper, silver, zinc, tellurium, and cerium are some of the metal ions that have been found to inhibit the growth of bacteria and control excessive inflammation effectively. These have become important therapeutic strategies. Due to the toxicity of silver and copper, our attention was drawn towards tellurium. Despite being considered a non-essential trace element, it has recently been investigated for its significant biological effects. For instance, the inorganic tellurium (IV) complex, named AS101, is the most studied compound, due to its potent immunomodulatory properties. Furthermore, phase I and II clinical trials of AS101 as a treatment for neovascular age-related macular degeneration have been completed (NCT03216538).

Chapter VII has been published as a 'research article' in Materials Science and Engineering: C with several authors as collaborators: Miola, Marta, Jonathan Massera, Andrea Cochis, Ajay Kumar, Lia Rimondini, and Enrica Vernè. 2021. "Tellurium: A New Active Element for Innovative Multifunctional Bioactive Glasses." (https://doi.org/10.1016/j.msec.2021.111957). In this paper, the contribution of the author is as follows:

Marta Miola and Enrica Verne: produced the glass composition by partially substituting SiO_2 with TeO_2. along with glass characterization and in vitro bioactivity test

Jonathan Massera: Characterized glasses with Raman spectroscopy.

Ajay Kumar: Performed the biological characterization of the samples in terms of cytocompatibility, anti-inflammatory effect, stem cell differentiation, antibacterial activity and co-culture studies.

Glass synthesis

The glasses were developed by partially substituting SiO_2 with TeO_2. The amount of TeO_2 was selected considering the possible toxic effect of this element and based on the author's previous experience with bioactive glass doping with therapeutic ions. The glasses were synthesized by melting and quenching process. The synthesized glasses were provided by the Politecnico di Torino and in collaboration with the Faculty of Medicine and Health Technology, Laboratory of Biomaterials and Tissue Engineering, Tampere University.

Abstract

Bioactive glasses have been widely investigated for their ability to release ions with therapeutic effects. In this paper, a silica-based bioactive glass was doped with a low amount of tellurium dioxide (1 and 5 mol%) to confer antibacterial and antioxidant properties. The obtained glasses were characterized in terms of morphology, composition, structure, characteristic temperatures and in vitro bioactivity. Moreover, comprehensive analyses were carried out to estimate the cytocompatibility, of the antibacterial and antioxidant properties of Te-doped glasses. The performed characterizations demonstrated that the Te insertion did not interfere with the amorphous nature of the glass, the substitution of SiO_2 with TeO_2 led to a slight decrease in Tg and a TeO_2 amount higher than 1 mol% can induce a change in the primary crystal field. In vitro, the bioactivity test demonstrated the Te-doped glass's ability to induce the precipitation of hydroxyapatite. Finally, the biological characterization showed strong antibacterial and antioxidant effects of Te-containing glasses in comparison with the control glass, demonstrating that Te is a promising element to enhance the biological response of biomaterials.

Introduction

Bioactive glasses, discovered by Professor Larry Hench fifty years ago, have been widely investigated for their role in bone tissue regeneration, since they can chemically bond to living bone through a well-known process, which involves a rapid ion exchange between glass surface and surrounding biological fluids, leading to the formation of biologically active hydroxyapatite (Hap) **(Cao and Hench 1996)**. Recently, the role of bioactive glasses in soft tissue regeneration has been also explored **(Miguez-Pacheco, Hench, and Boccaccini 2015) (Baino, Hamzehlou, and Kargozar 2018)** and it has been demonstrated that the controlled release of specific ions can stimulate several processes that regulate the regeneration of hard and soft tissues. For example, Si, Ca, P and Mg play a fundamental role in the formation and calcification of bone tissue, also Sr stimulates bone formation and reduces bone resorption. Other elements, such as Cu and Co, stimulate the proliferation of human endothelial cells and enhance the angiogenesis processes. Finally, different elements, such as Ag, Cu, Zn, and Ga, possess antimicrobial/anti-inflammatory properties.

In the last years, many efforts have been made to improve the biological activity of bioactive glasses, by the incorporation of tailored amounts of active elements, such as Sr, Cu, Ag, Zn, Mn, etc. in the glass formulation **(Isaac et al. 2011) (Vernè et al. 2005) (Miola and Verné 2016) (Miola et al. 2014)**. In this perspective, the efforts of the researchers have been addressed to design new bioactive glass compositions by doping both silica and phosphate-based glasses with therapeutic ions and investigating the effect of their release on cell viability and on gene stimulation towards regeneration and self-repair path (i.e. the genetic design of bioactive glasses **(Hench 2009) (Hoppe, Mouriño, and Boccaccini 2013).**

Among the functionalities that can be imparted by active ions, the antimicrobial properties are the most investigated **(Vernè et al. 2005) (Miola and Verné 2016) (E. Verné et al. 2008) (Palza et al. 2013)**. Moreover, the antioxidant effect of some bioactive glass formulations has been also explored **(Pedone et al. 2016).** The increasing growth of microorganisms is resistance to antibiotics **(Aslam et al. 2018)** leads the researchers to inspect the antimicrobial role of different agents and develop innovative materials able to reduce the adhesion and proliferation of bacteria, thus limiting infection development. Bioactive glasses compositions containing antibacterial elements, such as Ag, Cu, Zn and Ga, have been deeply examined **(Vernè et al. 2005) (Miola and Verné 2016) (E. Verné et al. 2008) (Palza et al. 2013)** and their ability to limit the bacterial growth was confirmed also towards antibiotic-resistant strains. However, recently, the ability of bacteria to develop resistance towards also metallic ions, such as silver ions, was observed **(Hobman and Crossman 2015) (Maillard and Hartemann 2012)** for this reason, there is a continuous need to create new solutions for infection control and to find new antimicrobial agents.

Among the poorly explored elements with potentially antibacterial and antioxidant properties, tellurium has attracted our attention since, although it is considered a non-essential trace element and shows a dose-related and chemical form-related toxicity, its important biological effects have been recently investigated **(Ba et al. 2010) (Zhong et al. 2013)**.

Tellurium (Te) is an element belonging to the chalcogens group showing different oxidation states that have been barely considered in biology and biochemistry. However, some studies demonstrated that Te, and its compounds, can be used as biomarkers, as well as possess antimicrobial, antioxidant and antitumoral effects **(Ba et al. 2010).** In particular, **(Zhong et al. 2013)** demonstrated that tellurium dioxide nanoparticles (TeO_2 NPs) have strong antioxidant activity and antimicrobial effect against some Gram-negative (*Escherichia coli, Salmonella enteritidis*) and Gram-positive (*Bacillus subtilis*) bacteria. Recently, another study **(Shakibaie et al. 2017)** investigated the antimicrobial and antioxidant activity of tellurium nanorods biologically synthesized by *Pseudomonas pseudoalcaligenes* in comparison to K_2TeO_3. This study showed a higher antioxidant effect of Te nanorods than K_2TeO_3; on the contrary, the antibacterial and antifungal activity of nanorods was significantly lower than K_2TeO_3. However, the authors affirmed that further investigations are required to investigate the mechanism of action of biosynthesized Te nanorods.

Besides, very few studies are concerned with the development of Te-doped biomaterials. **(Ma et al. 2011)** synthesized a tellurium/calcium silicate nanocomposite composed of tellurium nanorods dispersed in the calcium silicate matrix. This composite evidenced good biocompatibility at low nanorods concentration (10–20 μg/mL) towards human gastric carcinoma cells (MGC-803); nevertheless, the authors did not investigate the potential antimicrobial and/or antioxidant effect of the Te-containing composite. Moreover, based on the

authors' knowledge, there is only one study concerning the development of a bioactive glass containing tellurium **(El-Damrawi, Doweidar, and Kamal 2014)** synthesized tellurite glasses/glass ceramics, by completely substituting silica with TeO_2, and studied this composition from the viewpoint of bioactivity. They demonstrated the Te-based glasses/glass ceramics' ability to induce the nucleation of hydroxyapatite and thus the possibility of being used as a bioactive implant. However, this study did not evaluate the possible toxic effects of the Te-based material and did not investigate their possible efficacy in terms of antimicrobial and antioxidant effects.

In this work, we evaluate for the first time the possibility of developing innovative silica-based bioactive glasses containing a low amount of tellurium dioxide, in order to impart both antibacterial and antioxidant properties, maintaining contemporaneously the cytocompatibility. For this reason, we doped a bioactive glass composition with low amounts of TeO_2 (1 and 5 mol%), by substituting SiO_2 with TeO_2, and we characterized the obtained samples in terms of, morphology, composition, structure, reactivity in simulated physiological fluids and biological response (cytocompatibility, antioxidant and antibacterial effect).

6. Materials and Methods

Square samples measuring 10 × 10 × 1 mm samples were sterilized by heat for 3 hours at 100°C and then kept at room temperature shielded from light until the biological experiments. The samples' composition is shown in Table 6.1.

Table 6.1: The table represents the samples' names and composition.

No	Samples' names	Coating
1	STe0	NO coating (Control)
2	STe1	Tellurium dioxide 1 Mol%
3	STe5	Tellurium dioxide 5 Mol%

6.1 Biological Characterization

6.1.1 Cytocompatibility Evaluation

For cytocompatibility, human bone marrow-derived stem cells (hMSCs) were obtained from Merck (Promo Cell C-12974) and cultivated in low-glucose Dulbecco's modified Eagle Medium (DMEM, Merck) supplemented with 15% fetal bovine serum (FBS, Merck) and 1% antibiotics (penicillin/streptomycin, Merck) at 37°C, 5% CO_2 atmosphere. Cells were cultivated until 80-90% confluence, detached by a trypsin-EDTA solution (0.25% in PBS, from Merck), harvested, and used for the experiments.

Cells were directly seeded onto the samples' surface at a constant concentration (3×10^4 cells/sample) and cultivated for 1, 2 and 3 days. At each time point, the viability of the cells in direct contact with samples was

evaluated utilizing the metabolic colourimetric Alamar blue assay (AlamarBlue™, from Life Technologies) as previously explained in section 4.1.7.

6.1.2 ROS/RNS Scavenge

Cells were seeded onto samples' surfaces as previously described for the metabolic evaluation. At 1, 2 and 3 days, cells were treated with 300 µM H_2O_2 for 3 h/day to test tellurium antioxidant activity to scavenge the derived ROS and RNS species **(Lu et al. 2017).** Cell metabolism was checked by the Alamar blue to compare values pre- and after H_2O_2 treatment. The active species quantification was performed with the fluorescent OxiSelect™ assay (from Cell Biolabs) following manufacturers' instructions. Briefly, 50 µl of the test samples' supernatants were collected and mixed with 50 µl of catalyst and 100 µl of the DCFH solution (both provided from the kit); after 45 min incubation, the fluorescence signal was evaluated by spectrophotometer (Spark®, Tecan Trading AG, CH) using the following set-up: fluorescence excitation wavelength 480 nm, fluorescence emission reading 530 nm. Cells cultivated onto bioactive glasses without H_2O_2 stress were considered as controls.

6.1.3 Osteogenesis

Cells were directly seeded onto the samples' surface at a constant concentration (2×10^4 cells/sample) and cultivated for 7, 14 and 21 days in the presence of osteogenic medium (low-glucose DMEM supplemented with 10% FBS, 10−7 M dexamethasone, 50 µM β-glycerophosphate, 20 mM ascorbic acid). Cells were stressed with 300 mM H_2O_2 for 3 h/day as previously described; then, at each time-point, the supernatants were collected, and the alkaline phosphatase (ALP) activity was measured to evaluate osteogenesis progression in the presence of inflammation. ALP activity was evaluated by a colourimetric assay (ab83369, from Abcam, UK) following the Manufacturer's instructions: briefly, 80 µl of supernatants were collected from each sample and mixed with 50 µl of the pNPP solution and 10 µl of the ALP enzyme. After 60 minutes of incubation, the reaction was stopped and the optical density was measured by spectrophotometer (Spark®, Tecan Trading AG, CH) using a 405 nm wavelength.

After 21 days of culturing, the formation of calcium deposits was evaluated by the alizarin red staining. Briefly, cells were fixed (4% formaldehyde, 15 min) and then incubated for 30 min with the alizarin solution (from Sigma, 40 mM in PBS). Afterwards, deposited alizarin was solved with 10% acetic acid (5 min), collected and centrifuged to separate the pellet (20,000g, 15 min). Supernatant optical density was evaluated by a spectrophotometer (Spark®, Tecan Trading AG, CH) at 490 nm wavelength.

6.1.4 Antibacterial Activity

To test the antibacterial activity of the tellurium-doped glasses, the orthopedic-related strains *S. aureus* and *S. epidermidis.* Strain growth conditions were explained in section 5.2.11. were used bacteria concentration was adjusted to 1×10^5 cells/mL by diluting in fresh media until the optical density of 0.001 at 600 nm was reached as determined by spectrophotometer (Spark®, Tecan Trading AG, CH).

6.1.5 Biofilm Formation

Sterile samples were gently placed into a 24 multiwell plate with sterile tweezers avoiding any surface damages. Each sample was submerged with 1 mL of the 1×10^5 cells/mL broth bacteria culture prepared as prior described; the plate was incubated for 90 min in agitation (120 rpm) at 37^0C to allow the separation between adherent biofilm cells and not-adherent floating planktonic cells (separation phase) **(Cochis et al. 2016)**. Afterwards, supernatants containing planktonic cells were removed and replaced with 1 mL of fresh media to cultivate surface-adhered biofilm cells (growth phase). Biofilm was grown at 37°C for 1, 2 and 3 days before evaluations.

6.1.6 Biofilm Metabolic Evaluation

At each time-point, samples were gently washed 3 times with PBS to remove non-adherent cells and then moved to a new 24 multiwell plate where bacteria metabolic activity was evaluated by the Alamar blue assay as previously described in section 4.1.7.

6.1.7 hMSCs-Bacterial Culture

Samples' ability to preserve cells from infection was evaluated by a cells-bacteria co-culture assay as previously described by the Authors **(Jekabsone et al. 2019).** A defined number (3×10^4 cells/sample) of hMSCs were seeded onto the samples' surface and allowed to adhere and spread for 24 h at 37°C. The day after, the medium was removed, and samples were infected with 1 mL of antibiotics-free DMEM containing 1×10^5 bacteria (*S. aureus* or *S. epidermidis*). After 24 h infection, samples were collected and surface-adhered cells and bacteria were detached by trypsin digestion (10 min at 37°C); cells were marked by trypan blue and counted by a Burker chamber to determine the viable number, while bacteria were diluted by 6-ten-fold dilutions step and numbered by the CFU count, as prior described **(Fancello et al. 2020)**.

6.2 Results and Discussion

6.2.1 Cytocompatibility and ROS/RNS Scavenge Ability

Bioactive glasses are a well-known and established category of biomaterials aimed at bone replacement and repair due to their ability to promote naïve bone healing **(Baino, Hamzehlou, and Kargozar 2018) (Kaur et al. 2015) (Karadjian et al. 2019)**. The osteoinductive and osteoconductive properties of bioactive glasses are attributable to the continuous Ca^{2+} and Na^{+} ions release which leads to the formation of a hydrated silica gel layer on the surface that is fast crystallized into a hydroxycarbonate apatite layer **(Baino, Hamzehlou, and Kargozar 2018) (Kaur et al. 2015) (Karadjian et al. 2019)**. Moreover, many ions such as silver **(E. Verné et al. 2008) (Newby et al. 2011)**, copper **(Miola and Verné 2016)**, strontium **(Özarslan and Yücel 2016)** and magnesium **(Bellucci et al. 2017)** have been investigated to impart a therapeutic activity to the bioactive glasses; however, to the best of our knowledge, this is the first time that tellurium was used as a doping element in a bioactive glass composition to obtain an osteogenic, anti-bacterial and anti-inflammatory material. Accordingly, the first in vitro samples' cytocompatibility evaluation was done towards mesenchymal stem cells that were selected as representative cells deputed to undertake the self-healing process **(Lin et al. 2017)**.

Results are summarized in Figure 6.1a. In general, tellurium doping did not increase bioactive glass samples' toxicity; in fact, results obtained from cells metabolic activity assay were comparable between tellurium-doped samples (STe1 and STe5) and untreated controls (STe0, $p > 0.05$) within a 72-hour long test period. As prior mentioned, it is not easy to compare these findings with previous literature as tellurium was never applied to bioactive glasses cements or other bone-dedicated materials as well and only a few works deal with the cytocompatibility of tellurium for biomedical applications. However, in those few examples, tellurium was described as a safe element: **(Lu et al. 2017)** showed that a tellurium-based antioxidant was effective in modulating H_2O_2-induced inflammation and thus preserving the viability and the ALP release of MC3T3 pre-osteoblasts from oxidative stress without any side toxic effect. Similarly, **(Ada Vernet Crua et al. 2019)**. demonstrated that tellurium nanowires hold a targeted toxic effect towards cancerous melanoma cells while no side effects were noticed when the same materials were applied in contact with healthy dermal fibroblasts. However, despite these promising results, much more information is still required to better understand the safety range of tellurium; here, we can hypothesize that it is not toxic within a 5% molar range when combined with bioactive glasses.

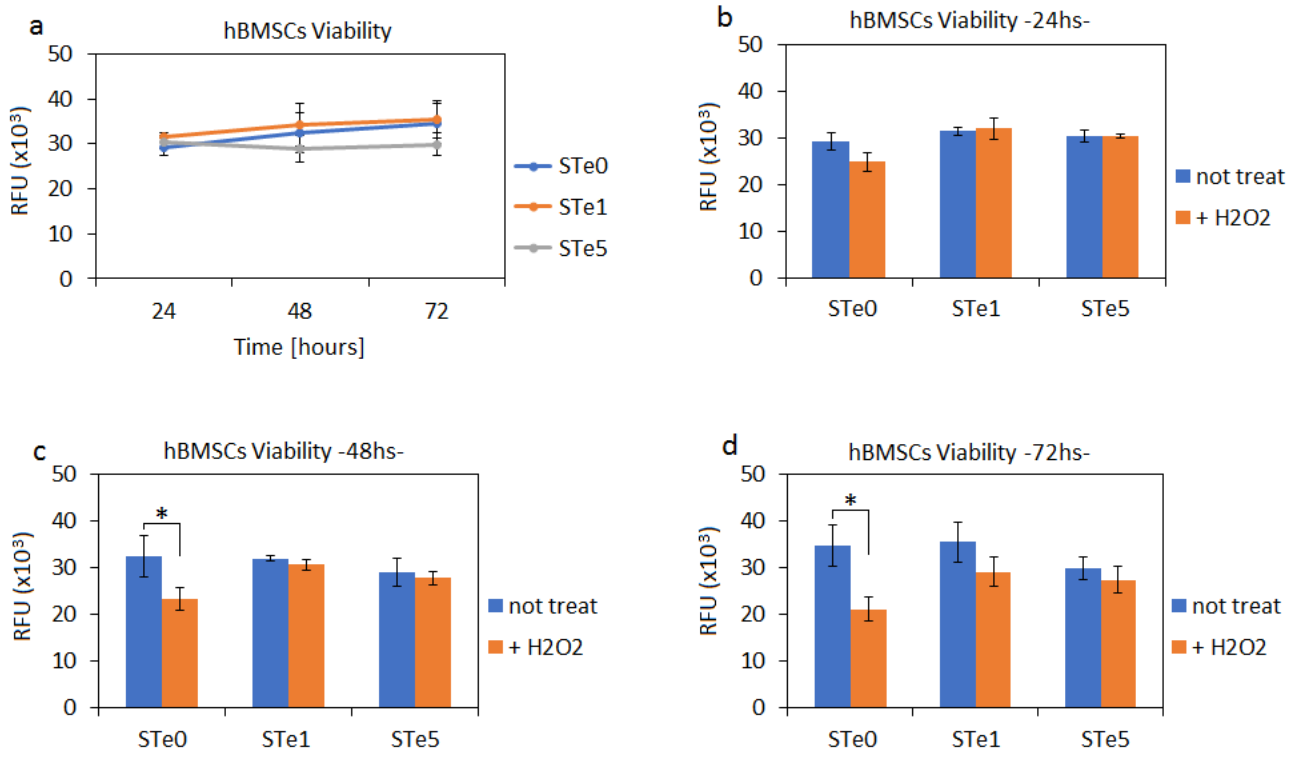

Figure 6.1: (a) hMSCs metabolic activity after 24-, 48- and 72-hour direct cultivation onto samples' surface. Tellurium doping (STe1-STe5) did not introduce toxic effects as the metabolism of cells cultivated onto doped samples was comparable to that obtained from control ones (STe0, $p > 0.05$). (b–d) hMSCs metabolic activity after 24 (b), 48 (c) and 72 (d) hours of direct cultivation onto samples' surface with (+ H_2O_2) and without (untreated) hydrogen peroxide treatment. While in the untreated controls STe0 samples' cell viability was significantly reduced after 48- and 72-hour H_2O_2 treatment ($p < 0.05$, indicated by *), the tellurium doped ones (STe1-STe5) preserved cell metabolic activity.

Unlike cytocompatibility, tellurium's anti-inflammatory properties have been proven. From this point of view, some very promising examples are reported in the literature: **(Dardik et al. 2016)** demonstrated that a small organotellurium compound octa-O-bis-(R, R)-tartarate ditellurane was effective in suppressing inflammation in human retinal pigment epithelium, while **(Brodsky et al. 2010)** showed how the use of tellurium was useful for macrophages modulation through the nitric oxide and NF-kappaB signalling. Very promising results were also obtained in vivo where tellurium compound AS101 was effective in reducing autoimmune encephalomyelitis by suppressing monocyte and T cell infiltration into the central nervous system in mice **(Jun Ho Lee et al. 2013)**.

Here we evaluated tellurium doping anti-inflammatory efficacy in terms of cell viability preservation **(Varini et al. 2019)** under oxidative stress conditions induced by a toxic H_2O_2 dosage (300 µM) **(Lu et al. 2017).** Results are summarized in Figure 6.1b–d. In general, tellurium insertion was effective in protecting cells from apoptosis induced by the H_2O_2 treatment. While in the untreated controls, STe0 samples' cell viability was significantly reduced after the H_2O_2 treatment after 48 and 72 h ($p < 0.05$, indicated by *), the tellurium doped

ones (STe1-STe5) preserved cells metabolic activity as no significant differences were obtained by comparing untreated and stressed samples (+ H_2O_2). So, our results seem to be in line with the previous literature thus confirming the cells-protective anti-inflammatory ability of tellurium even when used as a doping for bioactive glasses within a 1–5% molar range.

The correlation between tellurium, cell metabolism and oxidative stress has been confirmed by the supernatant active species (ROS/RNS) scavenge results that are reported in Table 6.2. In general, obtained values demonstrated that the lack of tellurium (STe0) determined the highest values of ROS/RNS in comparison with doped ones (STe1 and STe5) at all the time points without the oxidative stress induced by the H_2O_2. STe0 ranged from 2045 to 2198 RFU while STe1 from 1700 to 1931 and STe5 from 1606 to 1732, thus showing differences even at the basal level. When the H_2O_2 was added to introduce oxidative stress, a similar trend was observed: STe0 reported the highest values included from 2528 to 2735 RFU while STe1 from 2391 to 2613 and STe5 from 2387 to 2499. Accordingly, we can hypothesize that the hMSCs viability (Figure 6.1b–d) was not significantly decreased by the H_2O_2 stress due to the ability of tellurium to restrain the formation of toxic oxygen and nitrogen active species. So, we here confirmed the previously debated tellurium anti-inflammatory properties even when it was embedded into bioactive glasses.

Table 6.2: represents the supernatant release of ROS/RNS quantification (values are expressed in means ± standard deviation in relative fluorescent units – RFU).

Samples'	Timepoint (hours)	H_2O_2	ROS/RNS (RFU)
STe0	24	-	2045.3 (±25.0)
STeO+H_2O_2	24	+	2528.6 (±44.4)
STe1	24	-	1700.3 (±136.8)
Ste1+ H_2O_2	24	+	2391.6 (±59.6)
STe5	24	-	1606.6 (±76.5)
STe5+ H_2O_2	24	+	2387.6 (±121.0)
STe0	48	-	1975.6 (±96.7)
STeO+ H_2O_2	48	+	2677.0 (±7.5)
STe1	48	-	1723.0 (±99.4)
STe1+ H_2O_2	48	+	2588.6 (±194.9)
STe5	48	-	1547.3 (±27.6)
STe5+ H_2O_2	48	+	2462.6 (±123.0)
STe0	72	-	2198.0 (±223.9)
STeO+ H_2O_2	72	+	2735.0 (±75.1)
STe1	72	-	1931.0 (±42.2)
STe1+ H_2O_2	72	+	2613.0 (±242.0)
STe5	72	-	1732.6 (±48.3)
STe5+ H_2O_2	72	+	2499.0 (±245.4)

6.2.2 Antibacterial Activity

Unlike the lack of a large literature regarding tellurium and tellurium-doped composites cytocompatibility, its antibacterial properties have been demonstrated for many years. Moreover, the antibacterial effect ascribed to the tellurium seems to be broad-range and effective towards both planktonic and biofilm species. **(Zonaro et al 2015).** demonstrated that the use of Te0-based nanoparticles bio-synthesized from tellurite by *Stenotrophomonas maltophilia* and *Ochrobactrum* were effective in decreasing the viability of *E. coli, P. aeruginosa* and *S. aureus* planktonic cells as well as to eradicate the biofilm counterpart. Similarly, **(Chua et al. 2015)** identified in the secondary messenger cyclic di-GMP of *P. aeruginosa* the pathway affected by tellurite in planktonic and biofilm viability reduction.

Tellurium resulted as successful in introducing antibacterial properties even when used as a doping element into polymeric composites: 4 wt% tellurium-doped poly (methyl methacrylate) fibres resulted in resistance to *E. coli* K12 strain infection as demonstrated by the CFU count **(Mohan Edirisinghe et al. 2018a)**.

In this work, we decided to test tellurium-doped bioactive glasses towards *S. aureus* and *S. epidermidis* biofilm because they are the most frequent strains involved in orthopaedics infections **(Sorrentino et al. 2018)**. Results are summarized in Figure 6.2.

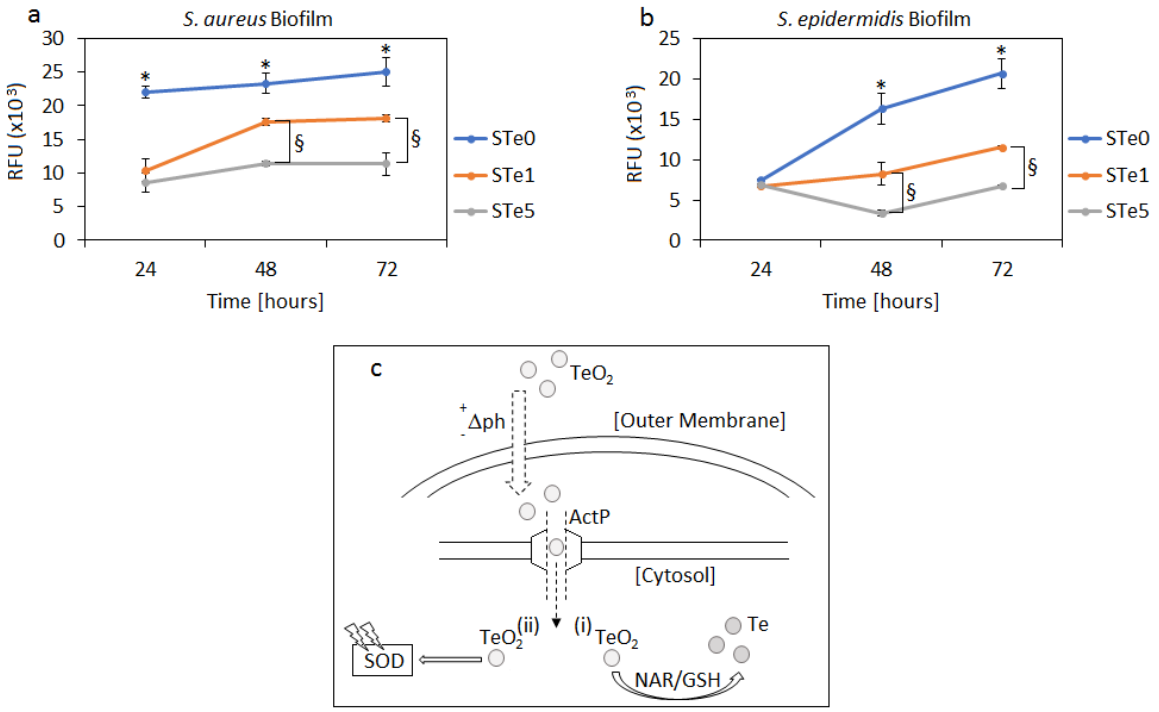

Figure 6.2: (a) *S. aureus* biofilm metabolic activity evaluation. Tellurium insertion (STe1 and STe5) determined a significant reduction of bacteria viability at a time-point in comparison with untreated control STe0 ($p < 0.05$, indicated by the *). However, the effect was dose-dependent as STe5 was significant in comparison with STe1 after 48 and 72 h ($p < 0.05$ indicated by the §). (b) *S. epidermidis* biofilm metabolic activity evaluation. Tellurium insertion (STe1 and STe5) determined a significant reduction of bacteria viability in comparison with untreated control STe0 ($p < 0.05$, indicated by the Again), a dose-dependent effect was observed as STe5 was significant in comparison with STe1 after 48 and 72 h ($p < 0.05$ indicated by the §). (c) Schematic representation of tellurium-derived toxicity in bacteria.

The tellurium insertion bestowed on glass a strong ability to inhibit biofilm formation, even if in a dose-dependent manner. In fact, STe1 and STe5 resulted as significant in terms of biofilm metabolic reduction in comparison with the untreated STe0 (considered as control) for both *S. aureus* (Figure 6.2a, $p < 0.05$, indicated by *) and *S. epidermidis* (Figure 6.2b, $p < 0.05$, indicated by *). However, the effect was dose-dependent as STe5 was significant in comparison with STe1 after 48 and 72 h (Figure 6.2a–b, $p < 0.05$ indicated by the §). Tellurium's antibacterial effect is due to a combination of different mechanisms that are probably not yet fully revealed; however, a clear explanation of some of the correlated events was given by **(Turner, Borghese, and Zannoni 2012)** and it is schematized and adapted in the cartoon in Figure 6.2c. Briefly, tellurite can exceed the outer membrane as a response to an environmental pH variation and then the toxic metalloid can reach the cytosolic space by exploiting the acetate permease (ActP) transport mechanism. Here, tellurite can be

toxic as it is by influencing the activity of the superoxide dismutase (SOD) that is required to counteract the oxygen species (ROS) formed due to the parallel Fenton reaction involving the metalloid reduction. The same reduction into metallic Te0 (for example through membrane-bound nitrate reductase NAR or thioredoxin-glutathione GSH system) can be toxic due to the accumulation that brings into homeostasis impairment. Based on these considerations, our results seem to be in line with the present literature thus opening to the use of tellurium as an interesting antibacterial tool to improve the resistance towards a possible infection of bioactive glasses.

6.2.3 Osteogenesis

As prior mentioned, bioactive glasses are materials mainly aimed at bone replacement and healing. Accordingly, here mesenchymal stem cells osteogenic differentiation was considered to study any eventual positive or negative event due to the presence of tellurium. Therefore, the activity of alkaline phosphatase (ALP) was considered over a 7–10–15–21-day period as an indicator of the progressive cell commitment. However, results did not reveal any significant differences in terms of ALP activity by comparing controls (STe0) and tellurium-doped samples (STe1 and STe5) thus not suggesting any improvement or worsening due to the presence of the metalloid (Figure 6.3a, $p > 0.05$). These findings are like those previously presented by **(Lu et al. 2017).** where the ALP activity of murine pre-osteoblasts MC3T3 cells was not affected after exposure to a tellurium-based antioxidant compound. However, very few works directly correlate tellurium and osteogenesis thus making necessary further study to fully evaluate this process.

Afterwards, keeping in mind the promising results obtained by the ROS/RNS scavenge activity, the ALP activity was further evaluated in the presence of H_2O_2-induced oxidative stress. Results are reported in Figure 6.3b. After 7 and 10 days, no significant differences were noticed between control (STe0) and tellurium-doped ones (STe1 and STe5), and ALP values were comparable to the previous assay performed in the absence of H_2O_2 (Figure 6.3a). However, after 15 and 21 days some differences were noted as STe1 and STe5 ALP results were significant towards STe0 controls (Figure 6.3b, $p < 0.05$, indicated by *) and comparable with the previous H_2O_2-free assay. A direct correlation between tellurium ROS scavenge activity and ALP activity preservation can be hypothesized because H_2O_2 is known to be effective in interfering with osteogenic differentiation including ALP and collagen type I expression by the ERK and ERK-dependent NF-kB activation **(Bai et al. 2004)**. Finally, to further prove the mesenchymal stem cells seeded onto STe1 and STe5 samples were correctly committed towards osteoblast lineage despite the oxidative stress induced by hydrogen peroxide, an alizarin red assay was performed to verify the presence of a bone-like mature calcified matrix. As previously shown by the ALP activity evaluation, alizarin staining confirmed that only untreated STe0 samples significantly decreased the number of calcified deposits by comparing results with and without H_2O_2 (Figure 6.3c, $p < 0.05$, indicated by the *). On the opposite, alizarin results for STe1 and STe5 were comparable between treated and

control groups. So, the tellurium activity in terms of ROS scavenges was effective in preserving the osteogenesis of cells cultivated on the surface of bioactive glasses imposed to an oxidative stress condition.

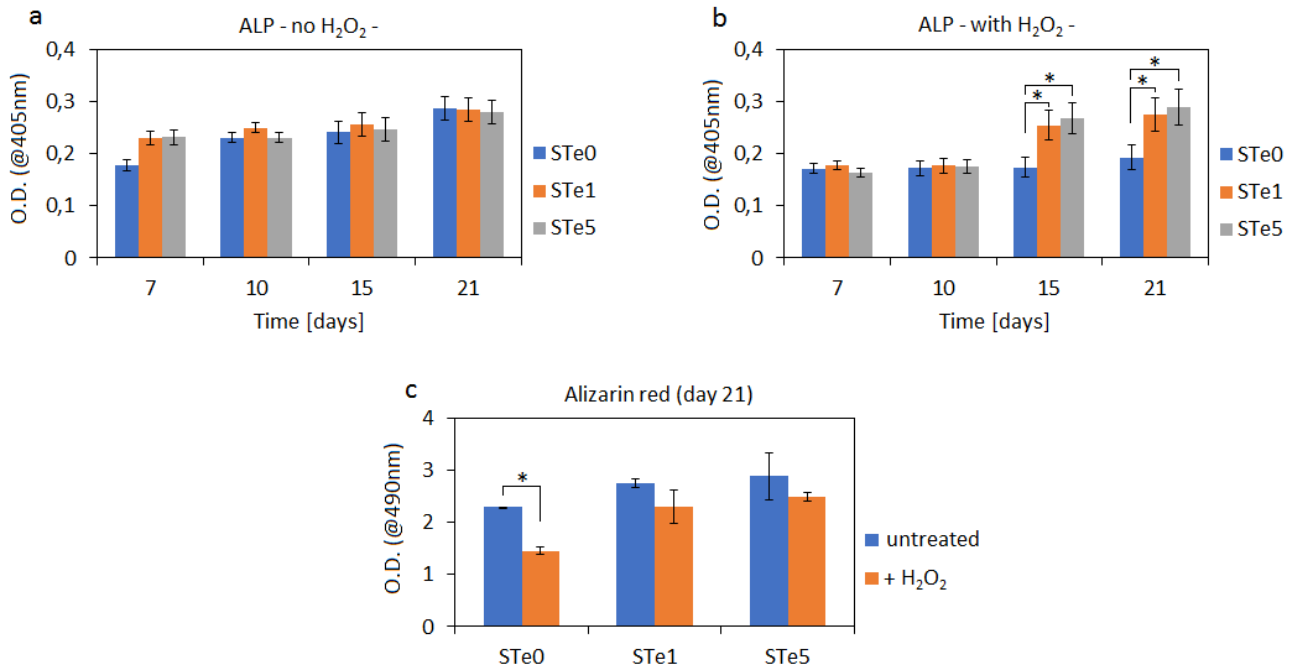

Figure 6.3: Alkaline Phosphatase and Alizarin red specific osteogenic markers evaluation. Tellurium doping (STe1 and STe5) did not increase ALP activity (a, $p > 0.05$) but preserved its expression in the presence of pro-inflammatory H_2O_2 (b, $p < 0.05$ vs STe0 control, indicated by *). As a confirmation, the amount of calcium deposit evaluated by alizarin red was preserved for STe1 and STe5 while was significantly reduced for STe0 control (c, $p < 0.05$, indicated by *).

6.2.4 hMSCs-Bacteria Culture

Further biological tests (hMSCs-Bacteria cultures) were applied to evaluate how the doped surfaces can act concerning the competition between cells and bacteria for surface colonization in a sort of "race for the surface" as first postulated by **(Gristina 1987)**. This assay was designed to resemble the most frequent clinical scenario where patients who underwent orthopaedic surgery and bone implantation are subjected to postoperative infection during late healing. Secondary infections are nowadays frequent increasingly, thus representing a huge problem for patients due to the need for a second surgery necessary to recover the device fixation **(Zhang et al. 2017)**. Accordingly, here we first seeded the cells directly onto the samples' surface and after 24 h of cultivation the infection was induced by inoculating *S. aureus* or *S. epidermidis* as schematized in Figure 6.4a. Similar procedures were previously applied in the literature to evaluate materials' surface properties to favour the device colonization from cells over bacteria **(Subbiahdoss et al. 2009) (McConda et al. 2016) (Lee et al. 2010).**

Our results were very promising from this point of view but unlike antibacterial assays (Figure 6.2), only STe5 samples were effective in significantly reducing bacteria number and preserving cell viability when they were cultivated in the same environment (Figure 6.4b–e). In fact, when the infection was done with *S. aureus*, the number of viable cells was significantly higher for STe5 in comparison with untreated STe0 (Figure 6.4b, $p < 0.05$, indicated by *) while STe1 was not significant towards control. Similarly, the CFU count reported a significant decrease in viable bacterial colonies only when they were cultivated onto STe5 surfaces (Figure 6.4d, $p < 0.05$, indicated by *). The difference between STe1 and STe5 was more evident by using *S. epidermidis* as both viable cells (Figure 6.4c) and CFU count (Figure 6.4e) revealed significant results by comparing STe5 vs Ste0 ($p < 0.05$, indicated by *) and STe5 vs STe1 ($p < 0.05$, indicated by #). Accordingly, only samples STe5 were effective in preventing infections by the co-culture assays.

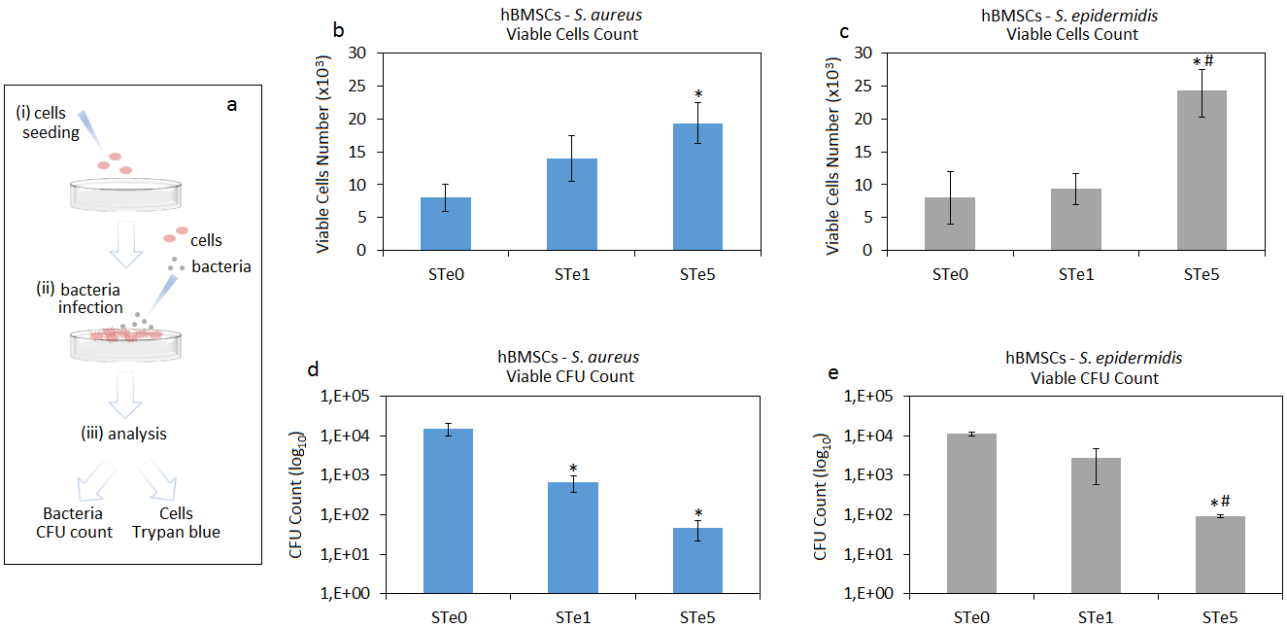

Figure 6.4: hMSCs-bacteria culture. (a) Samples were pre-seeded with cells and then infected using *S. aureus* (b–d) or *S. epidermidis* (c–e). Results showed that only STe5 were able to significantly preserve cells from the infection in comparison with STe0 (b and c, $p < 0.05$, indicated by the *) and STe1 (c, $p < 0.05$, indicated by the #); similarly, the CFU number was significantly decreased by STe5 in comparison with STe0 (b and c, $p < 0.05$, indicated by the *) and STe1 (c, $p < 0.05$, indicated by the #). Bars represent means and standard deviations.

6.3 Conclusion

In this work, Te-doped glasses were synthesized by melting and quenching process and characterized to investigate the influence of Te introduction in the glass properties and the possible biological effect imparted by Te presence. The performed analyses demonstrated that Te-containing glasses showed an amorphous structure and a slight change in characteristic temperature, in particular for glass doped with 5 mol% of TeO_2. The prepared glasses maintained a good degree of bioactivity since they can promote the in vitro precipitation of HAp in a few days.

The biological characterization demonstrated that Te-doped glasses preserved the cytocompatibility; moreover, tellurium insertion was effective in protecting the cell's metabolic activity from apoptosis induced by the H_2O_2 treatment. Antibacterial tests showed a clear antibacterial effect of Te-containing glasses and a strong ability to inhibit biofilm formation, in a dose-dependent manner. The evaluation of osteogenic markers confirmed the ability of Te-containing glasses to preserve the ALP and Alizarin red expression in the presence of oxidative stress. Finally, cell-bacteria co-cultures confirmed that Te presence significantly preserves cells from the infection, in particular for STe5 glass. Therefore, thanks to the strong antibacterial and antioxidant properties as well as the cytocompatibility here demonstrated, tellurium appears as a novel and interesting element to improve the biological properties of bioactive glasses, especially for the treatment of complicated cases such as infected and inflamed bone fractures.

6.4 References

Ada Vernet Crua, David Medina, Bohan Zhang, María Ujué González, Yves Huttel, José Miguel García-Martín, Jorge L Cholula-Díaz, and Thomas J Webster. 2019. "Comparison of Cytocompatibility and Anticancer Properties of Traditional and Green Chemistry-Synthesized Tellurium Nanowires." International Journal of Nanomedicine Volume 14 (May): 3155–76. https://doi.org/10.2147/ijn.s175640.

Aslam, Bilal, Wei Wang, Muhammad Imran Arshad, Mohsin Khurshid, Saima Muzammil, Muhammad Hidayat Rasool, Muhammad Atif Nisar, et al. 2018. "Antibiotic Resistance: A Rundown of a Global Crisis." Infection and Drug Resistance Volume 11 (11): 1645–58. https://doi.org/10.2147/idr.s173867.

Ba, Lalla Aicha, Mandy Döring, Vincent Jamier, and Claus Jacob. 2010. "Tellurium: An Element with Great Biological Potency and Potential." Organic & Biomolecular Chemistry 8 (19): 4203. https://doi.org/10.1039/c0ob00086h.

Bai, Xiao-chun, Di Lu, Jie Bai, Hang Zheng, Zi-yong Ke, Xiao-ming Li, and Shen-qiu Luo. 2004. "Oxidative Stress Inhibits Osteoblastic Differentiation of Bone Cells by ERK and NF-KB." Biochemical and Biophysical Research Communications 314 (1): 197–207. https://doi.org/10.1016/j.bbrc.2003.12.073.

Baino, Francesco, Sepideh Hamzehlou, and Saeid Kargozar. 2018. "Bioactive Glasses: Where Are We and Where Are We Going?" Journal of Functional Biomaterials 9 (1): 25. https://doi.org/10.3390/jfb9010025.

Bellucci, Devis, Antonella Sola, Roberta Salvatori, Alexandre Anesi, Luigi Chiarini, and Valeria Cannillo. 2017. "Role of Magnesium Oxide and Strontium Oxide as Modifiers in Silicate-Based Bioactive Glasses: Effects on Thermal Behaviour, Mechanical Properties and In-Vitro Bioactivity." Materials Science and Engineering: C 72 (March): 566–75. https://doi.org/10.1016/j.msec.2016.11.110.

Brodsky, Miri, Gilad Halpert, Michael Albeck, and Benjamin Sredni. 2010. "The Anti-Inflammatory Effects of the Tellurium Redox Modulating Compound, AS101, Are Associated with Regulation of NFκB Signaling Pathway and Nitric Oxide Induction in Macrophages." Journal of Inflammation 7 (1): 3. https://doi.org/10.1186/1476-9255-7-3.

Cao, Wanpeng, and Larry L. Hench. 1996. "Bioactive Materials." Ceramics International 22 (6): 493–507. https://doi.org/10.1016/0272-8842(95)00126-3.

Chua, Song Lin, Krishnakumar Sivakumar, Morten Rybtke, Mingjun Yuan, Jens Bo Andersen, Thomas E. Nielsen, Michael Givskov, et al. 2015. "C-Di-GMP Regulates Pseudomonas Aeruginosa Stress Response to Tellurite during Both Planktonic and Biofilm Modes of Growth." Scientific Reports 5 (1). https://doi.org/10.1038/srep10052.

Cochis, A., B. Azzimonti, C. Della Valle, E. De Giglio, N. Bloise, L. Visai, S. Cometa, L. Rimondini, and R. Chiesa. 2016. "The Effect of Silver or Gallium Doped Titanium against the Multidrug Resistant Acinetobacter Baumannii." Biomaterials 80 (February): 80–95. https://doi.org/10.1016/j.biomaterials.2015.11.042.

Dardik, Rima, Tami Livnat, Gilad Halpert, Shayma Jawad, Yael Nisgav, Shirley Azar-Avivi, Baoying Liu, Robert B Nussenblatt, Dov Weinberger, and Benjamin Sredni. 2016. “The Small Tellurium-Based Compound SAS Suppresses Inflammation in Human Retinal Pigment Epithelium.” PubMed 22 (January): 548–62.E.

Verné, M. Miola, C. Vitale Brovarone, M. Cannas, S Gatti, G. Fucale, G Maina, A. Massé, and S. Di Nunzio. 2008. “Surface Silver-Doping of Biocompatible Glass to Induce Antibacterial Properties. Part I: Massive Glass.” Journal of Materials Science. Materials in Medicine 20 (3): 733–40. https://doi.org/10.1007/s10856-008-3617-9.El-

Damrawi, G., H. Doweidar, and H. Kamal. 2014. “Characterization of New Categories of Bioactive Based Tellurite and Silicate Glasses.” Silicon 9 (4): 503–9. https://doi.org/10.1007/s12633-014-9248-5.Fancello, Francesco, Chiara Multineddu, Mario Santona, Pierfrancesco Deiana, Giacomo Zara, Ilaria Mannazzu, Marilena Budroni, Sandro Dettori, and Severino Zara. 2020. “Bacterial Biodiversity of Extra Virgin Olive Oils and Their Potential Biotechnological Exploitation.” Microorganisms 8 (1): 97. https://doi.org/10.3390/microorganisms8010097.

Gristina, A. 1987. “Biomaterial-Centered Infection: Microbial Adhesion versus Tissue Integration.” Science 237 (4822): 1588–95. https://doi.org/10.1126/science.3629258.

Hench, Larry L. 2009. “Genetic Design of Bioactive Glass.” Journal of the European Ceramic Society 29 (7): 1257–65. https://doi.org/10.1016/j.jeurceramsoc.2008.08.002.Hobman, Jon L., and Lisa C. Crossman. 2015. “Bacterial Antimicrobial Metal Ion Resistance.” Journal of Medical Microbiology 64 (5): 471–97. https://doi.org/10.1099/jmm.0.023036-0.

Hoppe, Alexander, Viviana Mouriño, and Aldo R. Boccaccini. 2013. “Therapeutic Inorganic Ions in Bioactive Glasses to Enhance Bone Formation and Beyond.” Biomater. Sci. 1 (3): 254–56. https://doi.org/10.1039/c2bm00116k.

Isaac, J, J Nohra, J Lao, E Jallot, J-M Nedelec, A Berdal, and J-M Sautier. 2011. “Effects of Strontium-Doped Bioactive Glass on the Differentiation of Cultured Osteogenic Cells.” European Cells and Materials 21 (February): 130–43. https://doi.org/10.22203/ecm.v021a11.

Jekabsone, Aiste, Inga Sile, Andrea Cochis, Marina Makrecka-Kuka, Goda Laucaityte, Elina Makarova, Lia Rimondini, et al. 2019. “Investigation of Antibacterial and Antiinflammatory Activities of Proanthocyanidins from Pelargonium Sidoides DC Root Extract.” Nutrients 11 (11): 2829. https://doi.org/10.3390/nu11112829.

Jun Ho Lee, Meital Halperin-Sheinfeld, Dolgar Baatar, Mohamed R Mughal, Hyun Jin Tae, Jie Wan Kim, Arnell Carter, et al. 2013. “Tellurium Compound AS101 Ameliorates Experimental Autoimmune Encephalomyelitis by VLA-4 Inhibition and Suppression of Monocyte and T Cell Infiltration into the CNS.” Neuromolecular Medicine 16 (2): 292–307. https://doi.org/10.1007/s12017-013-8277-3.

Karadjian, Maria, Christopher Essers, Stefanos Tsitlakidis, Bruno Reible, Arash Moghaddam, Aldo Boccaccini, and Fabian Westhauser. 2019. “Biological Properties of Calcium Phosphate Bioactive Glass Composite Bone

Substitutes: Current Experimental Evidence." International Journal of Molecular Sciences 20 (2): 305. https://doi.org/10.3390/ijms20020305.

Kaur, Gurbinder, Gary Pickrell, Nammalwar Sriranganathan, Vishal Kumar, and Daniel Homa. 2015. "Review and the State of the Art: Sol-Gel and Melt Quenched Bioactive Glasses for Tissue Engineering." Journal of Biomedical Materials Research Part B: Applied Biomaterials 104 (6): 1248–75. https://doi.org/10.1002/jbm.b.33443.

Lee, Joung-Hyun, Hongjun Wang, Jeffrey B. Kaplan, and Woo Y. Lee. 2010. "Effects of Staphylococcus Epidermidis on Osteoblast Cell Adhesion and Viability on a Ti Alloy Surface in a Microfluidic Co-Culture Environment." Acta Biomaterialia 6 (11): 4422–29. https://doi.org/10.1016/j.actbio.2010.05.021.

Lin, Weiping, Liangliang Xu, Stefan Zwingenberger, Emmanuel Gibon, Stuart B. Goodman, and Gang Li. 2017. "Mesenchymal Stem Cells Homing to Improve Bone Healing." Journal of Orthopaedic Translation 9 (April): 19–27. https://doi.org/10.1016/j.jot.2017.03.002.

Lu, Xunyu, Gemma Mestres, Vijay Pal Singh, Pedram Effati, Jia-fei Poon, Lars Engman, and Marjam Karlsson Ott. 2017. "Selenium- and Tellurium-Based Antioxidants for Modulating Inflammation and Effects on Osteoblastic Activity." Antioxidants 6 (1): 13–13. https://doi.org/10.3390/antiox6010013.

Ma, Ming-Guo, Jie-Fang Zhu, Run-Cang Sun, Feng Chen, and Ying-Jie Zhu. 2011. "Synthesis and Characterization of the Tellurium/Calcium Silicate Nanocomposite." Materials Letters 65 (3): 424–26. https://doi.org/10.1016/j.matlet.2010.10.083.

Maillard, Jean-Yves, and Philippe Hartemann. 2012. "Silver as an Antimicrobial: Facts and Gaps in Knowledge." Critical Reviews in Microbiology 39 (4): 373–83. https://doi.org/10.3109/1040841x.2012.713323.

McConda, David B., Jonathan M. Karnes, Therwa Hamza, and Brock A. Lindsey. 2016. "A Novel Co-Culture Model of Murine K12 Osteosarcoma Cells and S. Aureus on Common Orthopedic Implant Materials: 'the Race to the Surface' Studied in Vitro." Biofouling 32 (6): 627–34. https://doi.org/10.1080/08927014.2016.1172572.

Miguez-Pacheco, Valentina, Larry L. Hench, and Aldo R. Boccaccini. 2015. "Bioactive Glasses beyond Bone and Teeth: Emerging Applications in Contact with Soft Tissues." Acta Biomaterialia 13 (February): 1–15. https://doi.org/10.1016/j.actbio.2014.11.004.

Miola, Marta, Chiara Vitale Brovarone, Giovanni Maina, Federica Rossi, Loredana Bergandi, Dario Ghigo, S Saracino, et al. 2014. "In Vitro Study of Manganese-Doped Bioactive Glasses for Bone Regeneration." Materials Science and Engineering: C 38 (May): 107–18. https://doi.org/10.1016/j.msec.2014.01.045.

Miola, Marta, Jonathan Massera, Andrea Cochis, Ajay Kumar, Lia Rimondini, and Enrica Vernè. 2021. "Tellurium: A New Active Element for Innovative Multifunctional Bioactive Glasses." Materials Science and Engineering: C 123 (April): 111957. https://doi.org/10.1016/j.msec.2021.111957.

Miola, Marta, and Enrica Verné. 2016. "Bioactive and Antibacterial Glass Powders Doped with Copper by Ion-Exchange in Aqueous Solutions." Materials 9 (6): 405. https://doi.org/10.3390/ma9060405.

Mohan Edirisinghe, Zhalan Charani, Lena Ciric, Upulitha Eranka Illangakoon, and Mohan Edirisinghe. 2018. "Antimicrobial Activity of Tellurium-Loaded Polymeric Fiber Meshes." Journal of Applied Polymer Science 135 (25): 46368–68. https://doi.org/10.1002/app.46368.

Newby, P. J., R. El-Gendy, J. Kirkham, X. B. Yang, I. D. Thompson, and A. R. Boccaccini. 2011. "Ag-Doped 45S5 Bioglass®-Based Bone Scaffolds by Molten Salt Ion Exchange: Processing and Characterisation." Journal of Materials Science: Materials in Medicine 22 (3): 557–69. https://doi.org/10.1007/s10856-011-4240-8.

Özarslan, Ali Can, and Sevil Yücel. 2016. "Fabrication and Characterization of Strontium Incorporated 3-D Bioactive Glass Scaffolds for Bone Tissue from Biosilica." Materials Science and Engineering: C 68 (November): 350–57. https://doi.org/10.1016/j.msec.2016.06.004.

Palza, Humberto, Blanca Escobar, Julian Bejarano, Denisse Bravo, Mario Diaz-Dosque, and Javier Perez. 2013. "Designing Antimicrobial Bioactive Glass Materials with Embedded Metal Ions Synthesized by the Sol–Gel Method." Materials Science and Engineering: C 33 (7): 3795–3801. https://doi.org/10.1016/j.msec.2013.05.012.

Pedone, Alfonso, Francesco Muniz-Miranda, Antonio Tilocca, and Maria Cristina Menziani. 2016. "The Antioxidant Properties of Ce-Containing Bioactive Glass Nanoparticles Explained by Molecular Dynamics Simulations." Biomedical Glasses 2 (1). https://doi.org/10.1515/bglass-2016-0003.

Shakibaie, Mojtaba, Mahboubeh Adeli-Sardou, Tayebe Mohammadi-Khorsand, Mahdie ZeydabadiNejad, Ehsan Amirafzali, Sahar Amirpour-Rostami, Atefeh Ameri, and Hamid Forootanfar. 2017. "Antimicrobial and Antioxidant Activity of the Biologically Synthesized Tellurium Nanorods; a Preliminary in Vitro Study." Iranian Journal of Biotechnology 15 (4): 268–76. https://doi.org/10.15171/ijb.1580.

Sorrentino, Rita, Andrea Cochis, Barbara Azzimonti, Carlos Caravaca, Jerome Chevalier, Meinhard Kuntz, Alessandro Alan Porporati, Robert Michael Streicher, and Lia Rimondini. 2018. "Reduced Bacterial Adhesion on Ceramics Used for Arthroplasty Applications." Journal of the European Ceramic Society 38 (3): 963–70. https://doi.org/10.1016/j.jeurceramsoc.2017.10.008.

Subbiahdoss, Guruprakash, Roel Kuijer, Dirk W. Grijpma, Henny C. van der Mei, and Henk J. Busscher. 2009. "Microbial Biofilm Growth vs. Tissue Integration: 'the Race for the Surface' Experimentally Studied." Acta Biomaterialia 5 (5): 1399–1404. https://doi.org/10.1016/j.actbio.2008.12.011.

Turner, Raymond J., Roberto Borghese, and Davide Zannoni. 2012. "Microbial Processing of Tellurium as a Tool in Biotechnology." Biotechnology Advances 30 (5): 954–63. https://doi.org/10.1016/j.biotechadv.2011.08.018.

Varini, Elena, Sandra Sánchez-Salcedo, Gianluca Malavasi, Gigliola Lusvardi, María Vallet-Regí, and Antonio J Salinas. 2019. "Cerium (III) and (IV) Containing Mesoporous Glasses/Alginate Beads for Bone Regeneration: Bioactivity, Biocompatibility and Reactive Oxygen Species Activity" 105 (December): 109971–71. https://doi.org/10.1016/j.msec.2019.109971.

Vernè, E., S. Di Nunzio, M. Bosetti, P. Appendino, C. Vitale Brovarone, G. Maina, and M. Cannas. 2005. "Surface Characterization of Silver-Doped Bioactive Glass." Biomaterials 26 (25): 5111–19. https://doi.org/10.1016/j.biomaterials.2005.01.038.

Zhang, Xiaoming, Xuebin Zhan, Peng Zou, and Huixia An. 2017. "Factors Related to Infection after Fixation in the Process of Late Healed Bone Fracture." Experimental and Therapeutic Medicine 14 (2): 1126–30. https://doi.org/10.3892/etm.2017.4610.

Zhong, Cai Ling, Bi Yin Qin, Xin Yuan Xie, and Yan Bai. 2013. "Antioxidant and Antimicrobial Activity of Tellurium Dioxide Nanoparticles Sols." Journal of Nano Research 25 (October): 8–15. https://doi.org/10.4028/www.scientific.net/jnanor.25.8.

Zonaro, Emanuele, Silvia Lampis, Raymond J. Turner, S. Junaid S. Qazi, and Giovanni Vallini. 2015. "Biogenic Selenium and Tellurium Nanoparticles Synthesized by Environmental Microbial Isolates Efficaciously Inhibit Bacterial Planktonic Cultures and Biofilms." Frontiers in Microbiology 6 (June). https://doi.org/10.3389/fmicb.2015.00584.

Chapter VIII

Mesoporous Bioactive Glasses Doped with Cerium and Polyphenols

Aim

When a bone is fractured, the blood vessels and the surrounding tissue are damaged, which can lead to a significant decrease in blood and oxygen supply to the affected area. The interruption in blood supply can hinder the delivery of essential nutrients, growth factors, and cells necessary for bone repair. The lack of blood flow can also delay the removal of damaged tissue and the initiation of the healing process. Additionally, excessive production of ROS can occur, accompanied by cell death at the damaged site. Therefore, it is crucial to protect the cells from excessive ROS and inflammatory factors and encourage oxygen and blood vessel restoration at the damaged site. To address this issue, we have turned our attention to cerium. Cerium possesses therapeutic ions with unique biological activity. One of its defining features is its ability to change the oxidative state between Ce^{3+} and Ce^{4+} during redox reactions. In physiological pH conditions, it acts as an antioxidant (Ce^{3+}) and ROS scavenger, mediating oxygen within the microenvironment. As a result, cerium induces an anti-inflammatory response and osteogenesis. Cerium takes on the role of a pro-oxidant (Ce^{4+}) under low pH conditions. Thus, Ce generates ROS and causes cell damage. Furthermore, Ce enhances the formation of new blood vessels, which is important for tissue repair and can be a promising therapeutic option for tissue regeneration.

Chapter VIII has been published in a 'research article' in biomaterials and biosystems: Bifunctional Mesoporous Glasses for Bone Tissue Engineering: Biological Effects of Doping with Cerium and Polyphenols in 2D and 3D In Vitro Models. (https://doi.org/10.1016/j.bbiosy.2024.100095). In this paper, the contribution of the author is as follows:

Francesca Fraulini, Alfonso Zambon, and Gigliola Lusvardi: Synthesized the Ce-MBGs and Ce-MBGs polyphenols, along with chemical characterization.

Ajay kumar and Ksenia Menshikh: Performed the biological characterization of MBGs powders in terms of cytocompatibility, both in 2D and 3D models, and a 3D endothelial migration assay.

MBGs production

Ce-MBGs were synthesized using the modified sol-gel EISA method, and they were then ground to obtain powders in the range of 50-150 μm. The same powders were used and prepared as pellets. Polyphenols were extracted from chestnut flour. Loading was performed by soaking 0.1 g of each MBGs for 3 hrs at 37°C in 5 mL of loading solution. All samples were covered with aluminium foil to avoid exposure to light. Both the powders and pellets were provided by the University of Modena.

Abstract

This study evaluates the cytocompatibility of cerium-doped mesoporous bioactive glasses (Ce-MBGs) loaded with polyphenols (Ce-MBGs-Poly) for possible application in bone tissue engineering after tumour resection. We tested MBGs powders and pellets on 2D and 3D in vitro models using human bone marrow-derived mesenchymal stem cells (hMSCs), osteosarcoma cells (U2OS), and endothelial cells (EA.hy926). Promisingly, at a low concentration in culture medium, Poly-loaded MBGs powders containing 1.2 mol% of cerium inhibited U2OS metabolic activity, preserved hMSCs viability, and had no adverse effects on EA.hy926 migration. Moreover, the study discussed the possible interaction between cerium and Poly, influencing anti-cancer effects. In summary, this research provides insights into the complex interactions between Ce-MBGs, Poly, and various cell types in distinct 2D and 3D in vitro models, highlighting the potential of loaded Ce-MBGs for post-resection bone tissue engineering with a balance between pro-regenerative and anti-tumorigenic activities.

Introduction

Biomaterials, and specifically bioactive glasses (BGs), have been widely studied and used for the treatment of bone defects, as they are able to bind to the bone and stimulate osteogenesis through the release of biologically active ions (bioactivity) **(Baino, Hamzehlou, and Kargozar 2018) (Hench 2006) (El-Rashidy et al. 2017)**. The implant of a biomaterial often creates an inflammatory state with the production of reactive oxygen species (ROS) that can require lengthy drug treatments. In recent years, research in the field has focused on the development of biomaterials with antioxidant properties that can convert ROS into non-hazardous species and reduce post-implantation complications **(Zheng et al. 2021) (Rosenfeldt et al. 2013) (Firuzi et al. 2011) (Saeid Kargozar et al. 2022)**. To this end, one strategy employed is the doping of BGs with therapeutic inorganic ions (TIIs), which can confer antioxidant and/or osteogenic, angiogenic, cementogenic and antibacterial properties on the BGs **(Zhu, Zheng, and Boccaccini 2021) (O'Neill et al. 2018) (Mouriño et al. 2019)**. Among TIIs, cerium exhibits significant antioxidant and anti-inflammatory activities for its ability to quench ROS and regulate their level within the microenvironment and is thus of particular interest. Cerium-based compounds have long shown relevant pharmacological properties and have been used, for example, as antiemetics, bacteriostats and anticancer agents **(Zambon et al. 2021) (Nicolini et al. 2015) (Gigliola Lusvardi et al. 2022) (Łapa et al. 2019) (Atkinson et al. 2022) (Zheng et al. 2020)**.

Another well-established strategy to confer desirable biological properties on BGs is their loading with organic compounds able to elicit specific cellular responses onto the target tissue. These compounds include drugs and biomolecules and can add antioxidant properties, but also antitumour, antibacterial, anti-inflammatory, vasoprotective and bone-promoting effects to the loaded biomaterial **(Baino, Hamzehlou, and Kargozar 2018) (Cazzola et al. 2018) (Ferraris et al. 2017) (Sayed Abdelgeliel et al. 2019) (Schuhladen, Roether, and Boccaccini 2019) (Torre et al. 2020) (Cazzola et al. 2017) (Zhang et al. 2013) (Corazzari et al. 2016) (Giacomo**

Riccucci et al. 2021). Recently, we evaluated the effect of the loading of biomolecules (such as gallic acid, anthocyanins and polyphenols) on the antioxidant properties of Ce-doped BGs (specifically mesoporous bioactive glasses, Ce-MBGs). We found that doping with cerium does not affect the bioactivity of the BGs, while having a positive effect on their biocompatibility and giving the materials the ability to dismutase hydrogen peroxide, one of the main ROS species **(Gigliola Lusvardi et al. 2022)**. The loading of Ce-MBGs with polyphenols (Ce-MBGs-Poly) removes a second important ROS species, the superoxide anion, presumably by radical scavenging. Doping with cerium and loading with Poly thus add complementary antioxidant properties to MBGs, while maintaining their bioactivity.

In bone healing, osteogenesis and angiogenesis processes are closely connected. Newly formed vessels deliver not only necessary nutrients but also differentiation factors. Thus, it is of particular importance that the biomaterials designed for bone tissue engineering promote – or, at least, do not interfere in – angiogenesis **(Baino et al. 2016)**. Extracts of cerium-containing bioactive glasses were shown to promote proliferation, migration and lymphatic vascular network formation in an in vitro model set up with the use of lymphatic endothelial cells **(Baino, Hamzehlou, and Kargozar 2018)**.

Bone regeneration is a coordinated action of multiple cell types, such as mesenchymal stem cells, osteoblasts, chondrocytes, and immune and endothelial cells, which is why it is important to test material in various in vitro models **(Diomede et al. 2020)**. Additionally, for a multifunctional material aiming not only at assisting bone regeneration but also at suppressing cancer cell activity – which may be the case on the site of bone cancer resection – the activity towards cancer cells should also be taken into account **(Xie et al. 2022)**. Other factors, e.g. form, surface area and particle size of the material are to be considered in the design of the experiment to avoid interferences such as excessive absorption of nutrients from culture medium or blocking gas exchange by the material **(Jablonská et al. 2020) (Brookes et al. 2021)**. Nowadays, there is no universal testing method available that could be sufficient and applicable for a comprehensive biological evaluation of materials for bone repair. For these reasons, in the design of our study, we exploited different cell lines, as well as 2D and 3D in vitro models.

This study aims to evaluate the in vitro performance of Ce-MBGs and Ce-MBGs-Poly towards cell lines representing the bone microenvironment. First, to assess the cytocompatibility of the materials, we tested them in conventional 2D-monolayer in vitro models simulating “physiological” and “pathological” conditions – with human bone marrow-derived mesenchymal stem cells and human osteosarcoma cells, respectively. In the following steps, the cytocompatibility was evaluated in a 3D spheroid-based set-up using the same cell lines. Next, considering angiogenesis as a key factor in bone regeneration, we analysed the influence of Ce-MBGs on endothelial cell migration. Finally, considering the potential application of these materials, pellets of Ce-MBGs were produced and tested in vitro towards all three above-mentioned cell lines.

7. Materials and Methods

7.1 MBGs Powders Preparation for In Vitro Assays

MBGs powders were weighed and sterilized by heating at 160°C for 2 hrs or UV exposure for 20 min (for Poly-loaded powders) **(Xie et al. 2022) (Zheng et al. 2020).** Before each experiment, MBGs powders were quickly washed with phosphate-buffered saline (PBS, Sigma-Aldrich, USA). All MBGs (Table 7.1) were tested at concentrations of 1 and 5 mg/mL.

Table 7.1: Represents the composition of the Ce-MBGs and Ce-MBGs-Poly

Ce-MBGs	Ce-MBGs-Poly
MBG (control)	**MBG Poly (control)**
MBG 1.2%	**MBG 1.2% Poly**
MBG 3.6%	**MBG 3.6% Poly**
MBG 5.3%	**MBG 5.3% Poly**

7.1.1 2D Cytocompatibility

For the monolayer-based cytocompatibility assay, hMSCs were seeded in a 24 multiwell plate in a defined concentration ($1x10^4$ cells/well) and allowed to adhere and spread overnight. After this, the culture medium in the wells was substituted with MBGs powders suspension in the culture medium at concentrations 1 and 5 mg/mL. Fresh culture medium was added to the control, and cells were cultivated for 3 days.
After 24 and 72 h, the metabolic activity of the cells was evaluated by the fluorescent Alamar blue assay as previously described in section 4.1.7.

After the metabolic activity assay on the last day of the experiment, we furthermore visualized the hMSCs cell morphology by staining the cytoskeleton. For this, cells were washed with PBS and fixed with 4% paraformaldehyde (PFA, reagent grade, crystalline, Sigma-Aldrich, USA) solution at room temperature for 20 mins. Cells were washed with PBS again to eluate the fixative reagent and permeabilized for 10 mins with 0.5% Triton in PBS (Triton™ X-100, Sigma-Aldrich, USA) at RT. Furthermore, Alexa Fluor™ 488 Phalloidin (Life Technologies, USA) and 4,6-diamidino-2-phenylindole (DAPI, Sigma-Aldrich, USA) in PBS were added and incubated for 40 min at RT. Images were obtained with the EVOS Floid Microscope Imaging System (Invitrogen, USA).

7.1.2 3D Cytocompatibility Assay

For the spheroid-based cytocompatibility assay, firstly, wells of a 48-well plate were coated with 1.5 % agarose solution in sterile conditions and let solidify and sterilize at RT under UV exposure for 2 h. Then, were seeded

in the amount of $5x10^4$ cells per well of the agarose-coated plate. Cells were incubated in standard conditions with the medium being changed every 2 or 3 days. After the 7 days of complete self-aggregation of spheroids confirmed by light microscopy, the culture medium in the wells was substituted with MBGs powder suspension in the culture medium at concentrations of 1 and 5 mg/mL. Fresh culture medium was added to the control, and spheroids were cultivated for 7 days.

Metabolic activity assay was performed on the 1st, 3rd and 7th days as described in section 4.1.7. Additionally, the cell viability was further confirmed by evaluating them with the fluorescent live/dead assay (LIVE/DEAD, Invitrogen, L3224, Thermo Fisher, USA) following the manufacturer's instructions. Briefly, 2 µM Calcein AM and 4 µM EthD-1 solutions in fresh culture medium were added to spheroid-containing wells and then incubated in the dark for 45 min. After incubation, spheroids were visualized with Leica THUNDER Imager 3D Live Cell (Leica Microsystems, USA).

7.1.3 MBG Extracts Angiogenic Potential Assay

human endothelial umbilical vein cells (EA. hy926, American Type Culture Collection, Manassas, VA, USA, CRL-2922) were cultivated in high-glucose DMEM (Sigma-Aldrich, USA) supplemented with 10% FBS and 1% PS. All cell lines were cultivated at 37°C in the humidified atmosphere containing 5% CO_2. Before experiments, cells were cultivated until 80-90% confluence, detached by trypsin-EDTA solution (Sigma-Aldrich, USA), harvested, and used for experiments.

To estimate the potential influence of MBGs on angiogenesis, an endothelial cell spheroid migration assay was set up. For this, spheroids of endothelial EA.hy926 cells were prepared as described above. After spheroid maturation, spheroids were transferred to a new 24 multi-well plate and let adhere overnight. Ce-MBGs and Ce-MBGs-Poly weighed and sterilized powders were transferred into sterile 15-mL tubes and resuspended in a complete medium (up to concentrations of 1 and 5 mg/mL). Tubes were incubated at 37°C, 5% CO_2 in the humidified atmosphere, and extracts were obtained and added to the spheroids following ISO 10993-12. Spheroid migration was assessed after 0, 24, 48 and 72 h of incubation with extracts. At each time point, phase-contrast light microscopy images of spheroids were collected, and results were analysed in the ImageJ software with the use of a free toolset for cell invasion analysis **(Analyse Spheroid Cell Invasion In 3D Matrix, RRID: SCR_021204) (Backer V)**.

7.1.4 MBGs Pellets Preparation for In Vitro Assay

Biological characterization of 12-mm MBGs pellets (Table 7.1) was performed on hMSCs and EA.hy926 cells. Before incubation in direct contact with cells, the samples were sterilized by UV exposure for 1 h and placed in a 24 multiwell plate.

Cells were seeded dropwise directly onto the samples' surface at a defined concentration ($1.5x10^4$ cells/samples), allowed to adhere for 2 h, and then 1 mL of a relevant culture medium was added to the well. Cell-seeded pellets were incubated for 4 days. On the 1st, 3rd and 4th days, the metabolic activity of the cells in direct contact with samples was evaluated by the fluorometric Alamar blue assay as described before.

7.1.5 Statistical Analysis

Each group of samples was represented by three replicates. Results are shown as mean value ± standard deviation. Comparison between groups within experimental time points was performed in Prism (v8, GraphPad Software, USA) using two-way ANOVA with Dunnett's correction. Before that, Shapiro–Wilk's test for normal distribution and ROUT (Robust regression and Outlier removal) method for outliers' identification was performed. For each comparison, the difference was determined as significant for $p < 0.05$.

7.2 Results and Discussion

7.2.1 MBGs Powders Cytocompatibility Assay: 2D

There is a growing interest in applying tissue engineering to create in vitro 3D human models of healthy and pathological bone for drug development and systemic interactions. However, current models are not able to accurately simulate bone hierarchy and perfusable vasculature. As a result, there is a need to explore the development of more sophisticated models. Both cortical and trabecular bone possess a rich abundance of vascular supply, which plays a critical role in bone formation and remodelling processes. Vascularization contributes to the migration of mesenchymal stem cells (MSCs), the supply of oxygen and nutrients to metabolically active tissues, and the removal of waste by-products. Therefore, the exploration of more advanced models is necessary. for this purpose, we have chosen an In-vitro evaluation of MBGs powders' cytocompatibility done towards hMSCs, which were selected as representatives of the self-healing process during bone regeneration and endothelial (EA.hy926) cells as representatives of angiogenesis crucial for bone regeneration. First, we incubated MBGs powders with cells in a standard 2D monolayer to evaluate the direct influence of the material on cell metabolic activity.

The results of the cytocompatibility assay toward hMSCs are presented in Figure 7.1. After 1 day of direct contact, there is no significant difference in hMSCs metabolic activity observed between control and Ce-MBGs at 1 and 5 mg/mL and Ce-MBGs-Poly, at 1 mg/mL. Ce-MBGs-Poly at 5 mg/mL negatively influences the cell metabolic activity at the highest cerium amounts (3.6 and 5.3 mol %).

On the 2nd day of cultivation, the relative viability of cells drops below the standard threshold of 70 % **(ISO 10993-12)** in all groups of Ce-MBGs and Ce-MBGs-Poly at 1 mg/mL except those with the highest cerium amount, and in all groups at 5 mg/mL except MBG-Poly; however, this group is still significantly lower than the control in terms of raw RFU values.

On the 3rd day, it remains low for MBGs without cerium (1 and 5 mg/mL) and MBG1.2 at 1mg/mL. The same trend is observed for Ce-MBGs-Poly on the 3rd day at 1 mg/mL; at 5 mg/mL, on the contrary, the lowest metabolic activity is observed for the group with the highest amount of cerium (MBG5.3 Poly). Both Ce-MBGs and Ce-MBGs-Poly are generally well tolerated. Without Poly for both concentrations and with Poly at 1 mg/mL, the lowest hMSCs cell metabolic activity is correlated with the lowest cerium amount; in contrast, the highest cerium amount (5.3 mol %) in the Ce-MBGs-Poly at 5 mg/mL negatively affects cell viability.

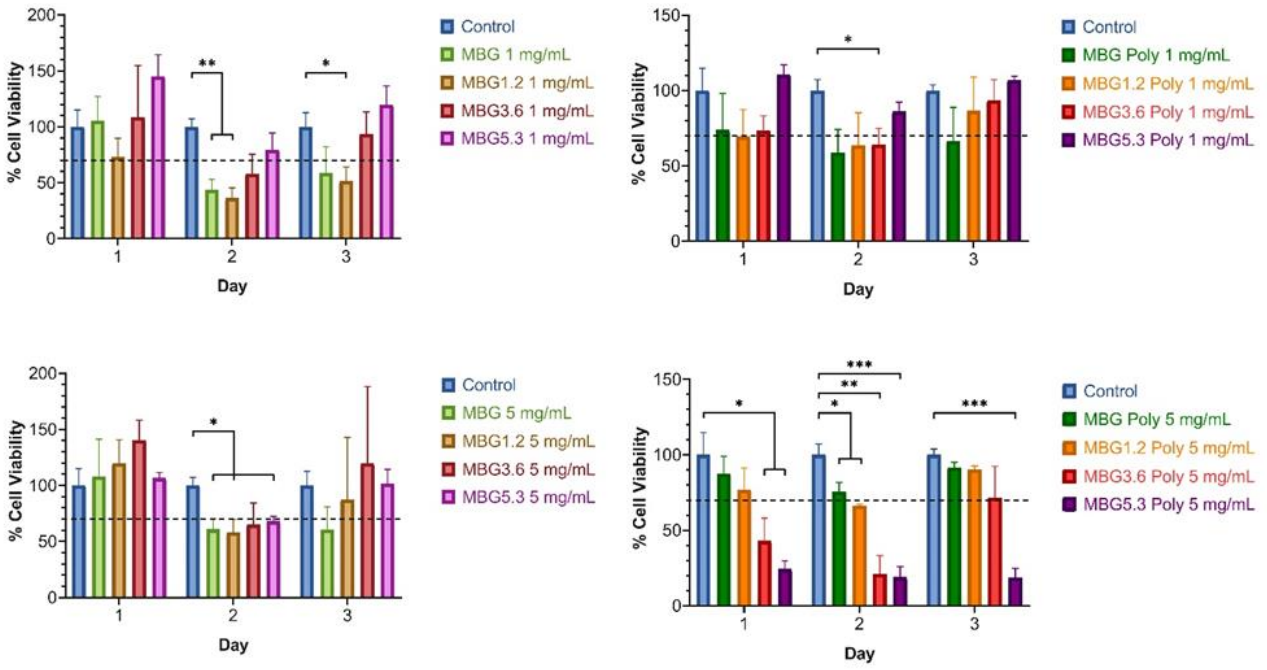

Figure 7.1: Metabolic activity of hMSCs cultivated in direct contact with Ce-MBGs and Ce-MBGs-Poly powders (1 and 5 mg/mL). 'Control' represents hMSCs cultivated in the medium without powders addition. The values are presented as mean ± SD of relative cell viability. Statistical analysis was performed on relative fluorescent units (RFU), * - significant differences between groups of samples, $p < 0.05$; ** - $p < 0.01$; * - $p < 0.001$.**

One possible way to explain the hMSCs toxicity is that Increased Ce and poly-induced ROS levels may be the cause of observed cellular damage and apoptosis. **(Kumari et al. 2014)** stated that Ce toxicity was dose-dependent toxicity in the human cell. The observed reduction in cell viability was due to the high concentration of MBGs powdered cytotoxic and it was more evident in Figure 7.2 However, no toxicity has been reported in 1 mg/mL. Furthermore, no changes in hMSCs morphology as shown in Figure 7.2 cells had elongated morphology and were well spread in the presence of powders. Moreover, Ce-MBGs powders were strongly attached to cells at all concentrations, which could also explain a slightly lower confluency of these samples: due to aggregation with particles, cells might have been rinsed off during the staining procedure. As for Ce-MBGs-Poly, the morphology of hMSCs was also found normal; in comparison to the Ce-MBGs groups, larger particles were attached to the cells. Very low confluency was observed in the group of MBG5.3 Poly 5

mg/mL with still some particles strongly attached to the remaining cells, in line with the metabolic activity results.

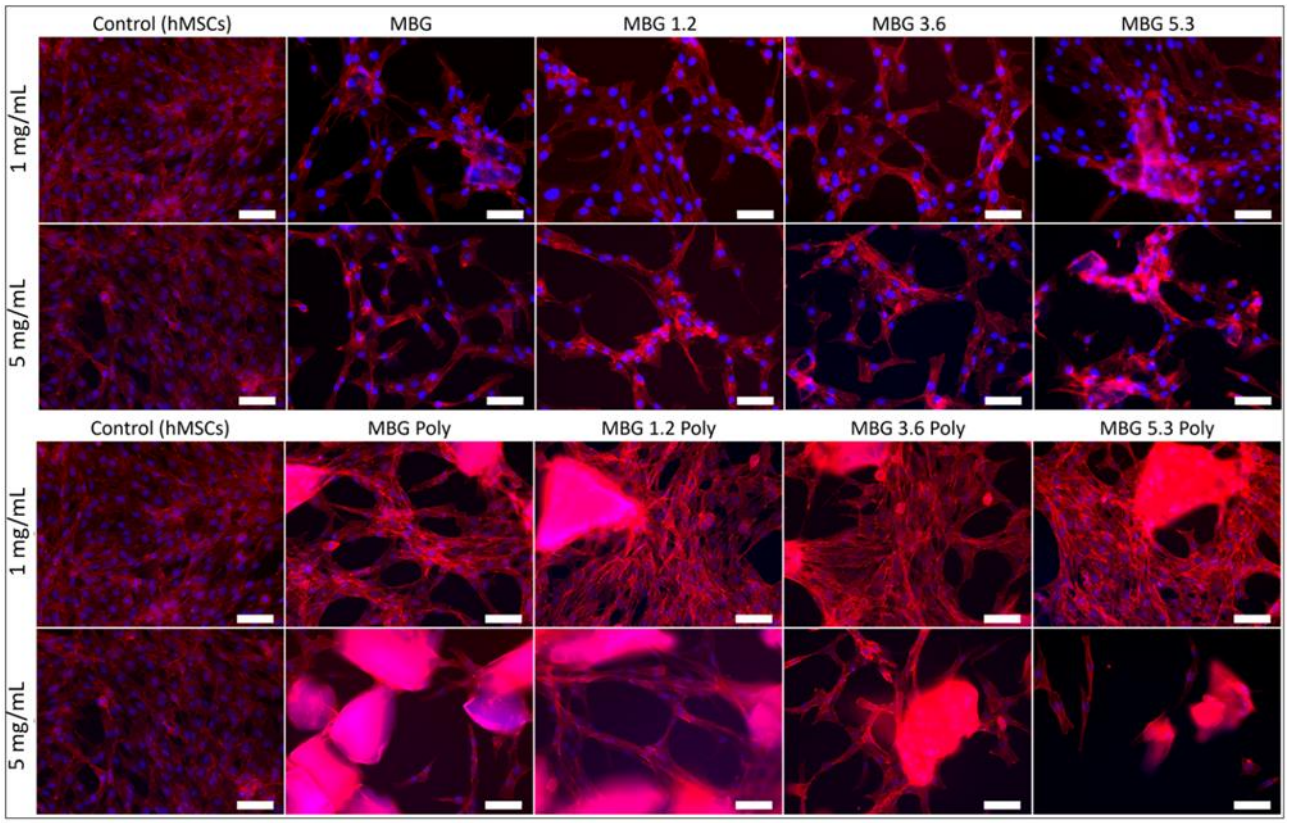

Figure 7.2: hMSCs morphology evaluation after 72 hrs of cultivation in direct contact with Ce-MBGs and Ce-MBGs-Poly powders (1 and 5 mg/mL). Actin cytoskeleton is stained red (Phalloidin) and nuclei are stained blue (DAPI). Scale bar 100 µm.

7.2.2 MBGs Powders Cytocompatibility Assay: 3D

After performing the cytotoxicity assay in a 2D monolayer, we further evaluated the MBGs powders in a 3D spheroid-based model in a prolonged direct contact experiment. Results are shown in Figure 7.3 on day 1, hMSCs cell viability for Ce-MBGs at both 1 and 5 mg/mL is slightly higher than control for the groups with higher cerium content (MGB3.6 and MGB5.3), while being significantly higher than control on day 3 for all cerium-doped groups. For Ce-MBGs-Poly cell viability is significantly higher than control for all groups on the 1st day both at 1 and 5 mg/mL and comparable to control on day 3. After 1 week, Ce-MBGs are generally in line with the control, and Ce-MBGs-Poly is generally slightly lower, except for the MBG5.3 Poly group at 5 mg/mL. Interestingly then, both doping with cerium and Poly loading seem to boost spheroids growth at early time points, but this effect wanes at longer cultivation times. One of the factors causing such diversity of results is the abundance of direct cell-material contact in the 2D model, while in a cell monolayer, the cells are equally exposed to the powders, in a spheroid, only the cells present in the outer layer are exposed. Next, direct contact with the material surface may alter the fate of a cell: the bioactive ions and biomolecules (which are, in our case, cerium and Poly) are being released in the culture medium, altering thus the biochemical

environment again, in contrast to cells in monolayer, there would be a gradient of cerium ions and Poly concentration reaching cells located in different layers of the spheroid **(Białkowska et al. 2020).** The heterogeneity of the results, which depend not only on the type of cells and presence of cerium and Poly but also on the testing approach (2D vs 3D), is of particular interest. Ce-MBGs Poly 1.2 (5 mg/mL) and 3.6 (1 and 5 mg/mL) are not cytotoxic in the 2D model but inhibit the proliferation of hMSCs spheroids.

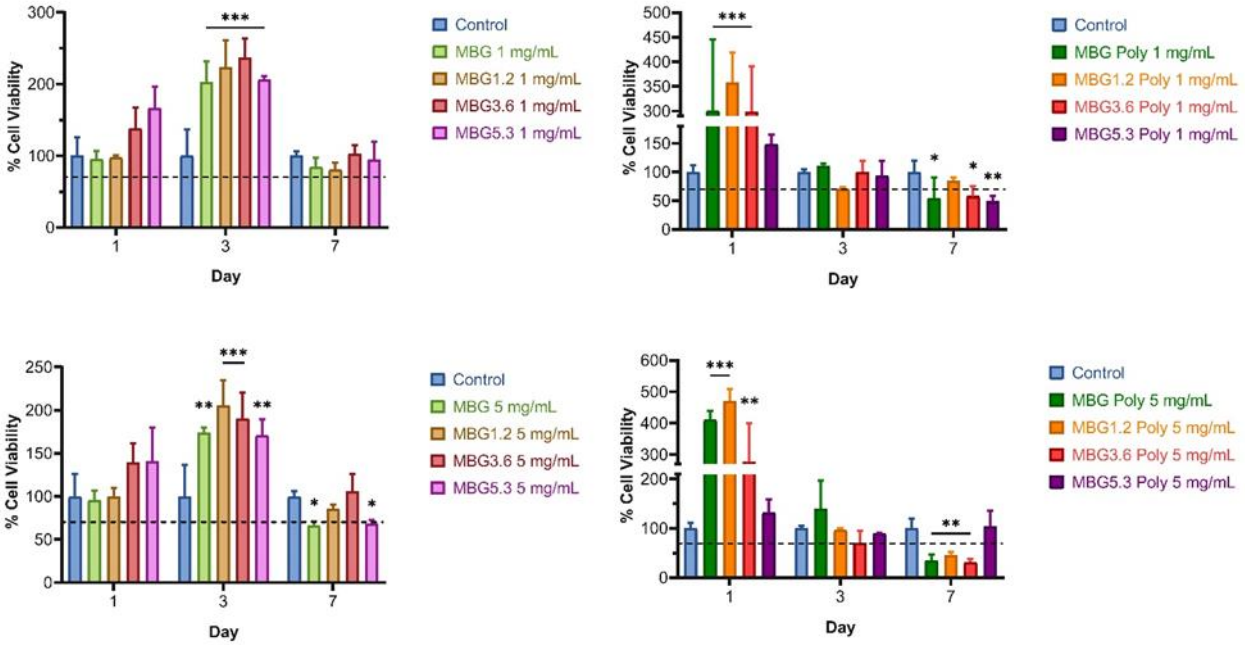

Figure 7.3: Metabolic activity of hMSCs cell spheroids cultivated in direct contact with Ce-MBGs and Ce-MBGs-Poly powders (1 and 5 mg/mL). 'Control' represents hMSCs cell spheroids cultivated in the medium without powders addition. The values are presented as mean ± SD of relative cell viability. Statistical analysis was performed on relative fluorescent units (RFU), * - significant difference compared to control, $p < 0.05$; ** - $p < 0.01$; * - $p < 0.001$.**

In addition to metabolic activity assay, spheroids cultivated in direct contact with the MBGs powders were visualized using light microscopy to assess the possible change in morphology of the cell spheroids. Figure 7.4a) illustrates the control hMSCs spheroids and the spheroids which demonstrated the lowest viability rates. Furthermore, hMSCs cell spheroids were stained with Calcein AM to visualize live cells. Interestingly, even though the spheroids were disaggregated throughout the experiment by the 2-week time point, cells of the disaggregated spheroid were attached to MBGs powders lining their surface (Figure 7.4b).

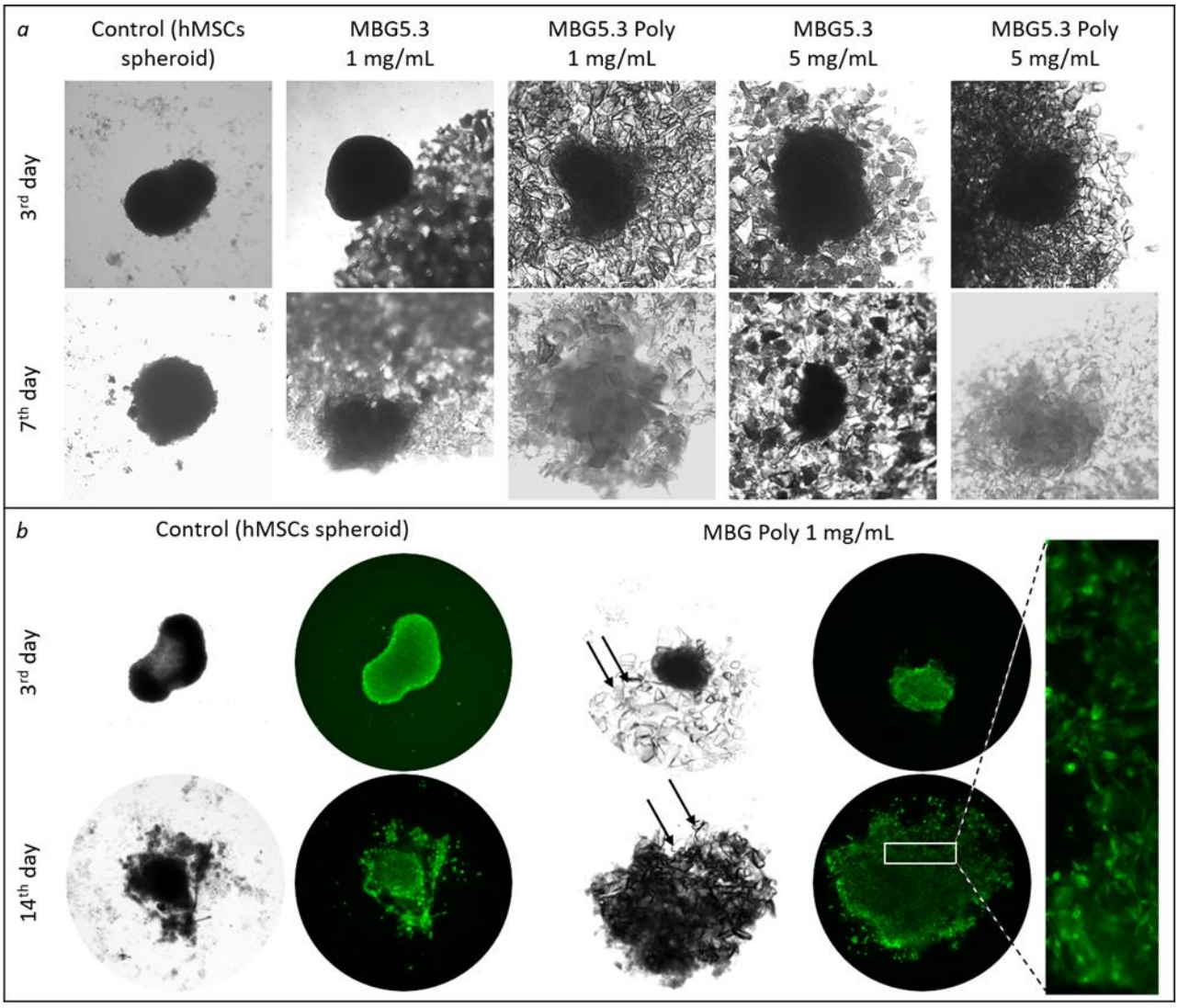

Figure 7.4: Bright-field (a and b left) and fluorescent (b right) microscopy images of hMSCs cell spheroids formed from 5 x 10^4 cells cultivated in standard conditions (Control) and MBGs powders for 3 days, 1 and 2 weeks. Live cells stained green (Calcein AM). Arrows indicate MBGs powders.

7.2.3 MBG Extracts Angiogenic Potential Assay

After performing the 2D-monolayer and 3D-spheroid cytocompatibility of MBGs powders, we further investigated the potential influence of the material on angiogenesis by setting up a spheroid migration assay. Figure 7.5 – 7.8 illustrates the principle of the assay of the Controls and MBGs and MBGs Poly of both 1 and 5 mg/mL. Quantitative analysis does not evidence any significant influence on endothelial cell migration in any of the experimental groups throughout the first 24 hrs. Migration is not altered also at 48 hrs in the case of Ce-MBGs, whereas it was inhibited by the extract of MBG3.6 Poly at the concentration of 1 mg/mL and MBG Poly, MBG3.6 Poly and MBG5.3 Poly of 5 mg/mL. By the 3rd day, in most of the spheroids monitored, there was a complete spread of cells within the area of observation. Inhibition of migration was only observed in two samples of 5 mg/mL – MBG3.6 and MBG5.3 Poly (Figure 7.9). Thus, extracts of the lowest (1 mg/mL)

MBGs powder concentrations had no inhibition effect on the migration of endothelial EA.hy926 cells from spheroid to monolayer.

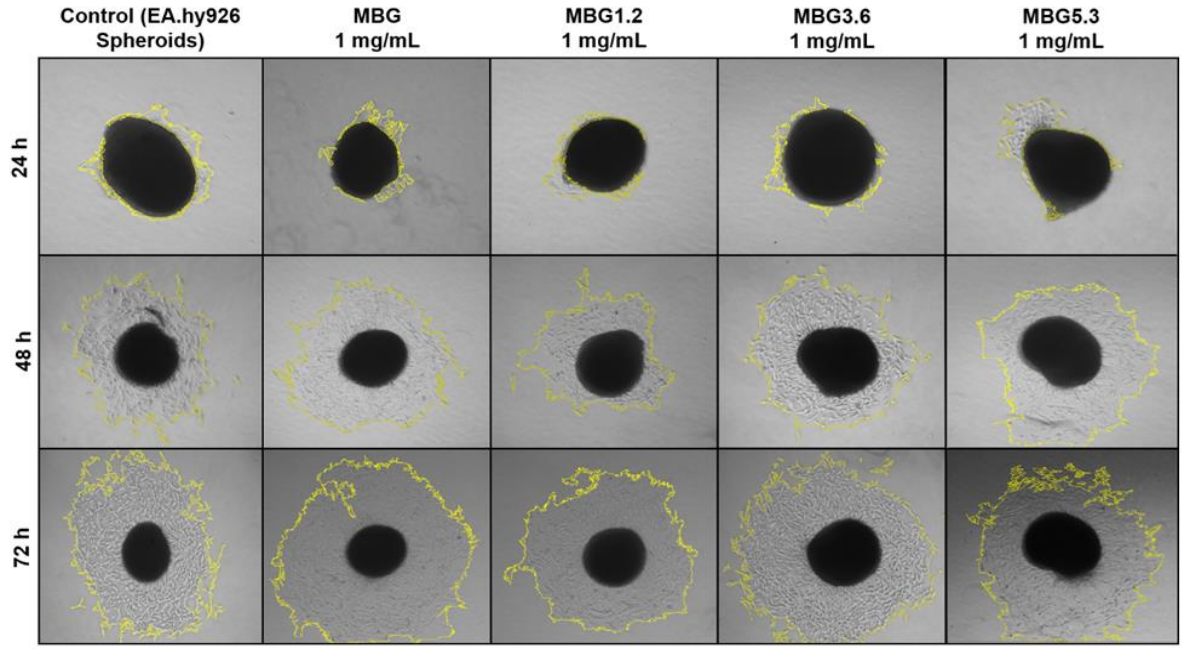

Figure 7.5: Light microscopy images of endothelial cell migration out of the spheroids after 24, 48 and 72 h of incubation with 1 mg/mL extracts of Ce-MBGs. The spheroid migration area is outlined in yellow.

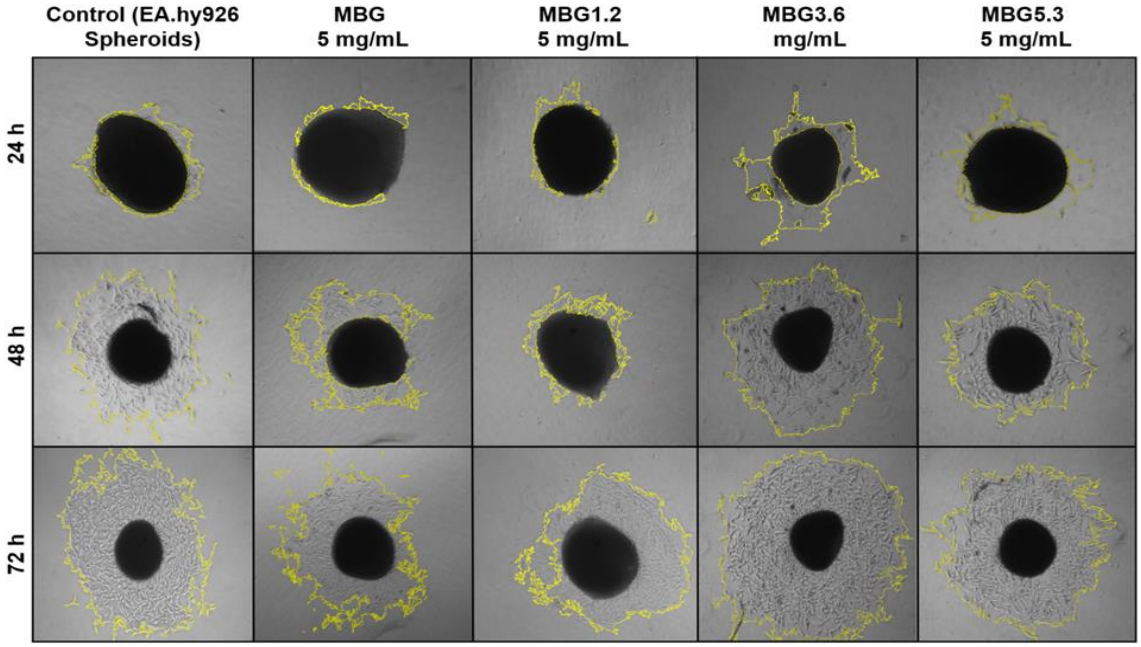

Figure 7.6: Light microscopy images of endothelial cell migration out of the spheroids after 24, 48 and 72 h of incubation with 5 mg/mL extracts of Ce-MBGs. The spheroid migration area is outlined in yellow.

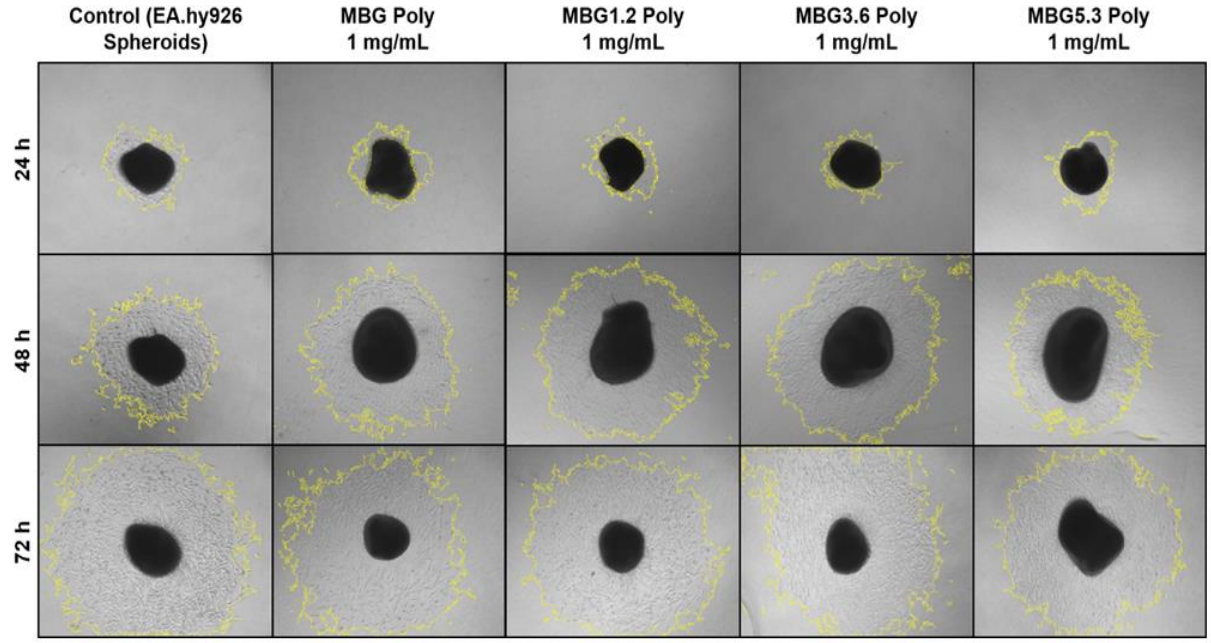

Figure 7.7: Light microscopy images of endothelial cell migration out of the spheroids after 24, 48 and 72 h of incubation with 1 mg/mL extracts of Ce-MBGs-Poly. The spheroid migration area is outlined in yellow.

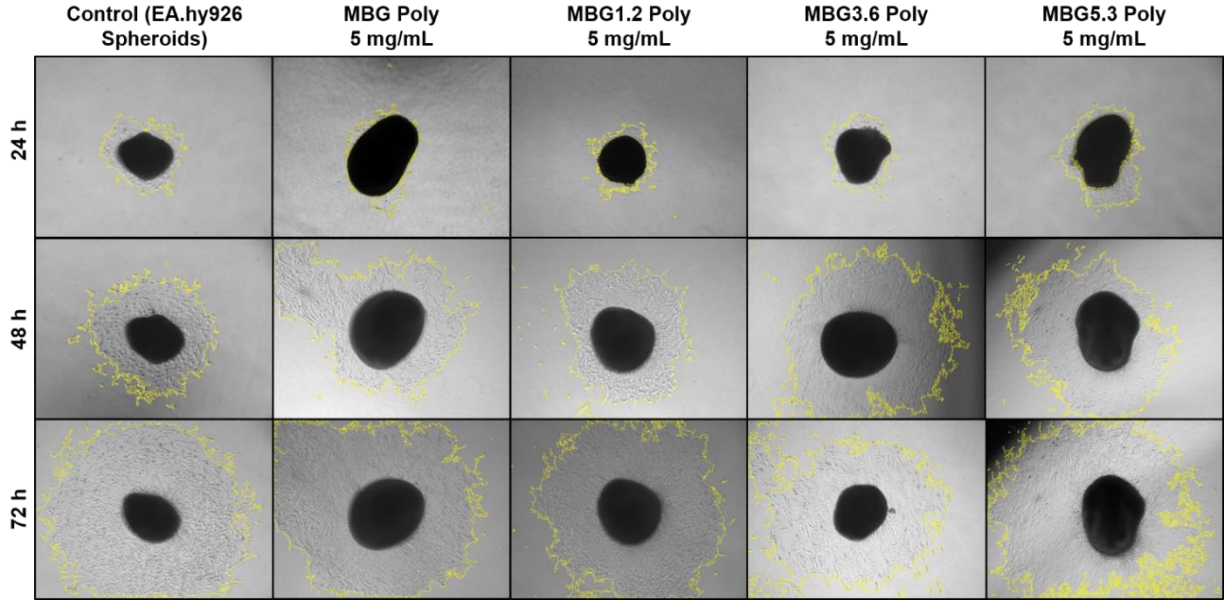

Figure 7.8: Light microscopy images of endothelial cell migration out of the spheroids after 24, 48 and 72 h of incubation with 5 mg/mL extracts of Ce-MBGs-Poly. The spheroid migration area is outlined in yellow.

High concentrations of Poly-loaded powders inhibited the migration at 48 h. However, by the end of the experiment, only marginal inhibition was observed in some groups of Ce-MBGs and Ce-MBGs-Poly at 5 mg/mL (MBG3.6 and MBG5.3 Poly)**. (Zambon et al. 2021)** proved that Ce-doped borate BGs exhibited increased formation of blood vessels in vivo. Research on rat cranial defect models showed that hollow mesoporous Ce-BG scaffolds promoted collagen deposition, osteoblast formation, and bone regeneration more effectively than BG scaffolds *in vivo*. Most of the literature studies documented a specific gene which is hypoxia-inducing

factor – 1α (HIF – 1α) regulates gene expression during angiogenesis. The reason for this transcription factor is the response to intracellular oxygen concentrations outcome in increased angiogenesis **(Das et al. 2012)**. Most of the research groups took advantage of the benefit of the oxygen capacity of the Ce ions to enhance the HIF – 1α and promote angiogenesis. **(Das et al. 2012)** assess the angiogenic ability of CNPs in both in vitro and *in vivo* models and the results demonstrated that the angiogenic capacity of CNPs mostly depends on the surface valence the authors conclude that the high surface area with increasing Ce^{3+} or Ce^{4+} ratios improve CNPs' more catalytically active towards modulating intracellular oxygen thus leading to induction of angiogenesis.

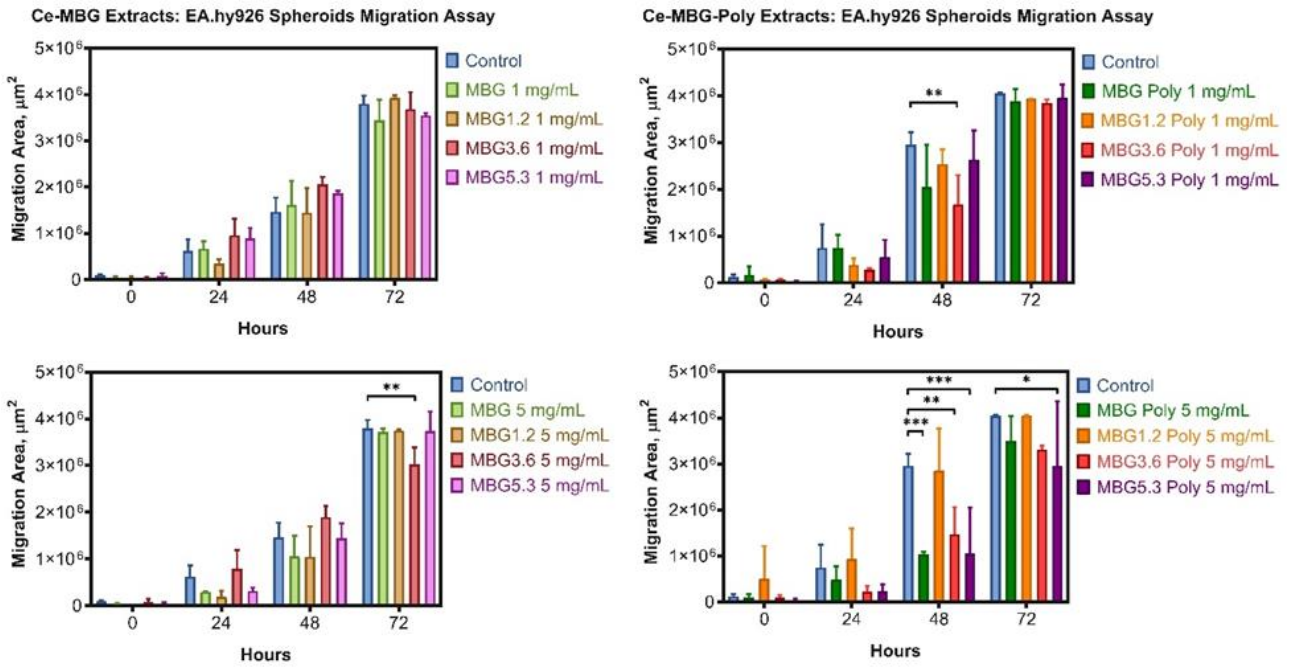

Figure 7.9: EA.hy926 endothelial cell spheroids migration assay. Spheroids migration was analysed by using ImageJ software by measuring the area of the cell migration after 0, 24, 48 and 72 hrs of incubation with MBGs extracts. The values are presented as mean ± SD, * - significant difference compared to control, p < 0.05; ** - p < 0.01; * - p < 0.001.**

7.2.4 MBGs Pellets Cytocompatibility Assay

The aim of the Ce-MBGs and Ce-MBGs-Poly powders is to promote bone repair by direct placement into the bone tumour resection site. So, the powders were compressed into composite disks and the disks' cytocompatibility was assessed in vitro towards hMSCs and EA.hy926 in direct contact. Due to the irrelevance of the comparison of cells seeded on polystyrene to cells seeded on the surface of the pellets, results were normalized and are reported as relative cell viability.

As shown in Figure 7.10a, for the viability of hMSCs after 1, 3 and 4 days of cultivation on the composites, no difference was noticed between MBG and MBG1.2, whereas in MBG3.6 and MBG5.3 the cell viability was almost two times lower. This trend was observed at all time points, however, neither of the groups

demonstrated any remarkable changes in relative cell viability between time points. As shown in Figure 7.10b, right panel, Ce-MBGs-Poly pellets appeared to be more cytocompatible in comparison with the MBG Poly without cerium; the loading with Poly concomitant with cerium doping thus preserves cell metabolic activity. In the case of direct contact with endothelial cells, both Ce-MBGs and Ce-MBGs-Poly did not show any cytotoxic effect on EA.hy926, and the cells showed an increase in metabolic activity, especially evident from 3 days onwards when cultured with all Ce-MBGs and in MBG5.3 Poly composites in comparison to MBG and MBG Poly, respectively (Figure 7.11 a and b).

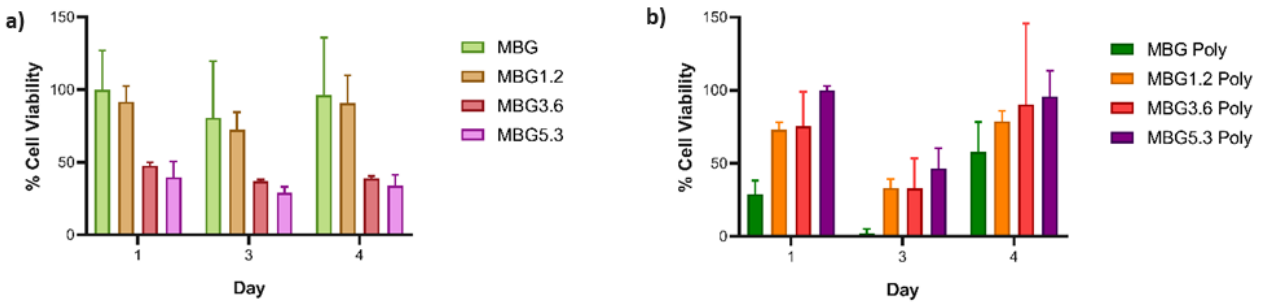

Figure 7.10: Ce-MBGs and Ce-MBGs-Poly pellets compatibility towards hMSCs. Values are presented as means of relative cell viability, and error bars represent SD.

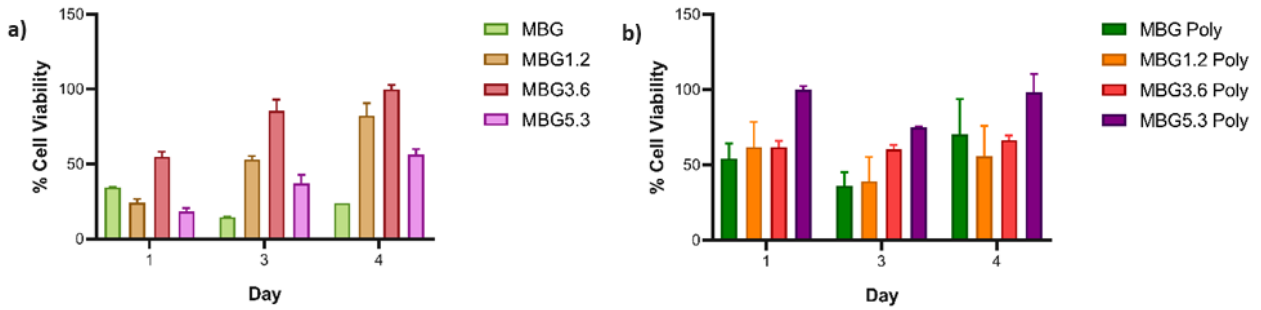

Figure 7.11: Ce-MBGs and Ce-MBGs-Poly pellets compatibility towards EA.hy926. Values are presented as means of relative cell viability, and error bars represent SD.

7.3 Conclusion

In our study, we examined the in vitro cytocompatibility of two types of mesoporous bioactive glasses with different antioxidant properties designed for bone tissue engineering, including tumour resection: MBGs doped with cerium and dually loaded with both cerium and polyphenols. By using both 2D and 3D in vitro models and relevant cell lines, we were able to demonstrate a complex relationship between the experimental design, material composition and dosage, and cellular responses. Variations in cytotoxicity between the 2D and 3D models highlighted how important it is to take different physiological circumstances into account. Factors such as direct cell-material contact, release of bioactive ions, and potential nutrient barrier effects influenced outcomes of cell metabolic activity, cell morphology, cell membrane integrity and migration assays. Furthermore, functionalization with polyphenols exhibited contrasting effects, showing mitigated cytotoxicity in comparison to Ce-MBGs without loading. Thus, supported by our previous observations of Ce release, the MBG1.2 Poly group at 1 mg/mL concentration emerged as promising in preserving hMSCs viability and endothelial cell migration. These findings highlight the importance of comprehensive evaluation approaches integrating diverse assay settings and cell types to enhance bioactive glasses research, as well as the need for further investigations of the biological effects of dual doping of MBGs with agents with distinct mechanisms of antioxidant activity.

7.4 References

Alaraby, Mohamed, Alba Hernández, Balasubramanyam Annangi, Eşref Demir, Jordi Bach, Laura Rubio, A. Creus, and Ricard Marcos. 2014. "Antioxidant and Antigenotoxic Properties of CeO2NPs and Cerium Sulphate: Studies withDrosophila Melanogasteras a Promisingin VivoModel." Nanotoxicology 9 (6): 749–59. https://doi.org/10.3109/17435390.2014.976284.

Atkinson, Irina, Ana Maria Seciu-Grama, Simona Petrescu, Daniela Culita, Oana Catalina Mocioiu, Mariana Voicescu, Raul-Augustin Mitran, Daniel Lincu, Ana-Maria Prelipcean, and Oana Craciunescu. 2022. "Cerium-Containing Mesoporous Bioactive Glasses (MBGs)-Derived Scaffolds with Drug Delivery Capability for Potential Tissue Engineering Applications." Pharmaceutics 14 (6): 1169. https://doi.org/10.3390/pharmaceutics14061169.

Baino, Francesco, Sepideh Hamzehlou, and Saeid Kargozar. 2018. "Bioactive Glasses: Where Are We and Where Are We Going?" Journal of Functional Biomaterials 9 (1): 25. https://doi.org/10.3390/jfb9010025.

Baino, Francesco, Giorgia Novajra, Valentina Miguez-Pacheco, Aldo R. Boccaccini, and Chiara Vitale-Brovarone. 2016. "Bioactive Glasses: Special Applications Outside the Skeletal System." Journal of Non-Crystalline Solids 432 (January): 15–30. https://doi.org/10.1016/j.jnoncrysol.2015.02.015.

Brookes, Marcus J., Corey D. Chan, Bence Baljer, Sachin Wimalagunaratna, Timothy P. Crowley, Maniram Ragbir, Alistair Irwin, et al. 2021. "Surgical Advances in Osteosarcoma." Cancers 13 (3): 388. https://doi.org/10.3390/cancers13030388.

Białkowska, Kamila, Piotr Komorowski, Maria Bryszewska, and Katarzyna Miłowska. 2020. "Spheroids as a Type of Three-Dimensional Cell Cultures—Examples of Methods of Preparation and the Most Important Application." International Journal of Molecular Sciences 21 (17): 6225. https://doi.org/10.3390/ijms21176225.

Cazzola, M., E. Vernè, A. Cochis, R. Sorrentino, B. Azzimonti, E. Prenesti, L. Rimondini, and S. Ferraris. 2017. "Bioactive Glasses Functionalized with Polyphenols: In Vitro Interactions with Healthy and Cancerous Osteoblast Cells." Journal of Materials Science 52 (15): 9211–23. https://doi.org/10.1007/s10853-017-0872-5.

Cazzola, Martina, Sara Ferraris, Francesco Boschetto, Alfredo Rondinella, Elia Marin, Wenliang Zhu, Giuseppe Pezzotti, Enrica Vernè, and Silvia Spriano. 2018. "Green Tea Polyphenols Coupled with a Bioactive Titanium Alloy Surface: In Vitro Characterization of Osteoinductive Behavior through a KUSA A1 Cell Study." International Journal of Molecular Sciences 19 (8): 2255. https://doi.org/10.3390/ijms19082255.

Corazzari, Ingrid, Maura Tomatis, Francesco Turci, Sara Ferraris, Elisa Bertone, Enrico Prenesti, and Enrica Vernè. 2016. "Gallic Acid Grafting Modulates the Oxidative Potential of Ferrimagnetic Bioactive Glass-Ceramic SC-45." Colloids and Surfaces. B, Biointerfaces 148 (December): 592–99. https://doi.org/10.1016/j.colsurfb.2016.09.034.

Das, Soumen, Sanjay Singh, Janet M. Dowding, Saji Oommen, Amit Kumar, Thi X.T. Sayle, Shashank Saraf, et al. 2012. "The Induction of Angiogenesis by Cerium Oxide Nanoparticles through the Modulation of Oxygen in Intracellular Environments." Biomaterials 33 (31): 7746–55. https://doi.org/10.1016/j.biomaterials.2012.07.019.

Diomede, Francesca, Guya Diletta Marconi, Luigia Fonticoli, Jacopo Pizzicanella, Ilaria Merciaro, Placido Bramanti, Emanuela Mazzon, and Oriana Trubiani. 2020. "Functional Relationship between Osteogenesis and Angiogenesis in Tissue Regeneration." International Journal of Molecular Sciences 21 (9): 3242. https://doi.org/10.3390/ijms21093242.

El-Rashidy, Aiah A., Judith A. Roether, Leila Harhaus, Ulrich Kneser, and Aldo R. Boccaccini. 2017. "Regenerating Bone with Bioactive Glass Scaffolds: A Review of in Vivo Studies in Bone Defect Models." Acta Biomaterialia 62 (October): 1–28. https://doi.org/10.1016/j.actbio.2017.08.030.

Ferraris, S., M. Miola, A. Cochis, B. Azzimonti, L. Rimondini, E. Prenesti, and E. Vernè. 2017. "In Situ Reduction of Antibacterial Silver Ions to Metallic Silver Nanoparticles on Bioactive Glasses Functionalized with Polyphenols." Applied Surface Science 396 (February): 461–70. https://doi.org/10.1016/j.apsusc.2016.10.177.

Firuzi, O., R. Miri, M. Tavakkoli, and L. Saso. 2011. "Antioxidant Therapy: Current Status and Future Prospects." Current Medicinal Chemistry 18 (25): 3871–88. https://doi.org/10.2174/092986711803414368.

Fröhlich, Eleonore. 2018. "Comparison of Conventional and Advanced in Vitro Models in the Toxicity Testing of Nanoparticles." Artificial Cells, Nanomedicine, and Biotechnology 46 (sup2): 1091–1107. https://doi.org/10.1080/21691401.2018.1479709.

Giacomo Riccucci, Martina Cazzola, Sara Ferraris, Virginia Alessandra Gobbo, Marta Miola, Antonella Bosso, Gissur Örlygsson, Chuen How Ng, Enrica Verné, and Silvia Spriano. 2021. "Surface Functionalization of Bioactive Glasses and Hydroxyapatite with Polyphenols from Organic Red Grape Pomace." Journal of the American Ceramic Society 105 (3): 1697–1710. https://doi.org/10.1111/jace.17849.

Gigliola Lusvardi, Francesca Fraulini, Sergio D'Addato, and Alfonso Zambon. 2022. "Loading with Biomolecules Modulates the Antioxidant Activity of Cerium-Doped Bioactive Glasses" 8 (7): 2890–98. https://doi.org/10.1021/acsbiomaterials.2c00283.

Hench, Larry L. 2006. "The Story of Bioglass®." Journal of Materials Science: Materials in Medicine 17 (11): 967–78. https://doi.org/10.1007/s10856-006-0432-z.

Jablonská, Eva, Diana Horkavcová, Dana Rohanová, and Delia S. Brauer. 2020. "A Review of in Vitro Cell Culture Testing Methods for Bioactive Glasses and Other Biomaterials for Hard Tissue Regeneration." Journal of Materials Chemistry B 8 (48): 10941–53. https://doi.org/10.1039/d0tb01493a.

K. Wittmaack. 2011. "Excessive Delivery of Nanostructured Matter to Submersed Cells Caused by Rapid Gravitational Settling." ACS Nano 5 (5): 3766–78. https://doi.org/10.1021/nn200112u.

Klimek, Katarzyna, Anna Belcarz, Robert Pazik, Paulina Sobierajska, Tomasz Han, Rafal J Wiglusz, and Grazyna Ginalska. 2016. "'False' Cytotoxicity of Ions-Adsorbing Hydroxyapatite — Corrected Method of Cytotoxicity Evaluation for Ceramics of High Specific Surface Area" 65 (August): 70–79. https://doi.org/10.1016/j.

Kumari, Monika, Shailendra Pratap Singh, Srinivas Chinde, Mohammed Fazlur Rahman, Mohammed Mahboob, and Paramjit Grover. 2014. "Toxicity Study of Cerium Oxide Nanoparticles in Human Neuroblastoma Cells." International Journal of Toxicology 33 (2): 86–97. https://doi.org/10.1177/1091581814522305.

Łapa, Agata, Mark Cresswell, Ian Campbell, Phil Jackson, Wolfgang H. Goldmann, Rainer Detsch, Andrew Parsons, Ifty Ahmed, and Aldo R. Boccaccini. 2019. "Ga and Ce Ion-Doped Phosphate Glass Fibres with Antibacterial Properties and Their Composite for Wound Healing Applications." Journal of Materials Chemistry B 7 (44): 6981–93. https://doi.org/10.1039/c9tb00820a

Leonelli, C., G. Lusvardi, G. Malavasi, L. Menabue, and M. Tonelli. 2003. "Synthesis and Characterization of Cerium-Doped Glasses and in Vitro Evaluation of Bioactivity." Journal of Non-Crystalline Solids 316 (2-3): 198–216. https://doi.org/10.1016/s0022-3093(02)01628-9.

Mouriño, V., R. Vidotto, J.P. Cattalini, and A.R. Boccaccini. 2019. "Enhancing Biological Activity of Bioactive Glass Scaffolds by Inorganic Ion Delivery for Bone Tissue Engineering." Current Opinion in Biomedical Engineering 10 (June): 23–34. https://doi.org/10.1016/j.cobme.2019.02.002.

Nicolini, Valentina, Elisa Gambuzzi, Gianluca Malavasi, Ledi Menabue, Maria Cristina Menziani, Gigliola Lusvardi, Alfonso Pedone, et al. 2015. "Evidence of Catalase Mimetic Activity in Ce3+/Ce4+ Doped Bioactive Glasses." Journal of Physical Chemistry B 119 (10): 4009–19. https://doi.org/10.1021/jp511737b.

Nicolini, Valentina, Gianluca Malavasi, Gigliola Lusvardi, Alfonso Zambon, Francesco Benedetti, Giuseppina Cerrato, Sergio Valeri, and Paola Luches. 2019. "Mesoporous Bioactive Glasses Doped with Cerium: Investigation over Enzymatic-like Mimetic Activities and Bioactivity." Ceramics International 45 (16): 20910–20. https://doi.org/10.1016/j.ceramint.2019.07.080.

O'Neill, Eric, Guleid Awale, Leila Daneshmandi, Obum Umerah, and Kevin Bryan Lo. 2018. "The Roles of Ions on Bone Regeneration" 23 (4): 879–90. https://doi.org/10.1016/j.drudis.2018.01.049.

Rosenfeldt, Franklin, Mark Wilson, Geraldine Lee, Christina Kure, Ruchong Ou, Lesley Braun, and Judy de Haan. 2013. "Oxidative Stress in Surgery in an Ageing Population: Pathophysiology and Therapy." Experimental Gerontology 48 (1): 45–54. https://doi.org/10.1016/j.exger.2012.03.010.

Saeid Kargozar, Sara Hooshmand, Seyede Atefe Hosseini, Sara Gorgani, Farzad Kermani, and Francesco Baino. 2022. "Antioxidant Effects of Bioactive Glasses (BGs) and Their Significance in Tissue Engineering Strategies." Molecules 27 (19): 6642–42. https://doi.org/10.3390/molecules27196642.

Sayed Abdelgeliel, Asmaa, Sara Ferraris, Andrea Cochis, Sara Vitalini, Marcello Iriti, Hiba Mohammed, Ajay Kumar, et al. 2019. "Surface Functionalization of Bioactive Glasses with Polyphenols from Padina Pavonica

Algae and in Situ Reduction of Silver Ions: Physico-Chemical Characterization and Biological Response." Coatings 9 (6): 394. https://doi.org/10.3390/coatings9060394.

Schuhladen, Katharina, Judith A. Roether, and Aldo R. Boccaccini. 2019. "Bioactive Glasses Meet Phytotherapeutics: The Potential of Natural Herbal Medicines to Extend the Functionality of Bioactive Glasses." Biomaterials 217 (October): 119288. https://doi.org/10.1016/j.biomaterials.2019.119288.

Torre, Elisa, Giorgio Iviglia, Clara Cassinelli, and Marco Morra. 2018. "Potentials of Polyphenols in Bone-Implant Devices." Polyphenols, July. https://doi.org/10.5772/intechopen.76319.

Torre, Elisa, Giorgio Iviglia, Clara Cassinelli, Marco Morra, and Nazario Russo. 2020. "Polyphenols from Grape Pomace Induce Osteogenic Differentiation in Mesenchymal Stem Cells." International Journal of Molecular Medicine, March. https://doi.org/10.3892/ijmm.2020.4556.

V, Bäcker . n.d. "Analyze Spheroid Cell Invasion in 3D Matrix." GitHub. Accessed April 11, 2024. https://github.com/MontpellierRessourcesImagerie/imagej_macros_and_scripts/wiki/Analyze-Spheroid-Cell-Invasion-In-3D-Matrix.

Xie, Hanyu, Sha Sha, Lingbo Lu, Geng Wu, Hongbing Jiang, Aldo R. Boccaccini, Kai Zheng, and Rongyao Xu. 2022. "Cerium-Containing Bioactive Glasses Promote in Vitro Lymphangiogenesis." Pharmaceutics 14 (2): 225. https://doi.org/10.3390/pharmaceutics14020225.

Zambon, Alfonso, Gianluca Malavasi, Annalisa Pallini, Francesca Fraulini, and Gigliola Lusvardi. 2021. "Cerium Containing Bioactive Glasses: A Review." ACS Biomaterials Science & Engineering 7 (9): 4388–4401. https://doi.org/10.1021/acsbiomaterials.1c00414.

Zhang, Xin, Sara Ferraris, Enrico Prenesti, and Enrica Verné. 2013. "Surface Functionalization of Bioactive Glasses with Natural Molecules of Biological Significance, Part I: Gallic Acid as Model Molecule." Applied Surface Science 287 (December): 329–40. https://doi.org/10.1016/j.apsusc.2013.09.151.

Zheng, Kai, Wen Niu, Bo Lei, and Aldo R. Boccaccini. 2021. "Immunomodulatory Bioactive Glasses for Tissue Regeneration." Acta Biomaterialia 133 (October): 168–86. https://doi.org/10.1016/j.actbio.2021.08.023.

Zheng, Kai, Elisa Torre, Alessandra Bari, Nicola Taccardi, Clara Cassinelli, Marco Morra, Sonia Fiorilli, Chiara Vitale-Brovarone, Giorgio Iviglia, and Aldo R. Boccaccini. 2020. "Antioxidant Mesoporous Ce-Doped Bioactive Glass Nanoparticles with Anti-Inflammatory and Pro-Osteogenic Activities." Materials Today Bio 5 (January): 100041. https://doi.org/10.1016/j.mtbio.2020.100041.

Zhu, Hui, Kai Zheng, and Aldo R. Boccaccini. 2021. "Multi-Functional Silica-Based Mesoporous Materials for Simultaneous Delivery of Biologically Active Ions and Therapeutic Biomolecules." Acta Biomaterialia 129 (July): 1–17. https://doi.org/10.1016/j.actbio.2021.05.007.

Chapter IX

Functionalization of Natural Polyphenols onto to Titanium Surface

Aim

The application of natural compounds, such as polyphenols, is becoming increasingly popular for tissue regeneration and wound healing. Polyphenols are bioactive compounds that have significant health effects. The beneficial effects of polyphenols on health and the protective effects of food as antioxidants have been extensively studied and widely accepted. Polyphenols are also known to have anti-inflammatory properties that can help reduce inflammation at damaged sites by inhibiting the production of inflammatory molecules and modulating the activity of inflammatory cells. This chapter examines the role of polyphenols and their applications in biomaterials. Moreover, polyphenols have been utilized for stabilizing collagen and enhancing its durability against degradation in biological systems. Numerous studies have shown enhanced bone formation, mineralization, proliferation, differentiation, and viability of osteoblasts. Polyphenols stimulate osteoblast cells and provide a protective barrier against oxidative stress and inflammatory cytokines, resulting in these effects. Furthermore, polyphenols prevent the differentiation of osteoclast cells. Together, these behaviours encourage the growth of bones and decrease bone resorption. In the present work, we evaluated titanium surface functionalization with tea polyphenols to prevent chronic inflammation during bone regeneration.

Chapter IX has been published in a 'research article' in MDPI Nanomaterials with several collaborators: Gamna, Francesca, Seiji Yamaguchi, Andrea Cochis, Sara Ferraris, Ajay Kumar, Lia Rimondini, and Silvia Spriano. 2023. Conferring Antioxidant Activity to an Antibacterial and Bioactive Titanium Surface through the Grafting of a Natural Extract. (https://doi.org/10.3390/nano13030479). In this paper, the contribution of the author is as follows:

Seiji Yamaguchi: Extraction of green tea leaves polyphenols and in vitro antibacterial activity.

Francesca Gamna, Sara Ferraris, and Silvia Spriano: Surface functionalization of titanium with polyphenols

Ajay Kumar: Performed the cytocompatibility and antioxidant properties.

Polyphenols Extraction and Surface functionalization

The polyphenols used in this work were extracted from green tea leaves (TPH) (Longjing, produced in Hangzhou, China). Commercially pure titanium samples were polished and subjected to a thermal-chemical surface treatment to create a calcium surface layer, and then iodine ions were introduced on the surface. Furthermore, samples were functionalized with TPH solution on the surface. Samples were provided by the Politecnico di Torino in collaboration with Chubu University, Japan.

Abstract

The main unmet medical need of bone implants is multifunctional activity, including their ability to induce rapid and physiological osseointegration, counteract bacterial biofilm formation, and prevent in situ chronic inflammation at the same time. This research starts from an already developed c.p. titanium surface with proven bioactive (in vitro hydroxyl apatite precipitation) and antibacterial activities, due to a calcium titanate layer with nano- and micro-scale roughness and loaded with iodine ions. Here, antioxidant ability was added to prevent chronic inflammation by grafting polyphenols of a green tea extract onto the surface, without compromising the other functionalities of the surface. The surface was characterized before and after functionalization through XPS analysis, zeta potential titrations, ion release measurements, in vitro bioactivity tests, SEM and fluorescence microscopy, and Folin–Ciocalteu and biological tests. The presence of grafted polyphenols as a homogeneous layer was proven. The grafted polyphenols maintained their antioxidant ability and were anchored to the surface through the linking action of Ca^{2+} ions added to the functionalizing solution. Iodine ion release, cytocompatibility towards human mesenchymal stem cells (hMSCs), and antibacterial activity were maintained even after functionalization. The antioxidant ability of the functionalized surface was effective in preserving hMSCs viability in a chemically induced pro-inflammatory environment, thus showing a scavenger activity towards toxic active species responsible for inflammation.

Introduction

Titanium and its alloys are widely used as materials for biomedical and prosthetic engineering, particularly for bone repair where large loads are involved, given their high mechanical properties. However, loosening of these implants is often reported, as bare, polished titanium has poor adhesion to bone and often requires a long period to achieve osseointegration **(Barfeie, Wilson, and Rees 2015).** Since the 1960s, when osseointegration was first observed, several surface modifications have been explored to give titanium and its alloys the ability to bond to bone following different treatments, such as chemical **(Le Guéhennec et al. 2007)**, mechanical **(Balza et al. 2013)**, hydrothermal **(E.B. Ansar et al. 2019),** ion implantation **(Nayab, Jones, and Olsen 2007),** and anodic oxidation **(J. Pavón et al. 2013).**

Despite the positive results of increased bone bonding and bone growth achieved with the various surface treatments, the challenge of providing titanium with antibacterial activity remains an unmet medical issue. The incidence of prosthetic joint infection is still around 2% and it is continuously increasing **(Tande and Patel 2014)**. To combat infections caused by pathogenic bacteria, antibiotic therapy is a widely used approach **(Ma et al. 2022)**. However, the main problem associated with antibiotic therapies is the increasing development of antibiotic-resistant bacterial strains and their narrow spectrum of activity, resulting in difficulty in treating infections caused by different bacteria **(Mancuso et al. 2021)**. For this reason, the scientific community began to investigate ways to make the titanium surface not only osseointegrated but also antibacterial, using different methods and antibacterial agents **(Ferraris and Spriano 2016)**. Current techniques to reduce

bacterial attachment and biofilm formation include antiadhesive function and bactericidal function **(Hasan, Crawford, and Ivanova 2013)**. The incorporation of metal ions, particularly silver, copper, and zinc, which have antibacterial action, is of great interest **(Orapiriyakul et al. 2018).** Unfortunately, a proper balance between effective antibacterial action and cytocompatibility is difficult to find **(Cazzola et al. 2022).** Attention then shifted to iodine ions as excellent candidates for antibacterial, biocompatible, and noncytotoxic agents. When an iodine-containing calcium titanate is produced on Ti by a chemical and heat treatment, the treated metal exhibits in vitro and in vivo antibacterial activity, in vitro apatite formation, and in vivo bone-bonding ability **(Ikeda et al. 2022).**

Another important factor that can lead to implant failure is inflammation; 47% of early implant failures are caused by inflammation **(Sun et al. 2017).** Again, the scientific literature has focused on the search for surface functionalization or coatings on titanium that can modulate inflammation to achieve a multifunctional surface **(Gamna et al. 2022).** One area of research of significant interest is the functionalization of titanium surfaces for biomedical implants with polyphenols. Polyphenols are a diverse group of phytochemicals found in fruits, vegetables, nuts, and other plant-based foods. They have potent antioxidant properties and anti-inflammatory effects on the body **(Scalbert, Johnson, and Saltmarsh 2005)**.

One of the main mechanisms by which polyphenols exert their antioxidant effects is by redox chemical action and scavenging free radicals. Free radicals are highly reactive molecules that can cause damage to cells and contribute to the development of chronic diseases such as cancer and heart disease. Polyphenols act as antioxidants and neutralize these free radicals, thereby preventing cellular damage **(Di Meo et al. 2013).**

In addition to their antioxidant properties, polyphenols also have anti-inflammatory effects on the body. Inflammation is a natural response to injury or infection, but chronic inflammation is linked to the development of many diseases. Polyphenols inhibit the production of inflammatory molecules and modulate the activity of inflammatory cells, which can help to reduce inflammation in the body **(Hans Konrad Biesalski 2007).** More controversial and still under study, is the antibacterial role of polyphenols. Studies can be found in the literature claiming the high antibacterial properties of polyphenols against certain bacteria strains. Research on polyphenols also shows that they may have beneficial effects on a wide range of health conditions, including cancer, heart disease, diabetes, and neurodegenerative diseases **(Kampa et al. 2007) (Barreto and Guedes 2012).** Indeed, polyphenols have gained great attention in different industrial fields due to their antioxidant, antibacterial, and anticarcinogenic capabilities. Their antioxidant action is strictly connected to the removal of radical oxygen species, and it resolves into an anti-inflammatory behaviour in a biological environment. Polyphenols are molecules that can be extracted from a large number of natural products, including waste products, economically and sustainably, representing an important approach to the ecological use of resources. In this paper, polyphenols extracted from green tea are specifically studied. The polyphenol family includes a wide range of substances containing one or more phenolic groups. All polyphenols are classified into two main categories: phenolic acids and flavonoids **(Cazzola et al. 2016)**.

Polyphenols contain both monomers and polymerized polyphenols. Green tea is very rich in catechins and their oligomers, which are part of the flavonoid family and are responsible for its renowned potential benefits, including antioxidant capacity. Among all catechins, epigallocatechin-3-gallate (EGCG) accounts for 60% of the catechins present in green tea **(Riccucci et al. 2021)**.

In this work, a surface functionalization protocol was optimized to graft tea polyphenols onto a titanium surface previously made bioactive (in vitro precipitation of hydroxyapatite) through specific heat treatment and made antibacterial through the loading of iodine ions. These substrates have been extensively characterized in previous works and their osseointegration ability is already verified. A high long-term sustainable bone-bonding capacity was confirmed by in vivo tests and mechanical and histological experiments **(Ikeda et al. 2022)**. In addition, the same type of green tea used here (TPH) has been previously tested and was found to have a good ability to promote osteoblast differentiation and mineralization **(Cazzola et al. 2018)**.

For functionalization, a specific focus was paid to the selection of the solvent medium and pH, the effect of Ca^{2+} ions in the solution on the grafting mechanism, and the concentration of the polyphenol source solution. A preliminary characterization of the functionalized surfaces was performed using the Folin–Ciocalteu photometric test and XPS (X-ray photoelectron spectroscopy) analysis, to verify the presence and activity of the grafted polyphenols. In vitro bioactivity, antibacterial activity, cytocompatibility, and antioxidant capacity were evaluated in the functionalized samples. Accordingly, the formation of apatite was observed, the ability to prevent the surface colonization from the pathogen *E. coli* was verified, and the antioxidant activity was confirmed by the possibility of protecting human cells from toxic active species in a pro-inflammatory environment by a scavenger mechanism.

This research aims to improve an already extensively studied surface with exceptional osseointegration capacity and antimicrobial properties by incorporating the renowned anti-inflammatory properties of tea polyphenols to create a multifunctional surface with osseointegration and antimicrobial and anti-inflammatory capabilities.

8. Materials and Methods

8.1. Cytocompatibility Evaluation

Biological characterizations were performed using square samples (10 mm × 10 mm × 1 mm) sterilized by UV light for 2 h. The samples' composition is shown in Table 8.1.

Table 8.1: Represents the samples' names and composition.

No	Samples' names	Coating
1	Ti	No coating (Control)
2	Ti_Ca+I	Calcium chloride ($CaCl_2$) and iodine ions (I)
3	TI_Ca+I+TPH	iodine ions and green tea leaves (TPH)

For the cytocompatibility studies, samples were gently placed into a 24 multi-well plate and hMSCs were seeded dropwise with a specific number of cells (1×10^4 cells/sample) onto the samples' surface and allowed to adhere for 4 h at 37°C before being submerged in 1 mL of medium. After 24 h of cultivation in direct contact with the sample surface, the cell viability was evaluated by their metabolic activity by the colourimetric metabolic Alamar blue assay as described previously in section 4.1.7. Moreover, cells adhered to the sample surface were investigated for their viability by the fluorescent live/dead assay (LIVE/DEAD, from Invitrogen, Milan, Italy); briefly, after washing with PBS, the solution was added to each sample and then incubated for 45 min. After incubation, the samples were washed with PBS and fluorescent images were collected by a confocal microscope (Leica SP8 confocal platform, Leica Microsystems, Germany).

8.1.1 Pre-inflammatory Model in Polystyrene

Before applying the pre-inflammatory protocol to the control and treated Ti samples, it was pre-validated by using the polystyrene gold standard as a substrate for cells' cultivation. Accordingly, 300 mM H_2O_2 was added into the medium to introduce toxic active species; after 3 hours, cells (hMSCs, $1x10^4$ cells/sample) were seeded onto the wells of a 24 multiwell plate and submerged with 1 mL/well of the pre-conditioned medium (schematized in Figure 8.2a). Cells were cultivated for 24 h and then their metabolic activity was evaluated by the alarm blue assay as detailed in the main paper. Moreover, to demonstrate that the toxic effect was due to the internalization of toxic active species, the specific CellRox reagent (CellROX™ Deep Red Reagent kit, from Thermo Fisher Scientific, Milan, Italy) was used to visualize the species in the intracellular compartment; cells were further co-stained with phalloidin (Alexa Fluor 488 Phalloidin, from Thermo Fisher Scientific, Milan, Italy) and 4,6-diamidino-2-phenylindole (DAPI, Sigma Aldrich, Milan, Italy) to visualize cytoskeleton F-actin filaments and nuclei, respectively. Cells cultivated in a regular medium were considered a positive control.

8.1.2 Pro-inflammatory Model in Polystyrene

Before applying the pro-inflammatory protocol to the control and treated Ti samples, it was pre-validated by using the polystyrene gold standard as a substrate for cells' cultivation. Accordingly, cells (hMSCs, $1x10^4$ cells/sample) were seeded onto the wells of a 24 multiwell plate and submerged with 1 mL/well of the medium. After 24 h, 300 mM H_2O_2 was added into the medium to introduce toxic active species (schematized in Figure 8.3a); after 3 h cells' metabolic activity was evaluated by the alarm blue assay as detailed in section 4.1.7. Moreover, to demonstrate that the toxic effect was due to the internalization of toxic active species, the specific CellRox reagent (CellROX™ Deep Red Reagent kit, from Thermo Fisher Scientific, Milan, Italy) was used to visualize the species in the intracellular compartment; cells were further co-stained with phalloidin (Alexa Fluor 488 Phalloidin, from Thermo Fisher Scientific, Milan, Italy) and 4,6-diamidino-2-phenylindole (DAPI, Sigma Aldrich, Milan, Italy) to visualize cytoskeleton F-actin filaments and nuclei, respectively. Cells cultivated in the regular medium were considered as positive control.

8.1.3 Antioxidant Properties Evaluation

The samples' ability to act as an antioxidant by scavenger process was evaluated regarding their ability to promote cell survival in a pro-inflammatory environment. Accordingly, the inflammation was chemically induced by adding hydrogen peroxide (H_2O_2, 3 h, 300 mM) into the medium to generate oxidative stress by toxic active species as previously shown by the authors **(Bonifacio et al. 2020)**. Accordingly, H_2O_2 was added before the cell seeding to resemble a pre-implant inflammation, or after the seeding to simulate a post-operative inflammation.

8.1.4 Statistical Analysis

Six replicates were utilized for conducting biological evaluations. The findings were assessed using SPSS software (v25, IBM, New York City, NY, USA) through one-way ANOVA followed by Tukey's test for post hoc analysis. The level of significance was established as $p < 0.05$.

8.2 Results and Discussion

To exclude any toxic effect, cytocompatibility was verified before moving to the antioxidant property evaluation. Given the potential application of the here-developed samples for bone repair, hMSCs were considered as a target model because of their pivotal role in the healing process. Moreover, cells were seeded directly in direct contact with the control and functionalized surfaces to study their ability to properly adhere, spread, and exploit metabolic activity, thus simulating possible colonization of the device after implantation by the cells recruited from the neighbour tissue towards the injury site **(Rivera et al. 2021).**

8.2.1 Cytocompatibility

Metabolic activity was considered as the parameter to determine the viability of the cells adhered to the sample surface after 24 h of cultivation, with the results reported in Figure 8.1. Neither of the treated surfaces (Ti_Ca+I or Ti_Ca+I+TPH) showed a reduction in the hMSCs metabolic activity in comparison to the untreated Ti control ($p > 0.05$), which was considered as a positive control given the large literature demonstrating its biocompatibility **(Zuo et al. 2021).** On the contrary, the presence of polyphenols (TPH) led to an increase (≈15%) in the metabolism in comparison to the Ti control which was assumed as 100% as discussed prior (Figure 8.1b). It can be hypothesized that the bioactivity of the functionalized samples was improved; thus, they are hypothetically able to improve/speed up the healing process. The previous literature demonstrates that green tea polyphenols can improve or increase the speed of different mechanisms related to mesenchymal stem cells, such as proliferation and differentiation **(Zhou et al. 2017)** or osteogenesis **(Chen et al. 2005),** by different molecular pathways, as reviewed by **(Trzeciakiewicz et al. 2009)**. when investigating bone physiology. Therefore, the polyphenols applied here from green tea demonstrated an interesting pro-regenerative potential similar to other well-known polyphenols, such as resveratrol **(Prakoeswa et al. 2020)**, which stimulates hMSCs to release growth factors in non-healing wounds, and curcumin, which improves BMP-2 and TGF-β production ameliorating osteogenesis in a pro-inflammatory environment **(Chen et al. 2021).** On the contrary, the iodine contribution appeared insignificant in terms of the hMSCs metabolism boost (≈5% improvement in comparison to Ti control); however, there is no evidence from previous research saying that iodine significantly helps stem cells as a pro-regenerative or pro-healing activity. Iodine is mostly recognized as a strong antioxidant through its action as an electron donor, and it can neutralize ROS or attach to the double bonds to some phospholipids on the cell membrane, making them less reactive to ROS (**Aceves et al. 2021)** as well as a potential antibacterial agent as previously demonstrated by **(Yamaguchi et al. 2021)**. To obtain a visual confirmation of the samples' successful colonization, live/dead fluorescent imaging (Figure 8.1c) was applied to confirm that cells were viable (stained in green) showing a correct fibroblast-like morphology and a comparable surface density between the control and functionalized samples.

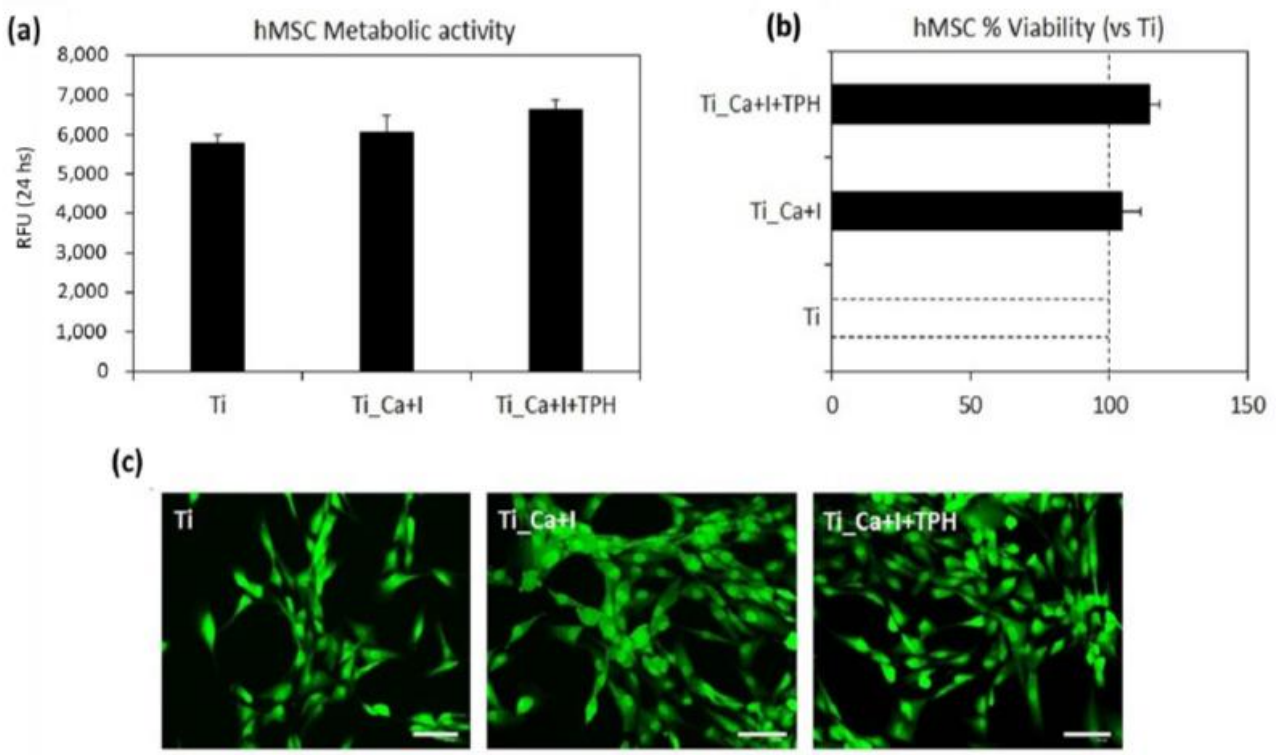

Figure 8.1: Cytocompatibility evaluation. Surface functionalization with iodine (Ti_Ca+I) and polyphenols (Ti_Ca+I+TPH) did not decrease hMSCs metabolic activity in comparison to the Ti controls ((a), $p > 0.05$) giving a positive boost of ≈5% and ≈15%, respectively. (c), Live/dead images confirmed that cells were viable (stained in green) with a proper morphology and comparable surface density. (b), bars represent means ± dev.st, replicates = 3. Images bar scale = 125 µm.

8.2.2 Pre-inflammatory Model

Pre-inflammatory results are reported in Figure 8.2. As can be noted by the metabolic assay (Figure 8.2b), the induced pro-inflammatory environment caused a significant reduction of the cell's metabolism (≈54%) being significant in comparison to the untreated controls ($p<0.05$, indicated by §). Therefore, the cells were able to sense the toxic environment reducing their metabolism and most likely their number as can be hypothesized from the density of the DAPI-labelled nuclei. As a confirmation of the cytotoxicity induced by the generated active species, the specific CellRox fluorescent dye was detected in the majority of the cells exposed to the H_2O_2-doped medium, thus confirming the suitability of the proposed protocol to resemble a material applied into an inflamed environment.

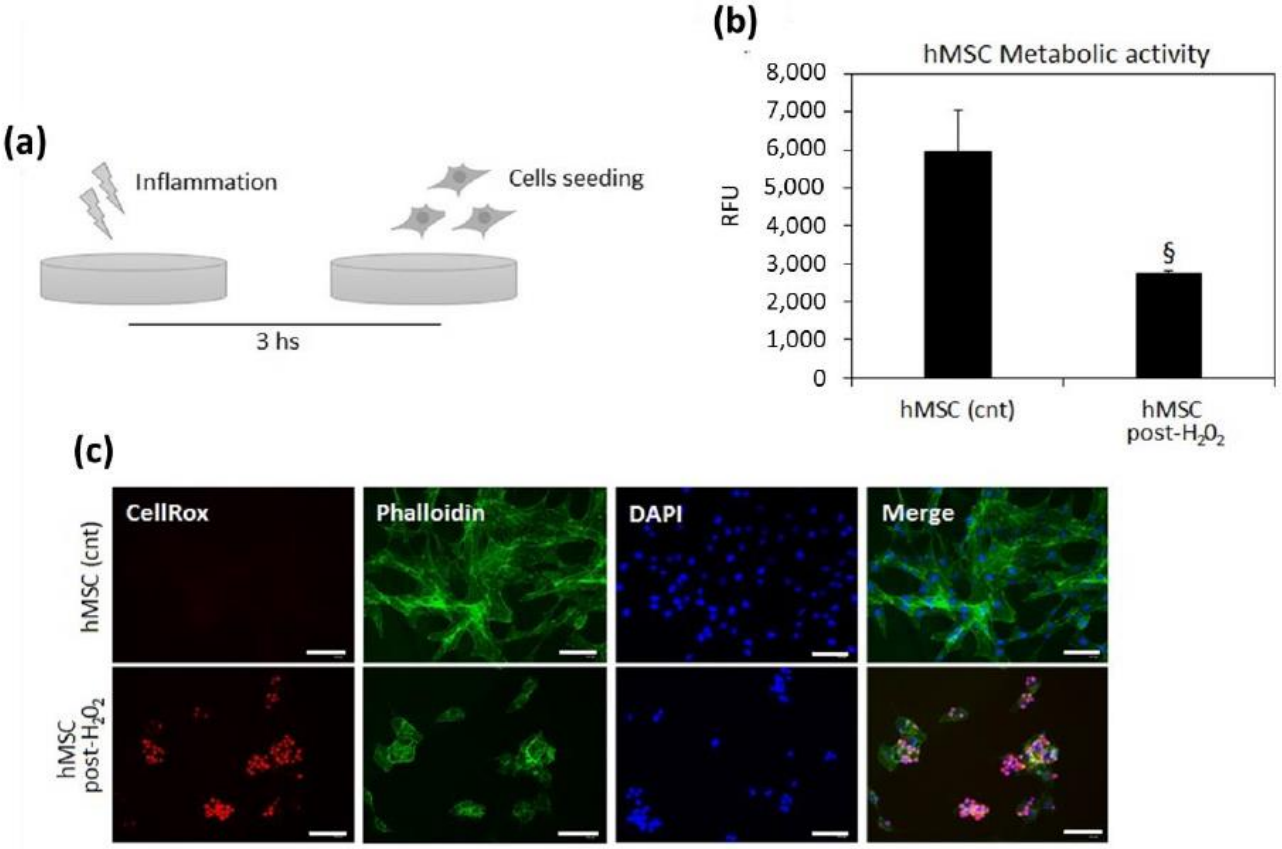

Figure 8.2: The use of H_2O_2 to pre-induce the formation of an inflammatory environment (a) determined a significant reduction of the cells' metabolism in comparison to the untreated controls ((b), $p<0.05$ indicated by §). As a confirmation, toxic active species were detected in the majority of the cells exposed to such pre-conditioned environment (c), positive cells stained in red by CellRox dye. Bars represent means±dev.st, replicates=3. Images bar scale=125 µm.

8.2.3 Pro-inflammatory Model

Pro-inflammatory results are reported in Figure 8.3. As can be speculated by the metabolic assay (Figure 8.3b), the introduction of toxic active species by H_2O_2 exposition caused a significant reduction of the cell's metabolism (≈62%) being significant in comparison to the untreated controls ($p<0.05$, indicated by §). Therefore, the cells reacted to the presence of such toxic elements by reducing their metabolism and most likely their number as can be hypothesized from the density of the DAPI-labelled nuclei. As a confirmation of the cytotoxicity induced by the generated active species, the specific CellRox fluorescent dye was detected in the majority of the cells exposed to the H_2O_2-doped medium, thus confirming the suitability of the proposed protocol to resemble the rise of a pro-inflammatory event after implantation.

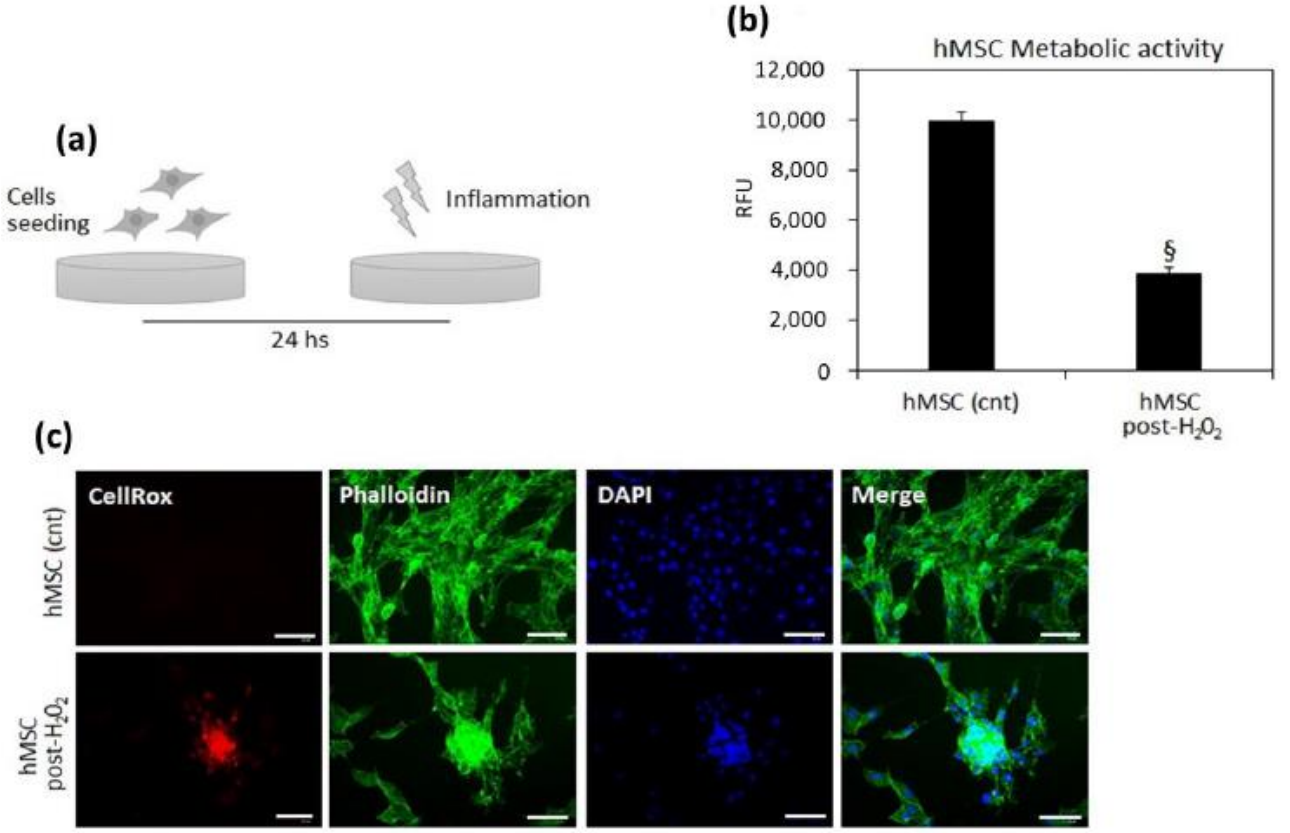

Figure 8.3: The use of H_2O_2 to generate toxic active species resembling an inflammatory environment (a) determined a significant reduction of the cells' metabolism in comparison to the untreated controls ((b), $p<0.05$ indicated by §). As a confirmation, toxic active species were detected in the majority of the cells exposed to H_2O_2-doped medium (c), with positive cells stained in red by CellRox dye). Bars represent means±dev.st, replicates=3. Images bar scale=125 µm.

8.2.4 Antioxidant Properties Evaluation

We imposed oxidative stress to the hMSCs seeded onto the surface of the control (Ti) and functionalized samples (Ti_Ca+I and Ti_Ca+I+TPH) by the generation of active species through H_2O_2 medium doping, to verify if any scavenger action was performed by the surfaces. In the first experimental set-up, a pro-inflammatory environment was induced before cell seeding to verify if the functionalization was effective in reducing the amount of free toxic active species, affecting the cells migrating towards the implant site.

Results related to the sample tests are reported in Figure 8.4. As expected, the lowest value in terms of cell metabolic activity was registered by the untreated Ti controls (Figure 8.4a); the lack of any protective effect was determined by a toxic environment driving cells mostly to the apoptotic stage, as seen by the SEM images (Figure 8.4b), where cells appeared mostly in the typical apoptotic round shape. On the contrary, iodine (Ti_Ca+I) provided first protection showing a significant improvement in comparison to the Ti control (Figure 8.4a, $p < 0.05$ indicated by §), but the best results were achieved by the combination of iodine + polyphenol (Ti_Ca+I+TPH), with changes that were significant in comparison to both the control and iodine (Figure 8.4a,

p < 0.05 indicated by § and #, respectively). SEM images (Figure 8.4b) confirmed that cells seeded onto the functionalized surfaces were able to adhere, spread, and maintain a proper fibroblast-like morphology. Their metabolism was also the highest when the Alamar blue assay was applied. Therefore, it can be hypothesized that iodine and polyphenols worked in synergy to maximize the capture of the active species, thus protecting cells from their toxic effect. To confirm this hypothesis, the specific fluorescent assay CellRox was applied to visualize the active species internalized by the cells. As displayed in Figure 8.4c, most of the cells cultivated onto Ti were positive to the red colour of the dye (indicated by the red arrows), whereas the number of cells positive decreased when iodine and iodine/polyphenols surfaces were analyzed. Moreover, as previously observed by SEM, cells on the Ti controls displayed mostly a round-shaped morphology, forming clusters. On the contrary, cells cultivated in the Ti_Ca+I+TPH samples showed the highest density, a proper morphology, and the lowest number of red-positive signals, thus giving confirming the starting hypothesis.

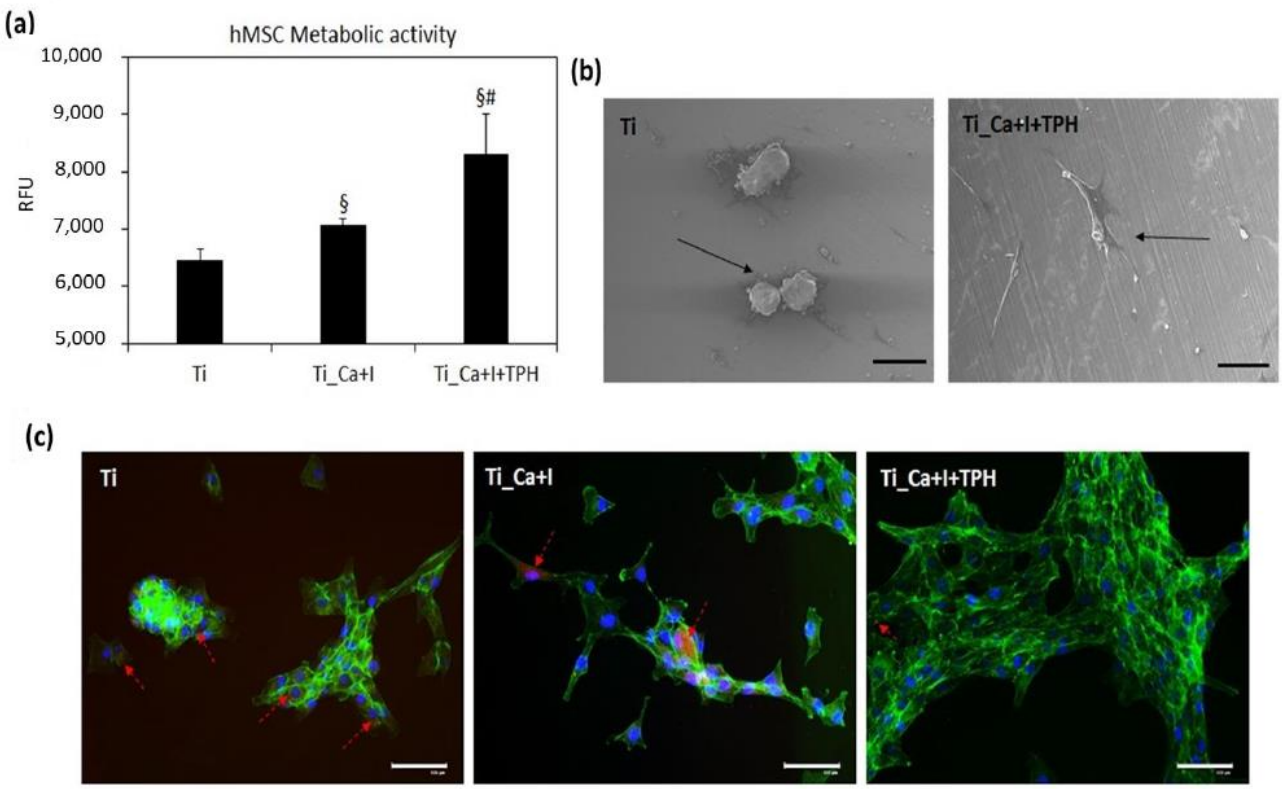

Figure 8.4: Pre-inflammatory evaluation. When the inflammatory environment was generated before cell seeding, the presence of iodine + polyphenols (Ti_Ca+I+TPH) protected cells from oxidative stress, as they showed the highest metabolism ((a), p < 0.05 in comparison with Ti and Ti_Ca+I, indicated by § and #, respectively) and a proper morphology in SEM images (b). The toxic effect was due to the active species internalization, as shown in the CellRox staining (c), positive cells stained in red) where most of the resulting cells were protected by the iodine and polyphenol. Bars represent means ± St. dev, replicates = 3. SEM images: 180× magnification, bar scale = 100 µm; fluorescent images bar scale = 125 µm.

In the second experimental set-up, the pro-inflammatory environment was induced after cell seeding to verify if the functionalization was effective in protecting from free toxic active species where the cells colonized the implant site. The protocol was first validated using polystyrene as a gold standard substrate for cell cultivation and the results are reported in Figure 8.3.

In a very similar way to the first experimental set-up, the lowest value in terms of cell metabolic activity was reported by the untreated Ti controls (Figure 8.5a); however, in this second pro-inflammatory condition only the functionalization based on the iodine + polyphenols reported significant results in comparison to both Ti controls and iodine functionalized Ti_Ca+I (Figure 8.5a, $p < 0.05$ indicated by § and #, respectively). Probably, the presence of the cells seeded before H_2O_2 administration reduced the scavenger activity of the surfaces by "screening" some of the surface-exposed iodine ions and polyphenols; therefore, only the combination was effective in protecting the cells from oxidative stress. Therefore, the very promising protective effect of the iodine + polyphenols combination was confirmed, as the cells maintained the correct morphology, as seen by the SEM images (Figure 8.5b) and minimized the toxic effect of the active species internalization, as confirmed by the CellRox fluorescent dye (Figure 8.5c). This assay was specifically chosen considering the hypothesis that TPH can act as a scavenger, thus preventing the intracellular accumulation of toxic active species generated by the H_2O_2 administration.

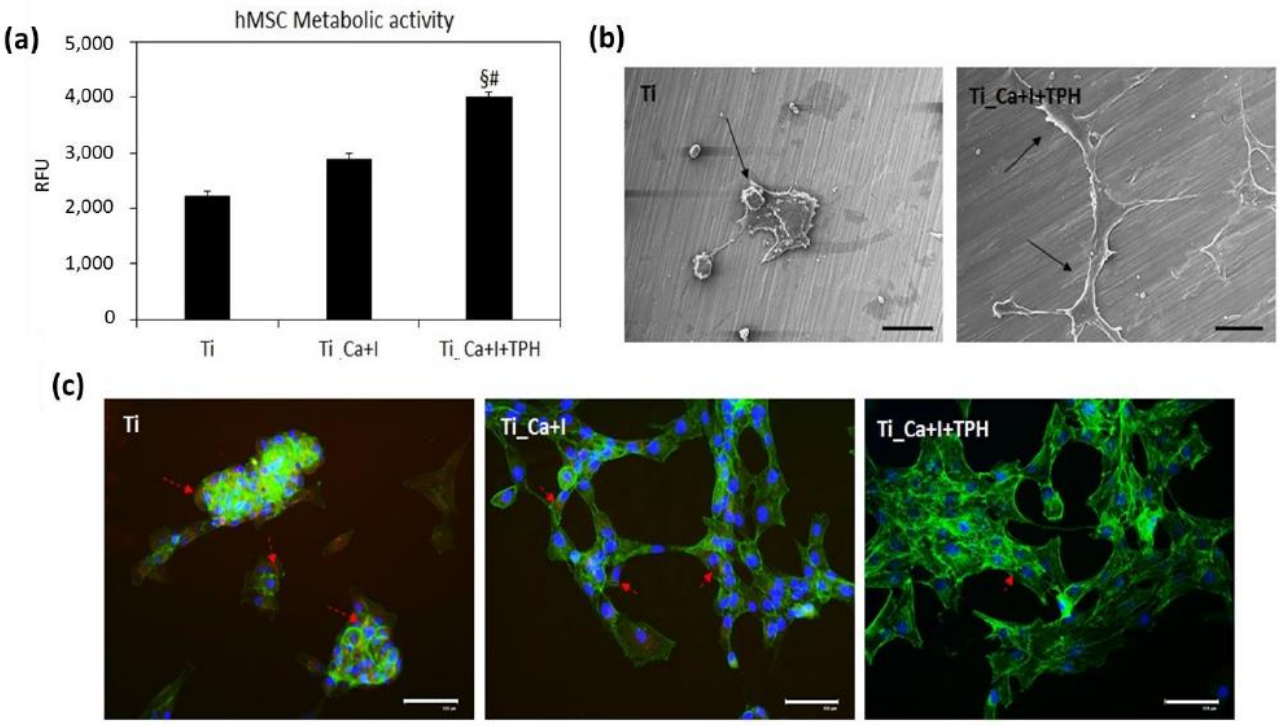

Figure 8.5: Pro-inflammatory evaluation. When the inflammatory environment was generated after cell seeding, the presence of iodine + polyphenols (Ti_Ca+I+TPH) protected cells from oxidative stress, as the highest metabolism was highest ((a), $p < 0.05$ in comparison with Ti and Ti_Ca+I, indicated by § and #, respectively), and a proper morphology in the SEM images (b). The toxic effect was due to the active species internalization as shown in the CellRox staining (c), positive cells stained in red), where most of the cells were protected by the iodine and polyphenol. Bars represent means ± St. dev, replicates = 3. SEM images: 180× magnification, bar scale = 100 µm; fluorescent images bar scale = 125 µm.

The results agree with the literature. Iodine is largely demonstrated to have an intrinsic antioxidant activity that can be exploited to reduce inflammation in situ upon implantation for tissue engineering purposes. Iodine is internalized by a facilitated diffusion system that is conserved and it directly neutralizes free radicals, induces the expression of type II antioxidant enzymes, or inactivates proinflammatory pathways **(Jekabsone et al. 2019)**. Moreover, here, iodine was combined with polyphenols, another element conferring strong antioxidant activity to the functionalized surfaces, as previously demonstrated also by the authors **(Jekabsone et al. 2019) (Savickiene et al. 2018)**. Polyphenols are very promising chemicals as they improve tissue repair under pro-inflammatory conditions. Regarding bone repair, polyphenols stimulate bone formation, mineralization, proliferation, differentiation, and the survival of osteoblasts by a protective effect against oxidative stress and inflammatory cytokines. In addition, polyphenols inhibit the differentiation of the osteoclast cells, thus favouring bone repair over resorption **(Shavandi et al. 2018)**.

The exploitation of the combination of TPH + iodine confirmed the starting hypothesis that this combination confers antioxidant properties to the ion-doped surface. Future further studies are still necessary to understand the cell response in terms of up-or down-regulation of pro- and anti-inflammatory markers to better define in which pathways THP and iodine are involved.

8.3 Conclusion

Green tea polyphenols were successfully grafted onto the surface of chemically treated titanium doped with iodine ions. Physicochemical characterization was performed, and the presence, amount, distribution, and release of the grafted polyphenols were evaluated. The reported results showed a stable molecular grafting, uniformly on the surface, which allowed hydroxyapatite precipitation. The polyphenols showed a good antioxidant effect in the biological environment and did not alter the antibacterial effect of iodine or the morphology of the surface, thus succeeding in obtaining a multifunctional surface with anti-inflammatory, antibacterial, and osseointegration capabilities. Cell assays confirmed that the functionalization was cytocompatible towards human mesenchymal stem cells and the combination of iodine and polyphenols demonstrated a strong ability to protect cells from chemically induced oxidative stress, thus representing a promising strategy to provide support in the healing process under pro-inflammatory conditions.

8.4 References

Aceves, Carmen, Irasema Mendieta, Brenda Anguiano, and Evangelina Delgado-González. 2021. "Molecular Iodine Has Extrathyroidal Effects as an Antioxidant, Differentiator, and Immunomodulator." International Journal of Molecular Sciences 22 (3): 1228. https://doi.org/10.3390/ijms22031228.

Balza, J C, Denise Zujur, Linda Gil, Raiza Subero, E Gutiérrez Domínguez, Pedro Delvasto, and Jonatán Pérez Álvarez. 2013. "Sandblasting as a Surface Modification Technique on Titanium Alloys for Biomedical Applications: Abrasive Particle Behavior." IOP Conference Series 45 (June): 012004–4. https://doi.org/10.1088/1757-899x/45/1/012004.

Barfeie, A., J. Wilson, and J. Rees. 2015. "Implant Surface Characteristics and Their Effect on Osseointegration." British Dental Journal 218 (5): E9–9. https://doi.org/10.1038/sj.bdj.2015.171.

Barreto, George E., and Rubem C. A. Guedes. 2012. "Polyphenols and Neurodegenerative Diseases." Nutritional Neuroscience 15 (3): 92–93. https://doi.org/10.1179/12z.00000000034.

Bonifacio, Maria A., Andrea Cochis, Stefania Cometa, Piergiorgio Gentile, Annachiara Scalzone, Alessandro C. Scalia, Lia Rimondini, and Elvira De Giglio. 2020. "From the Sea to the Bee: Gellan Gum-Honey-Diatom Composite to Deliver Resveratrol for Cartilage Regeneration under Oxidative Stress Conditions." Carbohydrate Polymers 245 (October): 116410. https://doi.org/10.1016/j.carbpol.2020.116410.

Cazzola, Martina, Jacopo Barberi, Sara Ferraris, Andrea Cochis, Grzegorz Cempura, Aleksandra Czyrska-Filemonowicz, Lia Rimondini, and Silvia Spriano. 2022. "Bioactive Titanium Surfaces Enriched with Silver Nanoparticles through an in Situ Reduction: Looking for a Balance between Cytocompatibility and Antibacterial Activity." Advanced Engineering Materials, October, 2200883. https://doi.org/10.1002/adem.202200883.

Cazzola, Martina, Ingrid Corazzari, Enrico Prenesti, Elisa Bertone, Enrica Verne, and Sara Ferraris. 2016. "Bioactive Glass Coupling with Natural Polyphenols: Surface Modification, Bioactivity and Anti-Oxidant Ability." Applied Surface Science 367 (March): 237–48. https://doi.org/10.1016/j.apsusc.2016.01.138.

Cazzola, Martina, Sara Ferraris, Francesco Boschetto, Alfredo Rondinella, Elia Marin, Wenliang Zhu, Giuseppe Pezzotti, Enrica Vernè, and Silvia Spriano. 2018. "Green Tea Polyphenols Coupled with a Bioactive Titanium Alloy Surface: In Vitro Characterization of Osteoinductive Behavior through a KUSA A1 Cell Study." International Journal of Molecular Sciences 19 (8): 2255. https://doi.org/10.3390/ijms19082255.

Chen, Chung-Hwan, Mei-Ling Ho, Je-Ken Chang, Shao-Hung Hung, and Gwo-Jaw Wang. 2005. "Green Tea Catechin Enhances Osteogenesis in a Bone Marrow Mesenchymal Stem Cell Line." Osteoporosis International 16 (12): 2039–45. https://doi.org/10.1007/s00198-005-1995-0.

Chen, Songfeng, Hang Liang, Yanhui Ji, Hongwei Kou, Chi Zhang, Guowei Shang, Chunfeng Shang, et al. 2021. "Curcumin Modulates the Crosstalk between Macrophages and Bone Mesenchymal Stem Cells to Ameliorate Osteogenesis." Frontiers in Cell and Developmental Biology 9 (February). https://doi.org/10.3389/fcell.2021.634650.

Cita R S Prakoeswa, Yuyun Rindiastuti, Yohanes Widodo Wirohadidjojo, Evelyn Komaratih, Nurwasis, Aristika Dinaryati, Ni, and Fedik A Rantam. 2020. "Resveratrol Promotes Secretion of Wound Healing Related Growth Factors of Mesenchymal Stem Cells Originated from Adult and Fetal Tissues." Artificial Cells, Nanomedicine, and Biotechnology 48 (1): 1159–66. https://doi.org/10.1080/21691401.2020.1817057.

Di Meo, Florent, Vincent Lemaur, Jérôme Cornil, Roberto Lazzaroni, Jean-Luc Duroux, Yoann Olivier, and Patrick Trouillas. 2013. "Free Radical Scavenging by Natural Polyphenols: Atom versus Electron Transfer." The Journal of Physical Chemistry A 117 (10): 2082–92. https://doi.org/10.1021/jp3116319.

E.B. Ansar, K Ravikumar, S. Suresh Babu, F.B Fernandez, Manoj Komath, Bikramjit Basu, and P.R. Harikrishna Varma. 2019. "Inducing Apatite Pre-Layer on Titanium Surface through Hydrothermal Processing for Osseointegration." Materials Science & Engineering. C, Biomimetic Materials, Sensors and Systems 105 (December): 110019–19. https://doi.org/10.1016/j.msec.2019.110019.

Ferraris, S., and S. Spriano. 2016. "Antibacterial Titanium Surfaces for Medical Implants." Materials Science and Engineering: C 61 (April): 965–78. https://doi.org/10.1016/j.msec.2015.12.062.

Gamna, F., A. Cochis, A.C. Scalia, A. Vitale, S. Ferraris, L. Rimondini, and S. Spriano. 2022. "The Use of Vitamin E as an Anti-Adhesive Coating for Cells and Bacteria for Temporary Bone Implants." Surface and Coatings Technology 444 (August): 128694. https://doi.org/10.1016/j.surfcoat.2022.128694.

Gamna, Francesca, Seiji Yamaguchi, Andrea Cochis, Sara Ferraris, Ajay Kumar, Lia Rimondini, and Silvia Spriano. 2023. "Conferring Antioxidant Activity to an Antibacterial and Bioactive Titanium Surface through the Grafting of a Natural Extract." Nanomaterials 13 (3): 479–79. https://doi.org/10.3390/nano13030479.

Giacomo Riccucci, Sara Ferraris, Camilla Reggio, Antonella Bosso, Gissur Örlygsson, Chuen H Ng, and Silvia Spriano. 2021. "Polyphenols from Grape Pomace: Functionalization of Chitosan-Coated Hydroxyapatite for Modulated Swelling and Release of Polyphenols." Langmuir 37 (51): 14793–804. https://doi.org/10.1021/acs.langmuir.1c01930.

Hans Konrad Biesalski. 2007. "Polyphenols and Inflammation: Basic Interactions" 10 (6): 724–28. https://doi.org/10.1097/mco.0b013e3282f0cef2.

Hasan, Jafar, Russell J. Crawford, and Elena P. Ivanova. 2013. "Antibacterial Surfaces: The Quest for a New Generation of Biomaterials." Trends in Biotechnology 31 (5): 295–304. https://doi.org/10.1016/j.tibtech.2013.01.017.

Ikeda, Norimasa, Shunsuke Fujibayashi, Seiji Yamaguchi, Koji Goto, Bungo Otsuki, Toshiyuki Kawai, Takayoshi Shimizu, et al. 2022. "Bioactivity and Antibacterial Activity of Iodine-Containing Calcium Titanate against Implant-Associated Infection." Biomaterials Advances 138 (July): 212952–52. https://doi.org/10.1016/j.bioadv.2022.212952.

J. Pavón, O Galvis, F. Echeverría, J G Castaño, M Echeverry, S Robledo, E. Jiménez-Piqué, A. Mestra, and M Anglada. 2013. "Anodic Oxidation of Titanium for Implants and Prosthesis: Processing, Characterization and

Potential Improvement of Osteointegration." IFMBE Proceedings, January, 176–79. https://doi.org/10.1007/978-3-642-21198-0_45.

Jekabsone, Aiste, Inga Sile, Andrea Cochis, Marina Makrecka-Kuka, Goda Laucaityte, Elina Makarova, Lia Rimondini, et al. 2019. "Investigation of Antibacterial and Antiinflammatory Activities of Proanthocyanidins from Pelargonium Sidoides DC Root Extract." Nutrients 11 (11): 2829. https://doi.org/10.3390/nu11112829.

Kampa, M., A.-P. Nifli, G. Notas, and E. Castanas. 2007. "Polyphenols and Cancer Cell Growth." Reviews of Physiology, Biochemistry and Pharmacology 159: 79–113. https://doi.org/10.1007/112_2006_0702.

Le Guéhennec, L., A. Soueidan, P. Layrolle, and Y. Amouriq. 2007. "Surface Treatments of Titanium Dental Implants for Rapid Osseointegration." Dental Materials 23 (7): 844–54. https://doi.org/10.1016/j.dental.2006.06.025.

Ma, Yan, Kai Jiang, Hongrang Chen, Qianqian Shi, Hang Liu, Xiaoyan Zhong, Haisheng Qian, Xulin Chen, Liang Cheng, and Xianwen Wang. 2022. "Liquid Exfoliation of V8C7 Nanodots as Peroxidase-like Nanozymes for Photothermal-Catalytic Synergistic Antibacterial Treatment." Acta Biomaterialia 149 (September): 359–72. https://doi.org/10.1016/j.actbio.2022.06.031.

Mancuso, Giuseppe, Angelina Midiri, Elisabetta Gerace, and Carmelo Biondo. 2021. "Bacterial Antibiotic Resistance: The Most Critical Pathogens." Pathogens 10 (10): 1310. https://pubmed.ncbi.nlm.nih.gov/34684258/.

Nayab, Saima N., Frances H. Jones, and Irwin Olsen. 2007. "Modulation of the Human Bone Cell Cycle by Calcium Ion-Implantation of Titanium." Biomaterials 28 (1): 38–44. https://doi.org/10.1016/j.biomaterials.2006.08.032.

Orapiriyakul, Wich, Peter S Young, Laila Damiati, and Penelope M Tsimbouri. 2018. "Antibacterial Surface Modification of Titanium Implants in Orthopaedics." Journal of Tissue Engineering 9 (January): 204173141878983. https://doi.org/10.1177/2041731418789838.

Rivera, Laura Ramos. 2021. "Antibacterial, Pro-Angiogenic and Pro-Osteointegrative Zein-Bioactive Glass/Copper Based Coatings for Implantable Stainless Steel Aimed at Bone Healing." Bioactive Materials 6 (5): 1479–90. https://doi.org/10.1016/j.bioactmat.2020.11.001.

Savickiene, Nijole, Aiste Jekabsone, Lina Raudone, Asmaa Abdelgeliel, Andrea Cochis, Lia Rimondini, Elina Makarova, et al. 2018. "Efficacy of Proanthocyanidins from Pelargonium Sidoides Root Extract in Reducing P. Gingivalis Viability While Preserving Oral Commensal S. Salivarius." Materials 11 (9): 1499. https://doi.org/10.3390/ma11091499.

Scalbert, Augustin, Ian T Johnson, and Mike Saltmarsh. 2005. "Polyphenols: Antioxidants and Beyond." The American Journal of Clinical Nutrition 81 (1 Suppl): 215S217S. https://doi.org/10.1093/ajcn/81.1.215S.

Shavandi, Amin, Alaa El-Din Ahmed Bekhit, Pouya Saeedi, Zohreh Izadifar, Adnan A. Bekhit, and Ali Khademhosseini. 2018. "Polyphenol Uses in Biomaterials Engineering." Biomaterials 167 (June): 91–106. https://doi.org/10.1016/j.biomaterials.2018.03.018.

Sun, Yuhua, Yiting Li, Baohua Wu, Jianxin Wang, Xiong Lu, Shuxin Qu, Jie Weng, and Bo Feng. 2017. "Biological Responses to M13 Bacteriophage Modified Titanium Surfaces in Vitro." Acta Biomaterialia 58 (August): 527–38. https://doi.org/10.1016/j.actbio.2017.06.019.

Tande, A. J., and R. Patel. 2014. "Prosthetic Joint Infection." Clinical Microbiology Reviews 27 (2): 302–45. https://doi.org/10.1128/cmr.00111-13.

Trzeciakiewicz, Anna, Véronique Habauzit, and Marie-Noëlle Horcajada. 2009. "When Nutrition Interacts with Osteoblast Function: Molecular Mechanisms of Polyphenols." Nutrition Research Reviews 22 (1): 68–81. https://doi.org/10.1017/s095442240926402x.

Yamaguchi, Seiji, Phuc Thi Minh Le, Seine A. Shintani, Hiroaki Takadama, Morihiro Ito, Sara Ferraris, and Silvia Spriano. 2021. "Iodine-Loaded Calcium Titanate for Bone Repair with Sustainable Antibacterial Activity Prepared by Solution and Heat Treatment." Nanomaterials 11 (9): 2199. https://doi.org/10.3390/nano11092199.

Zhou, Kang, Xiuli Ren, Mengen Zhao, Xifan Mei, Peng Zhang, Zhenhua Chen, and Xiangdong Zhu. 2017. "Promoting Proliferation and Differentiation of BMSCs by Green Tea Polyphenols Functionalized Porous Calcium Phosphate." Regenerative Biomaterials (Online) 5 (1): 35–41. https://doi.org/10.1093/rb/rbx031.

Zuo, Weiyang, Lingjia Yu, Jisheng Lin, Yong Yang, and Qi Fei. 2021. "Properties Improvement of Titanium Alloys Scaffolds in Bone Tissue Engineering: A Literature Review." Annals of Translational Medicine 9 (15): 1259–59. https://doi.org/10.21037/atm-20-8175.

9. Acknowledgement

I want to express my utmost thanks to my respected advisor, Prof. Lia Rimondini, for her unmatched help, direction, understanding, encouragement, passion, and extensive expertise throughout my PhD studies and research. Her consistent guidance has played a crucial role in developing my research and writing abilities, and I am extremely grateful for her role as an ideal advisor and mentor during my PhD experience.

Besides my advisor, I want to express my gratitude to my tutor, Dr Andrea Cochis, who has consistently motivated and encouraged me during the experiments, thus making the process easier and more enjoyable.

I would also like to express my sincere thanks to Prof. Dr Diego Cotella for leading me to work on diverse and exciting ongoing projects in their group and guiding me on the PhD project.

My gratitude also goes to my fellow lab mates for the stimulating discussions and valuable inputs that have helped me immensely in my research.

The University of Piemonte Orientale efforts have been critical to my academic and extracurricular achievements to date. The past four years have had a profound and important impact on the person I have become, and I am grateful for the people especially my lab and experiences that have contributed to this growth and for everyone who has helped me along my journey and appreciates me, value me and help me achieve my goals. I have pushed myself in my academic pursuits and delved into my passions. I am prepared to face the next stage in my life, thanks to the experiences I have gained so far.

10. Declaration of using software technologies in the writing process

During the preparation of the PhD thesis, I used Grammarly to increase the quality of writing. I also used some software like Image J, Excel, and GraphPad Prism to analyze the obtained results. Most Of the graphical abstracts were modified and created in Bio Render with the license.

11. Acronyms

ADP – Adenosine diphosphate

AKT – Serine/threonine kinase family

ALP – Alkaline phosphatase

AAs – Amino Acids

APQ – Aquaporins

AS101 – Tellurate

ATP – Adenosine triphosphate

BAI – Bacteria associate infection

BG – Bioactive glasses

BMSCs – Bone marrow Mesenchymal stem cells

BSP – bone sialoproteins

Ca – Calcium

$CaCl_2$ – Calcium chloride dihydrate

CBD – C – terminal Cell wall binding domain

CCL2 – Small inducible cytokine A2

Ce – Cerium

Ce^{3+} – Cerous

Ce^{4+} – Ceric

CeO_2 – Cerium oxide

CHAP – Cysteine-dependent peptidase

Cl- Chloride

CNPs – Cerium nanoparticles

CNS – Coagulase-negative staphylococci

CO_3^{2-} - Carbonate

COMP – Cartilage oligomeric matrix protein

CP – Calcium phosphate

Cu – Copper

DAMPS – Damage–associated signals

ECM – Extracellular matrix

EGF – Epidermal growth factor

F- - Fluoride

FRI – Fracture-related infections

FOXO – Forkhead box transcription factors

GPX – Glutathione peroxidase

GSH – Glutathione γ-glutamyl-cysteinyl-glycine

H2O2 – Hydrogen peroxide

H2SO4 – Sulfuric acid

HA – Hydroxyapatite

HCL – Hydrochloric acid

HIF – 1α – Hypoxia-inducible factor 1-alpha

HMGB1 – Extracellular S-100 proteins, high mobility group box-1

IAI – Chronic Orthopaedic Implant-Associated Infection

IL – Interleukin

I – Iodine ions

iONS – Inducible isoform

IEP – Isoelectric point

JNK – c – Jun N-terminal kinase

K – Potassium

LIPUS – low – intensity pulsed ultrasound

LPS – Lipopolysaccharides

Lys K – Staphylococcal phage – K endolysins

MAP – Mitogen-activated protein

MBGs – Mesoporous glasses

Mg – Magnesium

MgCl2 – Magnesium chloride hexahydrate

MICs – Minimum inhibitory concentrations

MnCl – Manganese chloride tetrahydrate

MRI – Magnetic resonance imaging

MRSA – Methicillin-resistant

MSCs – Mesenchymal stem cells

Mt – DNA – Mitochondrial DNA

N – Glc – N – acetylglucosamine residues

N – Mur – N – acetylmuramic acid

Na – Sodium

NAD – N – a terminal enzymatically active domain

NADPH – Nicotinamide adenine dinucleotide phosphate

NCPs – Non – collagenous proteins

NF-kB - Nuclear factor kappa B

NO – Nitric oxide

NOS – Nitric oxide synthase

NOX – NADPH oxidase enzymes

NPs – Nanoparticles

Nrf2 – Nuclear issues erythroid 2-related issues 2

NRF2 – Nuclear factor erythroid 2-related factor

O2 – Oxygen

O2.- – Superoxide radical

O2NO- – Peroxynitrite

OCN – Osteocalcin

OH – Hydroxyl radical

OR – Oral hygiene

OP – Phosphorylation

OPN – osteopontin

OS – Oxidative stress

P38MAPK – 38 Mitogen-activated protein kinases

PD – Parkinson's disease

PDGF – Platelet-derived growth factor

PEMF – Pulsed electromagnetic fields

PI3K – Phosphoinositide 3-kinases

PIKM – Peri-implant keratinized mucosa

PJI – Periprosthetic joint infections

PNA – Peptide nucleic acid

PO_4^{3-} - Phosphate

PRR – sophisticated pattern recognition

PT – Protein-tyrosine

PTH – parathyroid hormone

PTP – Protein-serine-threonine phosphatases

RBC – Red Blood Cells

RNS – Reactive nitrogen species

ROS – Reactive oxygen species

RTK - protein tyrosine kinases

SOD – Superoxide dismutase

Sr – Strontium

SSI – surgical site infection

SPIC – Supportive peri-implant care

Te – Tellurium

TIIS – Therapeutic inorganic ions

TE – Tissue engineering

TeO_3^{2-} - Tellurite

TeO_4^{2-} - Tellurate

TGF – β tumour growth factor – β

TiO_2 – Titanium dioxide

TLR – Toll-like receptors

TNF – α – Tumor necrosis factor-alpha

VEGF – Vascular endothelial growth factor

VEGFR – Vascular endothelial growth factor

WHO- World Health Organisation

Wnt/β – Wingless – related integration

YLDs – years lived with disability

Zn – Zinc

ZnO – Zinc oxide